Transvascular Transport of Sterically Stabilized Liposomes and Particles in Transplanted Tumors

by

Susan K. Hobbs

B.Ch.E., Department of Chemical Engineering, University of Minnesota, 1989

Submitted to the Department of Chemical Engineering
in partial fulfillment of the requirements for the degree of

Doctor of Philosophy
at the Massachusetts Institute of Technology

June 1998

Signature of Author: _____
Department of Chemical Engineering
May 22, 1998

Certified by: _____
Linda Griffith
Associate Professor of Chemical Engineering
Thesis Supervisor

_____
Rakesh K. Jain
Andrew Werk Cook Professor
Harvard Medical School
Thesis Supervisor

Accepted by: _____
Professor Robert E. Cohen
Chairman, Committee for Graduate Students

Transvascular Transport of Sterically Stabilized Liposomes and Particles in Transplanted Tumors

by
Susan K. Hobbs

Submitted to the Department of Chemical Engineering on May 22, 1998 in partial fulfillment of the requirements for the degree of Doctor of Philosophy in Chemical Engineering

Abstract

This thesis investigated macromolecular and nanoparticle transvascular transport within implanted tumors. The upper limit of the size of therapeutic agents that can traverse vessels of different tumors and how this is regulated is not well understood. Here we analyze the functional limits of transvascular transport and its modulation by the microenvironment. In situ studies of the extravasation of fluorescently labeled liposomes or latex beads were conducted in both the dorsal skin-fold chamber and the cranial window of immunodeficient mice. The pore cutoff size, a functional measure of transvascular gap size, was determined for various tumors.

Tumors grown in the subcutaneous microenvironment (dorsal chamber) were found to have tumor dependent pore cutoff sizes. The size of these pores (200 nm to 1.2 μm) indicated that the structures responsible for macromolecular or particulate extravasation are open gaps, either widened interendothelial junctions or transendothelial gaps. The permeability of the tumor microvessels to bovine serum albumin (≈ 7 nm) was not influenced by the pore cutoff size.

The microenvironment was modulated (*i*) temporally, by inducing vascular regression in hormone dependent tumors, and (*ii*) spatially, by growing tumors in subcutaneous or cranial locations. The onset of tumor regression following testosterone withdrawal in male mice resulted in an immediate and dramatic reduction in the pore cutoff size within 48 hours. Continuous vascular remodeling with further tumor growth did not influence the pore cutoff size.

There are local tissue differences in receptor expression, factor secretion, chemotherapy response, and metastatic potential of different tissues. One of the sites of most concern due to differences in treatment response is the brain. To determine the effect of the cranial microenvironment on the pore cutoff size, similar studies were performed on tumors grown in the cranial window. The pore cutoff size in the cranial window was less than that found in the dorsal chamber in three of the four tumor lines. However, the pore cutoff size was significantly greater than that of the host microvasculature at the cranial site. There was no macromolecular extravasation in a transplanted human glioma.

In an attempt to achieve a quantitative delivery system, we investigated the interaction of bFGF with sepharose-immobilized heparin as a first step in the controlled release process from calcium alginate gels. We found that a maximum of 80% of the initial bFGF was incorporated into the heparin-sepharose microbeads when heparin was in large excess. Modulation of heparin concentration, heparin immobilization, and accessibility did not increase the amount of bFGF which could be bound to these microbeads.

Characterization of vascular response to continuous local delivery was investigated by sucralfate-collagen system. Sustained delivery of growth factors released from sucralfate-collagen gels implanted in the dorsal chamber of immunodeficient mice induced angiogenesis. We found that bFGF containing gels induced an increased pore cutoff size on the order of tumor stimulated pore cutoff size, whereas VEGF containing gels induced no significant increase in pore cutoff size of the microvessels.

These results have major implications for the delivery of therapeutic agents. An understanding of the interaction of bFGF and immobilized heparin may improve the efficacy of

bFGF isolation and bFGF delivery from these devices. There are four major implications for the delivery of therapeutic agents to solid tumors: *(i)* delivery may be less efficient in cranial tumors than in subcutaneous tumors, *(ii)* delivery may be reduced during tumor regression induced by hormonal ablation, *(iii)* permeability to a molecule is independent of pore cutoff size as long as the diameter of the molecule is much less than the pore diameter, and *(iv)* chronic exposure to bFGF could affect the pore size in angiogenic and anti-angiogenic gel assays. Most encapsulated carriers and viral vectors proposed for therapeutic use are between 100 and 300 nm. An understanding of the limits and regulation of transvascular transport may offer modalities to increase the distribution or size of the transvascular transport pathways from optimized delivery and design of these large therapeutic agents.

Thesis Supervisor: Linda Griffith
Title: Associate Professor of Chemical Engineering
Thesis Supervisor: Rakesh K. Jain
Title: Andrew Werk Cook Professor

Acknowledgments

I would like to dedicate this work to my family. First to my parents, Sally and William, who instilled in their children the desire, drive, and strength to succeed at whatever we chose. To my brother Bill, who was gullible enough to follow his older sister down the MD/PhD path. To my older sisters, Yvone and Joan; even though we are separated by miles and differences, I still felt your support. And of course to the family pets, Ben and Skyler, who suffered through my various harried visits to Minneapolis.

I would like to thank my advisors, Linda Griffith and Rakesh Jain, for making this thesis possible with their support and their willingness to work through problems; and my committee members-Matthew Nugent, Fan Yuan, Bill Deen, and Doug Lauffenberger- for their invaluable input to my research.

Thanks to the group at MGH who welcomed me when I first came to the lab: Larry Baxter, Bob Melder, Yves Boucher, Sylvie Roberge, Michael Leunig, and Fan Yuan. Michael Leunig was probably the best teacher I had, I owe my microsurgery technique to you (Never drink the night before operating...right!). My mentor Fan Yuan, for his honesty, lack of bitterness, intelligence, and patience. Thanks so much to Julia Kahn and Sylvie Roberge; Julia made many of the dorsal chambers and implanted many of the tumors as well as provided tons of information on animal care and conversations in the colony. Sylvie maintained the cell lines, and even when I was a flake she came through for me (not to mention the great books she read). To Melody: thanks for the gripe sessions. And importantly, thank you to Wayne Monskey, for your hard work, enthusiasm, and your words of advice and encouragement. Too bad we won't be working together at BIDMC (although I am secretly glad that I am not staying around Boston--Go Gophers!!!).

I'd like to thank the other MD/PhD students in the department, Bobby Satcher, Jim Oliver, and Ed Perez. You guys always had an encouraging word about the benefits of obtaining both degrees (I never knew if you truly believed it...). To the other MD/PhD students: Ann West (even if you are from Cornell), Pat Senatus for talks on life in general, Colleen Buggs for her dignity and strength, and Mike Root for his never-ending enthusiasm for everything. We are finally OUTTA HERE!!!!

I would like to thank my "best friend" in the Chemical Engineering department; Mary Jane. It was great "not being a real Chemical Engineer" with you for five whatever years. I don't know if all our chats over beer or coffee helped but I sure enjoyed them. Thanks for all the dinners, the running, and the friendship. Don't let the corridor monsters make you too bitter, you are still a great person! Thanks to Talid Sinno for his refreshing insights from day 1. What would I have done without your sense of humor, your sarcasm, and your homework? You were one of the few who never made me feel stupid. I do wish you would stop trying to kill yourself, though. Thanks to the rest of "the boys" for the nights of drinking and dancing and generally cutting loose.

Thanks to my Minnesota fan club: Kim Didier, John Lee, Dawn Tilbury, Rosie Gaynor, Toby Smith, Lisa Monsour, Peggy Bartz, Bruce Anderson, Marianne Loken, and Roxanne Hall for listening, keeping the faith, and for putting up with my inconsistent communication. Especially Dawn, thank you so much for your continued support and advice from someone "in the trenches" and for our discussions outside of science. You helped me through many difficult times (but Michigan?--Go Gophers!!!).

Special thanks go out to various people I have met along this journey: Catherine Shaw-Reid and Araba Lamouse-Smith for keeping our group together, Judy Chen, words cannot describe this crazy woman, Stephanie Lopina for her positive attitude in the face of adversity, Howard Covert for all his help with mathematical modeling and my car, Peter Chefalo (although I may never forgive you) for the company during the most difficult 2 years at MIT, Andre Lecesne, for having the strength to make the right decision and for all the fun we have in New Orleans, Minnesota home boy Colin Wolden for all the music talks and the free tickets to fabulous concerts! and to Diana, Danny, Anais, and now Gavril-I am going to miss my step-family!

I must send out a note of appreciation to my roommates, Carrie and Ratna, for their understanding when I was a slob, absent-minded, strung out, a zombie, inconsiderate, forgetful, and all the things normal people would be committed for. Especially to Ratna, it seems almost unbelievable how much the two of us have gone through in the past 9 years (can you believe it?!). You have always been there for me, I only wish I could say the same. I will never forget your glazed eyes while listening to me practice my qualifying presentation.

And finally, a note of great thanks goes out to Jim, the guy at the photo shop. Without him the completion of this thesis would not have been possible.

Table of Contents

List of Figures

List of Tables

Chapter 1.
MOTIVATION

Cancer is second to heart disease as the cause of death and accounts for approximately 22% of the mortality in the United States [1]. There are three established methods of cancer therapy: surgery, radiation, and chemotherapy; and three experimental methods of cancer therapy: immunotherapy, hyperthermia, and photodynamic therapy. The latter three treatment methods have seen little clinical application. Surgery and radiation therapy are local treatment modalities. Surgery, while it has the advantage of removing a local tumor mass at once, is limited by anatomical and functional constraints. In approximately 50% of patients surgical excision of the primary neoplasm is not curative because metastasis have already occurred [2]. Radiation therapy has the capacity of damaging infiltrating malignant cells. However, the effectiveness is limited by dose-toxicity to normal tissue and the inherent kinetics of cell regrowth, as well as being a local agent. Chemotherapy delivers the cytotoxic agent throughout the body via the bloodstream and thus, it has the ability to reach disseminated cancer cells. The disadvantage is toxicity to high perfusion organs such as the liver and kidney, or to rapidly dividing cells such as in bone marrow and in the gastrointestinal system which limits the dose. In addition to the toxicity of the drugs, the limitations to drug delivery include 1) decreased flow within the tumor, 2) increased plasma or tissue clearance, 3) decreased transvascular transport.

Treatment choice is tumor dependent and not always successful. Molecular biology and genetic engineering have led to the discovery and development of numerous molecules which could aid in the detection and treatment of cancer. In parallel, encapsulated drug technology has the potential to reduce drug toxicity in normal tissues. However, to achieve clinical success the antibodies, macromolecules, or nanoparticles must be delivered selectively and at therapeutic levels to the target tissue [3]. Transvascular transport is one of the physical barriers to delivery of intact drug. Knowledge of the significant structures in the macromolecular or nanoparticle transvascular passage is crucial for the potential use of antibodies, macromolecules, and particles in clinical

detection of and treatment of cancer. The focus of this thesis is to elucidate the nature of the microvascular barrier to delivery of nanoparticles utilizing sterically protected liposomes and latx beads as representative delivery vehicles. A flow chart of the thesis is shown in Figure 1-1.

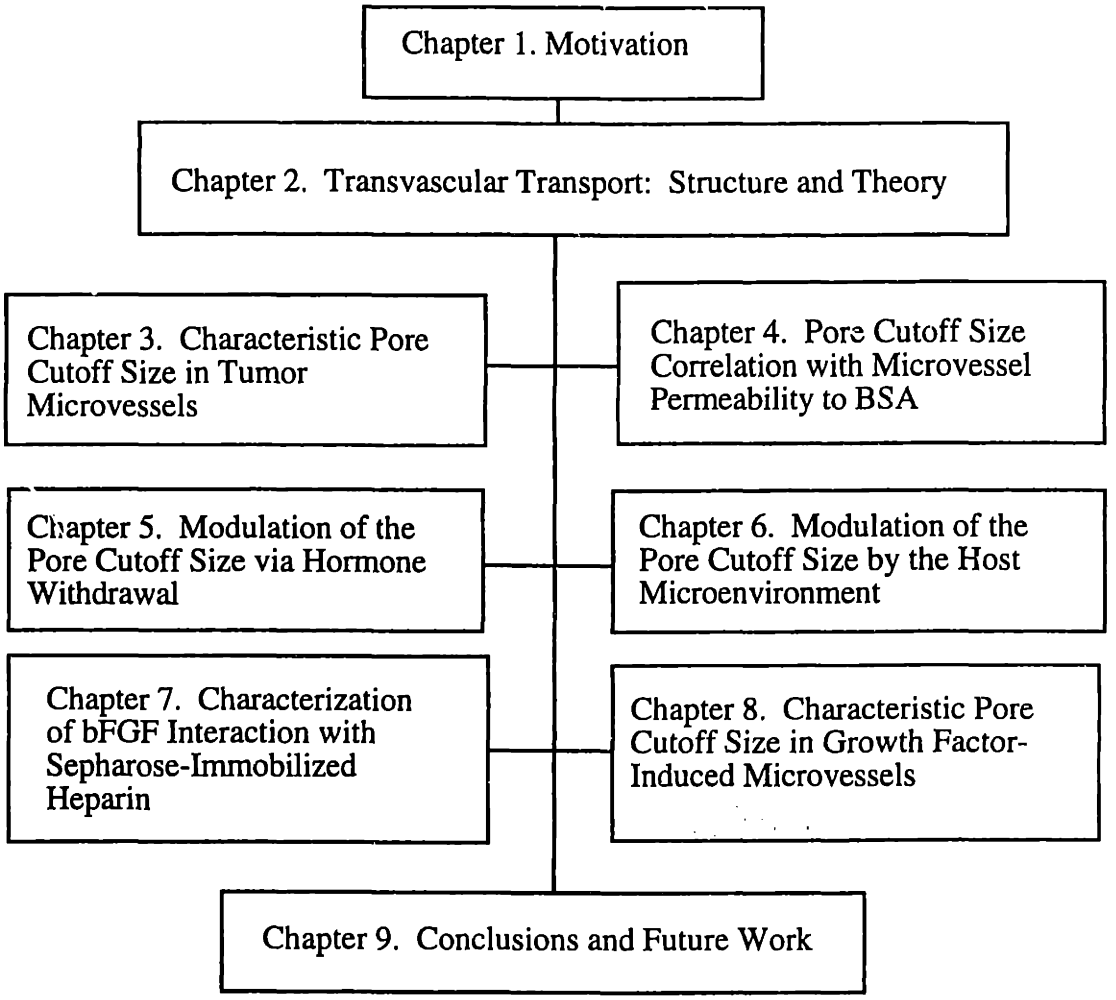

Figure 1-1. Outline of thesis

References

1. United States Department of Health and Human Services, Vital Statistics of the United States 1992. Mortality Part A. Vol. 2. 1996, Hyattsville, Maryland: Public Health Service, and Center for Disease Control and Prevention.

2. Fidler, I. and L. Ellis, The implications of angiogenesis for the biology and therapy of cancer metastasis. Cell. **79**: 185-188 (1994).

3. Jain, R., Delivery of molecular medicine to solid tumors. Science. **271**: 1079-1080 (1996).

Chapter 2.

TRANSVASCULAR TRANSPORT: STRUCTURE AND THEORY

2.1 Microcirculation

The microcirculation is a complex interacting unit that reacts to all variables of any subcellular or tissue system. The vessels included in the microcirculation are the arteriole, terminal arteriole, capillary, postcapillary venule and venule (Figure 2-1). Although lymphatic vessels are intertwined with the blood vessels they are not classically included in the description of the microcirculation. The arterioles, afferent vessels, control the inlets to the capillary bed. The capillary is the site of nutrient and oxygen exchange for waste and carbon dioxide. Macromolecular transport also occurs at this level.

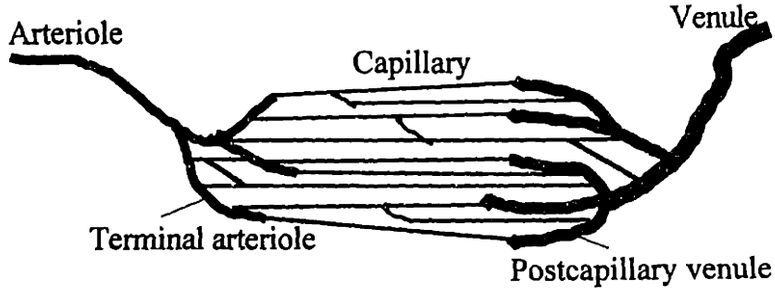

Figure 2-1. Components of the microcirculation

2.1.1 Endothelium

The endothelium forms the luminal lining of blood vessels (Figure 2-2). These cells are differentiated to permit large-scale exchange of molecules between blood plasma and interstitial fluid. The exchange of small molecules and water is via coated pits/vesicles, plasmalemmal vesicles, caveolae, pinocytic transport vesicles, and other cell surface associated openings which are characteristics of endothelial cells [1]. Transvascular exchange of macromolecules rarely occurs in normal vessels. The endothelial cells form the most important barrier to macromolecular leakage from the vessels into the interstitium.

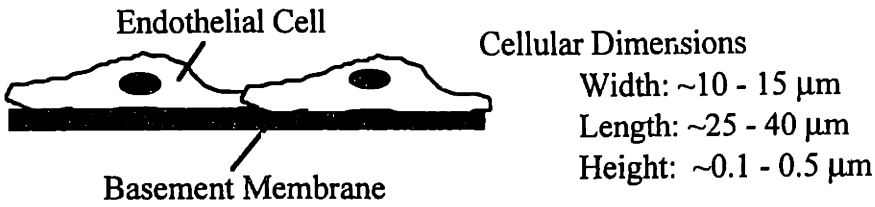

Figure 2-2. Schematic of the microvessel endothelium (adapted from [2])

Capillary endothelium have been classified into three categories: continuous, fenestrated, and discontinuous. Continuous endothelium, the most common type, is found in skin, connective tissue, skeletal and cardiac muscle, lung, and brain. Fenestrae are small attenuations of the endothelial thickness (diameters in the range of 40-80 nm) which do not affect the continuity of the cell membrane. The fenestrae can be open or covered by a thin diaphragm (60 -80 Å thick) composed of a radial array of fibers which meet in the center to form a knob-like structure and carries a net negative charge. Fenestrated endothelium is found in intestinal mucosa, pancreas, glomerulus, peritubular capillaries, endocrine glands, choroid plexus, and ciliary body of the eye. These locations are associated with increased filtration or increased transendothelial transport. Sinusoids or discontinuous capillaries contain wide openings between endothelial cells and discontinuous or absent basal lamina. This type of endothelium is most commonly found in the liver, spleen, and bone marrow.

2.1.2 Basement Membrane

The basement membrane to which endothelial cells are attached is a 40-80 nm thick matrix of collagens, glycoproteins, laminin, and fibronectin (Figure 2-2). Its function is to maintain the blood vessel shape, control cell configuration, limit the flow of solutes across the wall, and participate in local responsive reactions (i.e. inflammation). In normal microvasculature the basement membrane does impart some inhibition to macromolecular transport.

2.1.3 Angiogenesis and Tumor Microcirculation

Angiogenesis is the result of the release of several factors working in concert to cause digestion of the extracellular matrix, endothelial cell migration, and endothelial cell differentiation [3]. This results in sprouting, anastamosis, and vascular remodeling. This process is fundamental to reproduction, development, wound healing, and pathology. In adult tissues angiogenesis is infrequent; occurring during wound healing or in pathology. Pathology includes but is not limited to neoplasms, diabetic retinopathy, rheumatoid arthritis, and psoriasis.

The ability to induce expansion of the vascular network to provide nutrients is essential for cellular proliferation [4]. The vasculature in a tumor may bear little resemblance to normal vasculature. It is anatomically heterogeneous, characterized by a chaotic network of tortuous, dilated vessels and sluggish blood flow. Due to release of various factors and cytokines, the number of vesicles, fenestrae, and widened interendothelial junctions is increased. In addition tumor vessels exhibit transendothelial gaps similar to sinusoids found in the liver or spleen. The basement membrane is discontinuous, absent, and the fiber structures may be disorganized when compared to the normal basement membrane [5]. A common characteristic of tumor microvessels is the vascular hyperpermeability to circulating macromolecules.

2.2 Macromolecular Transvascular Transport

2.2.1 Structural Barriers

The primary sites for transvascular exchange are capillaries and post-capillary venules because of their large surface area and thin walls. In general, small hydrophilic molecules and lipophilic substances readily pass through the endothelial cell from the circulation to the interstitial space. The barriers to macromolecular transport from the blood vessel to the tissue site include the endothelial cell layer, the basement membrane, the interstitial space, and the intervening parenchyma (Figure 2-3). The normal microvasculature is composed of endothelial cells which act as molecular sieves allowing passage of water, ions, and small hydrophilic molecules, but acting

as a barrier to the passage of macromolecules. Endothelial impermeability maintains a protein concentration difference across the vessel wall and results in differential fluid distribution in the plasma and interstitial spaces. The prevalent model of transvascular transport consists of two cylindrical pore populations; a small pore (effective radius 6 nm) for the transport of water and small solutes up to the size of albumin and a large pore (effective radius 10 nm) for the passage of macromolecules [6].

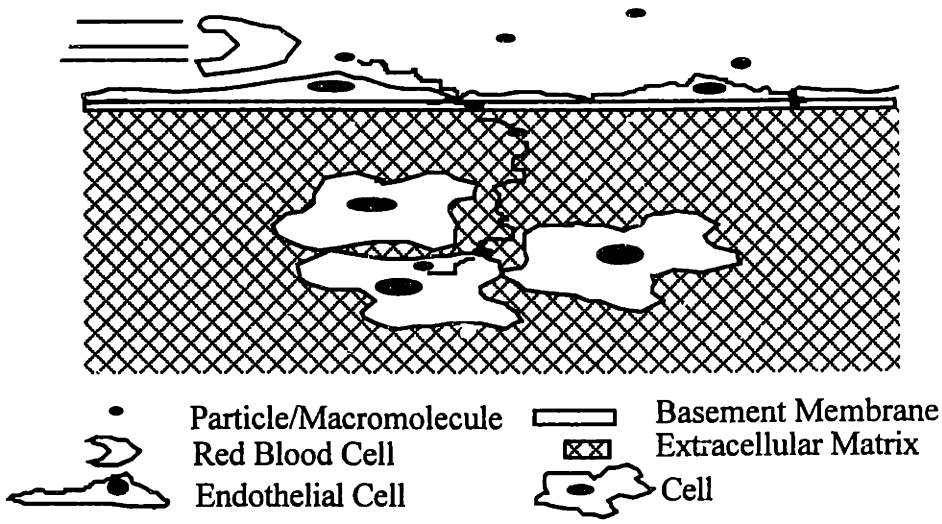

Figure 2-3. Barriers to particulate or macromolecular transport. These include transport in the vessels, transport across the endothelium, transport across the basement membrane, transport through the extracellular matrix, and transport across the target cell membrane.

Transport across the microvascular wall includes passage through the endothelial cell and the basement membrane. On a more detailed scale, transport will depend on the microarchitecture of the endothelial cell and the arrangement of fibers in the basement membrane. Five processes found in the normal endothelium could be important in transcellular or paracellular macromolecular (size >> 5 nm diameter) transport: interendothelial junctions, vesicles, transendothelial channels, fenestrae, and phagocytosis (Figure 2-4).

The interendothelial junction or cleft is a 6-7 nm space between two adjacent endothelial cells. Endothelial cells form adhering and occluding junctional complexes which serve as diffusive pathways for small molecules [7]. Although these channels occupy less than one thousandth of the surface area, it is thought that they are the primary pathways for hydrophilic molecules. This

interendothelial junction may increase in size in response to released cytokines. Vascular endothelial growth factor (VEGF) has been shown to open endothelial junctions within 10 minutes after topical administration [8]. The gaps can be up to 1 μm wide [9]. The enlargement is believed to result from endothelial contraction and junctional separation [9-12].

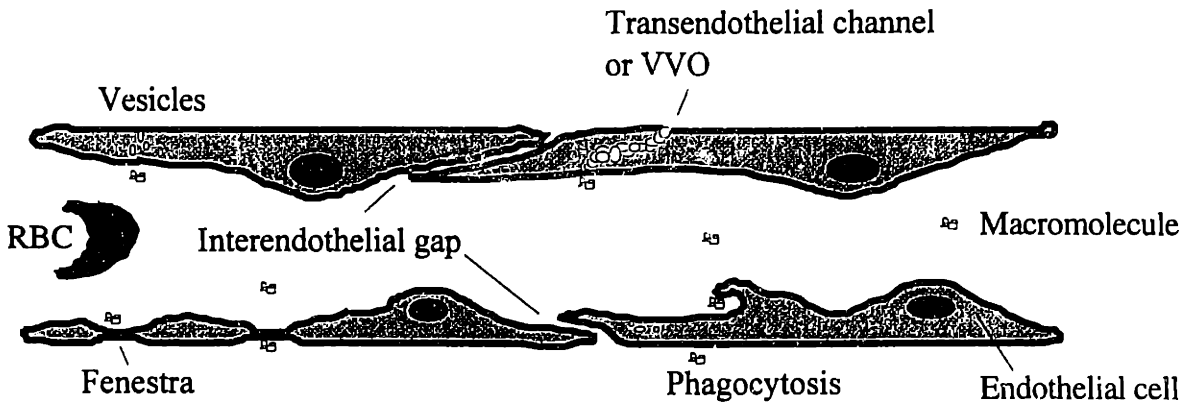

Figure 2-4. Microvascular transport processes. These are the processes which may be important to macromolecular transport through the endothelium.

Endothelial cells contain numerous vesicles which may be responsible for transporting particles and macromolecules back and forth (transcytosis) [13]. Since their discovery, they have been the subject of much controversy concerning their function in macromolecular transport. In 1993, Predescu reported that particles of 12 - 14 nm did not permeate the interendothelial gaps but were found in the plasmalemmal vesicles and in the pericapillary space near a discharging vesicle [14]. The diameter of these vesicles was approximately 70 nm [13-18]. Vesicles do not appear to contain surface anionic sites in contrast to fenestrae and coated pits. Initially, it was thought that the vesicles operated like shuttles from the luminal side to the abluminal side of the endothelium [18]. Later, it was proposed that repeated fusion and fission of a series of closely spaced vesicles might be the transport mechanism [19].

Vesicles can remain fused together to form chains or transendothelial channels. Bundegaard observed clusters of vesicles linked together with 20 - 40 nm strictures at the junction between two vesicles in transmission electron micrographs [16]. These transendothelial channels are proposed to be the large pore pathway. Recently, this stationary organelle was described in

tumor microvessels and normal postcapillary venules as vesiculo-vacuolar organelles (VVOs) [15]. VVOs are clusters of vesicles and larger sized vacuoles interconnected by stomata which may be open or closed by thin diaphragms. Serial tissue sections obtained after VEGF injection revealed ferritin (~11 nm diameter) extravasation associated with the VVOs, and no observable ferritin associated with the closed interendothelial junctions [20]. Unlike transendothelial channels, the VVOs are composed of vesicles and vacuoles. On average the vesicles involved in VVOs are larger than vesicle size (108 ±32 nm inner diameter) [20].

The fourth important structure in macromolecular transvascular transport are fenestrae. Normal fenestrated endothelium is found in the liver, spleen, and bone marrow. Endothelial cells in the liver contain large fenestrae approximately 150-175 nm in diameter [21]. However, fenestrae can be larger than this average; 10 μm liposomes extravasated through the liver endothelium [22]. Fenestrae may be open or closed, and contain a high population of heparan sulfate proteoglycans imparting a negative charge. Fenestrae have been shown to have an increased frequency with the addition of VEGF [8, 23].

Phagocytosis comprises the final transport process. However, not much is known about this pathway in vivo. Endothelial cells in cell culture are capable of phagocytosis in response to perfusion of the lung with 5-10 μm beads [24].

The above discussion pertains to normal vasculature. The situation is more complex in tumor microvasculature due to anatomical heterogeneity and heterogeneous hyperpermeability to circulating macromolecules [25-29]. In addition, the tumor microenvironment contains various growth factors [3, 25, 28, 30-33] which may influence the macromolecular transport. For example, VEGF production is upregulated in tumors [8, 23, 29, 34-36], and has been shown to induce increased fenestration [8, 23]; Dvorak, 1995 #49; Feng, 1996 #55].

2.2.2 Theoretical Description of Transvascular Transport

Starling's hypothesis of fluid transport between the plasma and the interstitium has undergone significant modification since 1896. Starling proposed that the balance of hydrostatic

pressure (P) difference between the capillary and interstitial space and colloid osmotic pressure (π) difference between the plasma osmotic pressure and the interstitial osmotic pressure describes the steady state transcapillary fluid balance [37]:

$$P_p - P_{\text{int}} = \pi_p - \pi_{\text{int}} \tag{2-1}$$

Landis modified the Starling hypothesis by introducing dynamic fluid flow [38]:

$$J_v = K_f\left[\left(P_p - P_{\text{int}}\right) - \left(\pi_p - \pi_{\text{int}}\right)\right] \tag{2-2}$$

J_V represents the fluid volume flux (cm^3/s), and K_f a proportionality constant. However, this equation does not take into account the effect of membrane properties on fluid transport. The influence of membrane permeability to a solute on its osmotic force was introduced by Kedem in 1958 [39]:

$$J_v = L_p S\left[\left(P_p - P_{\text{int}}\right) - \sigma\left(\pi_p - \pi_{\text{int}}\right)\right] \tag{2-3}$$

where K_f is replaced by the product of hydraulic conductivity, L_p ($cm^3/s/dyne$), and capillary surface area, S (cm^2). The solute reflection coefficient, σ, ranges from permeability equal to water ($\sigma = 0$) to complete impermeability ($\sigma = 1$).

Transport of macromolecules is a function of coupled diffusion and convection described by the Staverman-Kedem-Katchalsky equation [40]:

$$J_s = PS\left(c_p - c_{\text{int}}\right) + J_v(1-\sigma)\left(\frac{c_p - c_{\text{int}}}{\ln\left(\frac{c_p}{c_{\text{int}}}\right)}\right) \tag{2-4}$$

where P is the diffusive permeability of the membrane to the solute (cm/s), c_p and c_{int} are the plasma and interstitial solute concentrations (moles/cm^3). This description of transport includes the fact that the distribution of the extracellular fluid is governed by forces controlling interstitial drainage and lymph flow. The lymphatics carry proteins and macromolecules in addition to excess fluid away from the interstitial spaces. This movement continues the protein filtration loop which begins with "leakage" of proteins from the circulation.

Another commonly used description of transport across a porous membrane, originally described by Patlak, is the following [41]:

$$J_s = J_v(1-\sigma_s)\left[\frac{c_p - c_{int}e^{-Pe}}{1-e^{-Pe}}\right] \tag{2-5}$$

Pe is the Peclet number, a ratio of convective transport to diffusive transport:

$$Pe = \frac{J_v(1-\sigma)}{PS} \tag{2-6}$$

When the system is in steady state or the transcapillary transport is equal to transport into the lymphatics, the above expression (2-5) can be separated into diffusive and convective terms:

$$J_s = \frac{PS(c_p - c_{int})Pe}{e^{Pe}-1} + J_v(1-\sigma)c_p \tag{2-7}$$

This equation provides a complete description of solute flux through a homoporous membrane. If convection is assumed to be negligible, equation (2-7) can be simplified in terms of an effective microvascular permeability coefficient:

$$J_s = P_{eff}(c_p - c_{int}) \tag{2-8}$$

It must be emphasized that the above equations of solute flux are valid for homoporous membranes. In reality, microvascular membranes are not homoporous. There are many different possible pathways as illustrated in Figure 2-3. The cylindrical two-pore theory postulates that there are two populations of pores: small pores (5-6 nm) and large pores (20 - 35 nm) [42]. The large pores allow bulk filtration of macromolecules due to the hydrostatic pressure gradient in the pores. The general description for fluid transport in a multi-pore model is:

$$J_v = \sum_{i=1}^{m} J_{v,i} = \sum_{i=1}^{m} \alpha_i L_p S \left(\Delta P - \sum_{j=1}^{n} \sigma_{i,j} \Delta \pi_j \right) \qquad (2\text{-}9)$$

where m is the number of pores of size i, n is the number of solutes in the system which exert an osmotic pressure, α_i is the fraction of hydraulic conductance attributed to pore type i.

The role of cytoplasmic vesicles as a prominent macromolecular transport mechanism is under debate [13, 14, 16, 18-20, 43-46]. There are three contested mechanisms of action: 1) shuttle hypothesis where a vesicle buds from one membrane surface and moves freely to fuse with the opposite surface, 2) fusion-fission hypothesis where the vesicles move until they fuse with another vesicle, transfer their contents and then move away, and 3) the vesicles form transendothelial channels that are permanent structures. To incorporate these mechanisms in the above transport descriptions the following equation has been used; $(PS)_{total} = (PS)_{vesicles} + (PS)_{pores}$ [42].

The transport of a macromolecule or nanoparticle may be affected by diffusion and convection constraints through the pores. Hindered transport theory has been used to understand the transvascular transport through capillaries [47]. If the size of the macromolecule is on the order of magnitude of the pore structure, the diffusional transport is much slower than that in the bulk solution. This can be explained by the steric and, in some cases, long-range interactions of the macromolecule with the pore wall which prevents the free access of the macromolecule to the entire pore fluid volume. Similar arguments are proposed for convective transport.

The partitioning of the macromolecule into the pore is described by [48]:

$$\phi = \left(1 - \frac{r_s}{r_p}\right)^2 \qquad (2\text{-}10)$$

where Φ is the partitioning coefficient described as the ratio of r_s, radius of the solute, and r_p, radius of the pore. Solute flux of macromolecules will be modified by hindrance factors which depend on the partitioning coefficient and the radial position within the pore. The hindrance factors account for the effects of finite pore size. As discussed earlier, transvascular transport in tumor microvessels appears to be dominated by diffusional transport, therefore, the permeability (P_{eff} in Equation 2-8) of the porous membrane is directly modified by the diffusional hindrance factor.

2.3 Summary

A blood-borne cancer therapeutic agent must make its way into the tumor blood vessels, cross the vessel wall, migrate through the interstitium to reach the target cell. Tumors have developed means to hinder or halt this process. The goal of this thesis was to analyze the macromolecular transvascular transport step experimentally. This will allow better understanding in development and design of novel therapeutic agents.

2.4 References

1. Palade, G., The microvascular endothelium revisited, in Endothelial Cell Biology in Health and Disease, N. Simionescu and M. Simionescu, Editors. 1988, Plenum Press: New York. p. 3-22.

2. Simionescu, M. and N. Simionescu, Ultrastructure of the microvascular wall: functional correlations, in Handbook of Physiology, E. Renkin and C. Michel, Editors. 1984, American Physiological Society: Bethesda. p. 41-101.

3. Bicknell, R. and A. Harris, Novel growth regulatory factors and tumor angiogenesis. European Journal of Cancer. 27(6): 781-785 (1991).

4. Denekamp, J., Review article: Angiogenesis, neovascular proliferation and vascular pathophysiology as targets for cancer therapy. British Journal of Radiology. **66**(783): 181-196 (1993).

5. Paku, S. and N. Paweletz, First steps of tumor-related angiogenesis. Laboratory Investigation. **65**(3): 334-346 (1991).

6. Curry, F., Determinants of capillary permeability: A review of mechanisms based on single capillary studies in the frog. Circulation Research. **59**(4): 367-380 (1986).

7. Lum, H. and A. Malik, Regulation of vascular endothelial barrier function. American Journal of Physiology. **267**: L223-L241 (1994).

8. Roberts, W. and G. Palade, Increased microvascular permeability and endothelial fenestration induced by vascular endothelial growth factor. Journal of Cell Science. **108**: 2369-2379 (1995).

9. Majno, G. and G. Palade, Studies on inflammation 1. The effect of histamine and serotonin on vascular permeability: an electron microscopic study. Journal of Biophysics Biochemistry and Cytology. **11**: 571-605 (1961).

10. DeClerck, F., M. Brabender, H. Neels, and V.V.d. Velde, Direct evidence for the contractile capacity of endothelial cells. Thrombosis Research. **23**: 505-520 (1981).

11. Majno, G., S. Shea, and M. Levethal, Endothelial contraction induced by histamine-type mediators. Journal of Cell Biology. **42**: 647-672 (1969).

12. Boswell, C., G. Majno, I. Joris, and K. Ostrum, Acute endothelial cell contraction *in Vitro*: A comparison with vascular smooth muscle cells and fibroblasts. Microvascular Research. **43**: 178-191 (1992).

13. Palade, G. Fine structure of blood capillaries. in Electron Microscope Society of America. 1953. Pokonos, Pennsylvania: Journal of Applied Physics.

14. Predescu, D. and G. Palade, Plasmalemmal vesicles represent the large pore system of continuous microvascular endothelium. American Journal of Physiology. **265**: H725-H733 (1993).

15. Kohn, S., J. Nagy, H. Dvorak, and A. Dvorak, Pathways of macromolecular tracer transport across venules and small veins. Laboratory Investigation. **67**(5): 596-607 (1992).

16. Bundgaard, M., J. Frøkjaer-jensen, and C. Crone, Endothelial plasmalemmal vesicles as elements in a system of branching invaginations from the cell surface. Proceedings of the National Academy of Sciences. **76**(12): 6439-6442 (1979).

17. Bundgaard, M., The paracellular pathway in capillary endothelia, in Advances in Experimental Medicine and Biology, S. Chien, Editor. 1988, Plenum Press: New York. p. 3-8.

18. Palade, G. and R. Burns, Structural modulations of plasmalemmal vesicles. Journal of Cell Biology. **37**: 633-653 (1968).

19. Clough, G. and C. Michel, The role of vesicles in the transport of ferritin through frog endothelium. Journal of Physiology. **315**: 127-142 (1981).

20. Feng, D., J. Nagy, J. Hipp, H. Dvorak, and A. Dvorak, Vesiculo-vacuolar organelles and the regulation of venule permeability to macromolecules by vascular permeability factor, histamine, and serotonin. Journal of Experimental Medicine. **183**: 1981-1986 (1996).

21. Ballet, F., Hepatic circulation: Potential for therapeutic intervention. Pharmaceutical Therapeutics. **47**: 281-328 (1990).

22. Poste, G., C. Bucana, A. Raz, P. Bugelski, R. Kirsh, and I. Fidler, Analysis of the fate of systemically administered liposomes and implications for their use in drug delivery. Cancer Research. **42**: 1412-1422 (1982).

23. Roberts, W. and G. Palade, Neovasculature induced by vascular endothelial growth factor is fenestrated. Cancer Research. **57**: 765-772 (1997).

24. Ryan, U., The endothelial surface and responses to injury. Federation Proceedings. **45**: 101-108 (1986).

25. Ausprunk, D. and J. Folkman, Migration and proliferation of endothelial cells in preformed and newly formed blood vessels during tumor angiogenesis. Microvascular Research. **14**: 53-65 (1977).

26. Dvorak, H., J. Nagy, J. Dvorak, and A. Dvorak, Identification and characterization of the blood vessels of solid tumors that are leaky to circulating macromolecules. American Journal of Pathology. **133**(1): 95-109 (1988).

27. Heuser, L. and F. Miller, Differential macromolecular leakage from the vasculature of tumors. Cancer. **57**: 461-464 (1986).

28. Leunig, M., F. Yuan, M. Menger, Y. Boucher, A. Goetz, K. Messmer, and R. Jain, Angiogenesis, microvascular architecture, microhemodynamics, and interstitial fluid pressure during early growth of human adenocarcinoma LS174T in SCID mice. Cancer Research. **52**: 6553-6560 (1992).

29. Senger, D., S. Galli, A. Dvorak, C. Perruzza, V. Harvey, and H. Dvorak, Tumor cells secrete a vascular permeability factor that promotes accumulation of ascites fluid. Science. **219**: 983-985 (1983).

30. Andrade, S., Y. Bakhle, I. Hart, and P. Piper, Effects of tumour cells on angiogenesis and vasoconstrictor responses in sponge implants in mice. British Journal of Cancer. **66**(5): 821-6 (1992).

31. Fenselau, A., Tumor and related angiogenesis factors, in Growth and Maturation Factors, G. Guroff, Editor. 1984, John Wiley & Sons: New York. p. 88-129.

32. O'Reilly, M., L. Holmgren, Y. Shing, C. Chen, R. Rosenthal, M. Moses, W. Lane, Y. Cao, E. Sage, and J. Folkman, Angiostatin: A novel angiogenesis inhibitor that mediates the suppression of metastases by a Lewis lung carcinoma. Cell. **79**: 315-328 (1994).

33. Peverali, F., S. Mandriota, P. Ciana, R. Marelli, P. Quax, D. Rifkin, G.D. Valle, and P. Mignatti, Tumor cells secrete an angiogenic factor that stimulates basic fibroblast growth factor and urokinase expression in vascular endothelial cells. Journal of Cellular Physiology. **161**: 1-14 (1994).

34. Dvorak, H., L. Brown, M. Detmar, and A. Dvorak, Vascular permeability factor/Vascular endothelial growth factor, microvascular hyperpermeability, and angiogenesis. American Journal of Pathology. **146**(5): 1029-1039 (1995).

35. Q-Hong, J. Nagy, D. Senger, H. Dvorak, and A. Dvorak, Ultrastructural localization of vascular permeability factor/vascular endothelial growth factor (VPF/VEGF) to the abluminal plasma membrane and vesiculovacuolar organelles of tumor microvascular endothelium. Journal of Histochemistry and Cytochemistry. **43**(4): 381-389 (1995).

36. Senger, D., L. Brown, K. Claffey, and H. Dvorak, Vascular permeability factor, tumor angiogenesis and stroma generation. Invasion Metastasis. **14**: 385-394 (1994-95).

37. Starling, D., On the absorption of fluids from connective tissue spaces. Journal of Physiology. **19**: 312-326 (1896).

38. Landis, E., Micro-injection studies of capillary permeability. II. The relation between capillary pressure and the rate at which fluid passes through the walls of single capillaries. American Journal of Physiology. **82**: 217-238 (1927).

39. Kedem, O. and A. Katchalsky, Thermodynamic analysis of the permeability of biological membranes to non-electrolytes. Biochimica et Biophysica Acta. **27**: 229-246 (1958).

40. Curry, F., Mechanics and thermodynamics of transcapillary exchange, in Handbook of Physiology, E. Renkin and C. Michel, Editors. 1984, American Physiological Society: Bethesda. p. 309-374.

41. Rippe, B. and B. Haraldsson, Transport of macromolecules across microvascular walls: The two-pore theory. Physiological Reviews. **74**(1): 163-219 (1994).

42. Jain, R., Transport of molecules across tumor vasculature. Cancer and Metastasis Reviews. **6**: 559-593 (1987).

43. Michel, C., The Transport of Albumin: A critique of the vesicular system in transendothelial transport. American Review of Respiratory Disease. **146**: s32-s36 (1992).

44. Predescu, D., R. Horvat, S. Predescu, and G. Palade, Transcytosis in the continuous endothelium of the myocardial microvasculature is inhibited by N-ethylmaleimide. Proceedings of the National Academy of Sciences - USA. **91**: 3014-3018 (1994).

45. Palade, G. and A. Milici, Vascular Endothelium: role in albumin transport. Molecular mechanisms in cell growth and differentiation. **2**: 223-247 (1991).

46. Taylor, A. and D. Granger, Equivalent pore modeling: vesicles and channels. Federation Proceedings. **42**: 2440-2445 (1983).

47. Renkin, E., Capillary Transport of macromolecules:pores and other endothelial pathways. Journal of Applied Physiology. **58**(2): 315-325 (1985).

48. Deen, W., Hindered transport of large molecules in liquid-filled pores. AIChE Journal. **33**(9): 1409-1425 (1987).

Chapter 3.
CHARACTERISTIC PORE CUTOFF SIZE IN TUMOR MICROVESSELS

3.1 Motivation and Background

Molecular biology and genetic engineering have led to the discovery and development of numerous molecules which could aid in the detection and treatment of cancer. In parallel, encapsulated drug technology has the potential to reduce drug toxicity in normal tissues [1]. However, to achieve clinical success the antibodies, macromolecules, or particles must be delivered selectively and at therapeutic levels to the target tissue. The hyperpermeability of tumor microvessels to large molecules has been observed in numerous studies and it has been speculated that large therapeutic agents could be selectively delivered to the tumor [2]. However, the upper limit of the size of the therapeutic agent that can traverse vessels of different tumors and how this is regulated is not well understood.

The barriers to transport from the blood vessel to the tissue site include the endothelial cell layer, the basement membrane, the interstitial space, and the target cell (Figure 2-3). The normal microvasculature is composed of endothelial cells which act as molecular sieves allowing passage of water, ions, and small hydrophilic molecules, but acting as a barrier to passage of macromolecules. Endothelial impermeability maintains a protein concentration difference across the vessel wall and results in differential fluid distribution in the plasma and interstitial spaces. The prevalent model of transvascular transport consists of two cylindrical pore populations; a small pore (effective radius 6 nm) for the transport of water and small solutes up to the size of albumin and a large pore (effective radius 10 nm) for the passage of macromolecules [3]. Due to inconsistencies in both the model and experimental measurements, a thorough investigation into the potential structural pathways is needed.

Numerous structural studies have been conducted to elucidate the transvascular pathway in tumors (Table 3-1). The potential for artifacts as a result of various fixation techniques exists. It

has been proposed that the physical characteristics of the tracer (colloidal carbon, ferritin, monastral blue) may interact with the endothelium to induce gap formation [4]. Furthermore, these studies describe various processes that are present but do not provide information on the modes of macromolecular transport across the vessel wall.

In situ studies showing the diameters of tracer particles moving along a given pathway, rather than studies of fixed tissue, may provide more reliable information about transvascular transport in tumors [5]. Previous in vivo studies have demonstrated the extravasation of macromolecules such as FITC-Dextrans (up to 150 kDa) [6], colloidal carbon (50 nm diameter) [7], and liposomes of diameter 30 - 90 nm [8, 9]. In an in situ study using stealth liposomes, the LS174T human colon adenocarcinoma implanted into the mouse dorsal skinfold chamber exhibited a pore cutoff size between 400 and 600 nm [10].

The specific objective of the work presented in this chapter is to determine the characteristic pore cutoff size, a functional description of the size of transvascular gaps, in a variety of tumors. The in situ model chosen was the dorsal skinfold chamber implanted into SCID (Severe Combined Immuno-Deficient) mice (Appendix A). The pore cutoff size was determined using stealth liposomes or latex beads. Liposomes have been investigated as drug delivery devices due to the decreased tissue toxicity with antitumor/antifungal drugs, the ability to target antiparasitic drugs to the reticuloendothelial system (RES), and the enhancement of the immune response to encapsulated antigens [11] (Further details of liposome properties are given in Appendix B). Our hypothesis is that macromolecular transvascular transport in tumors is primarily due to widened interendothelial junctions and transendothelial gaps (similar to sinusoids) and not due to vesicles, transendothelial channels (or VVOs), fenestrae, or phagocytosis.

Table 3-1a. Structural Studies of Tumor Vessels: Tumor Type and Host

Study #	Host	Tumor	Control Tissue	Comments	Reference
1	rat	W256			[12]
2	rat	astrocytoma	brain		[13]
3	human	renal carcinoma	brain	1 case	[14]
4	human	brain tumors	brain		[15]
5	guinea pig	line 1 bile duct carcinoma	ND		[7]
6	guinea pig	line 2 bile duct carcinoma	ND		[7]
7	mice	Lewis Lung carcinoma	ND		[7]
8	mice	TA3/St	ND		[7]
9	mice	Mouse ovarian tumor	ND		[7]
10	human	glioblastoma multiforme (GM)	brain	more clustered vesicles, smaller clusters	[16]
11	mice	mammary carcinoma M1S			[17]
12	mice	rhabdomyosarcoma			[17]
13	mice	glioblastoma U87			[17]
14	human	astrocytoma	brain	attenuated or plump endothelial cells	[18]
15	human	GM	brain	thickened and multilayered BM	[18]
16	human	giant cell glioblastoma	brain	# vesicles varied	[18]
17	human	astrocytoma	brain	endothelial cell multilayers	[19]
18	human	GM	brain		[19]
19	rat	R175A	brain	microvilli, multilayers, and nuclear pleomorphism	[20]
20	human	astrocytoma	brain	hyperplastic cells, elongated and tortuous junctions	[21]
21	human	glioma	brain	attenuated cells, elongated and tortuous junctions	[21]
22	human	glioma	brain	elongated and tortuous junctions	[21]
23	human	giant cell granuloma	none	extraluminal PMNs	[22]
24	rat	C6 astrocytoma (13 days)	muscle brain	tumor vessels did not exhibit site differences	[23]
25	human	prolactinoma		endothelial blebs and swelling	[24]
26	rat	RD/2 Sarcoma			[25]

Table 3-1b. Structural Studies of Tumor Vessels

Study #	Fenestrae	Vesicles	Transendo-thelial Channels	Basement Membrane Abnormalities	Widened Interendo-thelial Junctions
1	++	ND	ND	ND	ND
2	++	++	ND	ND	+
3	++	ND	ND	ND	ND
4	++	++	ND	+	+
5	ND	ND	++	+	+
6	ND	ND	++	+	+
7	ND	ND	++	+	+
8	ND	ND	++	+	+
9	ND	ND	++	+	+
10	-	+	ND	ND	++
11	++	ND	++	++	++
12	++	ND	++	++	++
13	++	ND	++	++	++
14	ND	+	ND	++	+
15	ND	++	ND	++	+
16	ND	++	ND	++	+
17	++	++	ND	++	+
18	++	++	++	++	+
19	ND	++	ND	++	ND
20	-	++	ND	++	++
21	-	++	ND	++	++
22	-	+	+	+	+
23	ND	ND	ND	++	+
24	-	+	ND	ND	++
25	++	++	ND	++	ND
26	ND	ND	ND	ND	++

++ greater than normal, + similar to normal, - not present, ND not determined

3.2 Materials and Methods

Dorsal Chamber Implantation. The method used was previously described in Leunig et al [26]. Briefly, all experiments were performed in SCID mice, bred and maintained in a specific pathogen germ free environment in the Steele Laboratory. For the surgical implantation of the chamber, animals (25 - 30 g body weight) were anesthetized by intramuscular injection of 0.3 µl of anesthesia (9 parts saline: 1 part ketamine: 0.1 parts Xylazine). Prior to chamber implantation, the entire back of the animals was shaved and depilated and two symmetrical titanium frames (weight 3.2 g) which are mirror images of each other (Radiation Oncology, MGH) were implanted

so as to sandwich the extended double layer of skin. One layer of the skin was removed in a circular area of approximately 15 mm in diameter, and the remaining layer, consisting of epidermis, subcutaneous tissue, and striated skin muscle, was covered with a cover slip incorporated into one of the frames (Figure 3-1). All surgical procedures were performed under aseptic conditions. During surgery the body temperature of the animals was kept constant at 36 - 37 °C by means of a heating pad. Following implantation of the transparent access chamber, the animals were allowed to recover for 24 hours from the microsurgery and anesthesia. Preparations fulfilling the criteria of intact microcirculation were utilized as sites for tumor implantation.

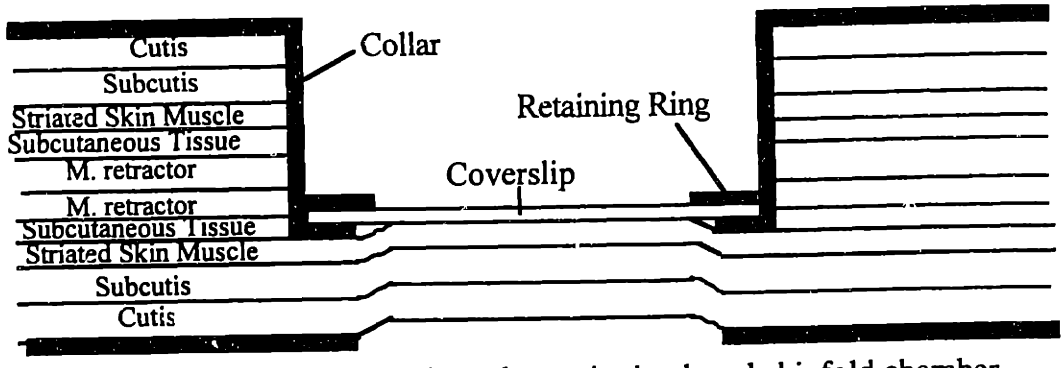

Figure 3-1. Cross-section through the tissue layers in the dorsal skinfold chamber

Tumor Implantation. The cell lines studied were LS174T (ATCC), MCa IV, HCa-1, Shionogi (kindly provided by M. E. Gleaze, Division of Urology, University of British Columbia, Vancouver, Canada), ST-8, and ST-12 (all ST-tumors were kindly provided by Dr. L. Gerweck and T. Syed, Radiation Oncology, Massachusetts General Hospital, Boston). MCa IV tumors were maintained by cell slurry injection into the thighs of C3H mice. HCa-1, Shionogi, ST-8, and ST-12 were maintained by transplanting a tumor chunk into the flank of SCID mice. LS174T was used as a dense cell suspension. Cultured cells were dispersed with Trypsin/EDTA and transferred into Dulbecco's Modified Eagles Medium (DMEM). They were centrifuged twice and resuspended in DMEM to give a final concentration of 10^8 cells. Two microliters of this dense suspension (containing ~2 x 10^5 cells) was inoculated onto the striated muscle layer of the subcutaneous tissue in the chambers. A piece of tumor tissue, 1 mm in diameter (0.5 µl), was placed onto the striated

muscle layer of the subcutaneous tissue in the chambers for all other tumor types. This size was selected on the basis that excessively small pieces delay the induction of vascularization and that larger pieces develop necrotic centers [27]. The experiments were performed between 14 and 20 days after tumor implantation, dependent on the growth and vascularization of the tumor. Tumor size was within 30 - 50% of chamber window size at the time of studies.

Liposome Preparation. Liposomes were prepared by Professor Vladimir P. Torchillin and Dr. Vladimir Trubetskoy at the Center for Imaging and Pharmaceutical Research, MGH. The liposomes were prepared according to Yuan et al [9]. Briefly, sterically protected liposomes were prepared by octyl glycoside dialysis method and labeled with Rhodamine-phosphatidylethanolamine (Rho-PE). The molar ratio of egg phosphatidylcholine:cholesterol: polyethylene glycol conjugated with distearoylphosphatidylethanolamine (PEG-DSPE):Rho-PE was 10:5:0.8:0.1. Liposomes obtained were sized by multiple passage through polycarbonate filters with pore diameters dependent on the target size. All liposome preparations had a narrow size distribution (95% of liposomes within a ±15-nm interval for 100 and 200 nm and within a ±25 nm interval for 400 and 600 nm liposomes). In addition, surface modified polystyrene latex beads (Sigma Chemical Co., St. Louis, MO)were used for the 600 nm and 800 nm sizes. Latex:PEG-DSPE:Rho-PE were mixed together in a 1:10:0.1 weight ratio.

Microscopy. Animals bearing the dorsal chamber were anesthetized as described above. A 200 µl suspension of liposomes or latex beads was injected into the tail vein of the mouse. The extent of particle extravasation was observed 24 hours after injection. For observation, the animals were anesthetized as described above and immobilized in a polycarbonate tube. The animal was mounted on the microscope stage (Axioplan, Zeiss) and observed using a 20x objective (LD Achroplan, Zeiss). Transillumination was achieved with a 100 W halogen lamp (Zeiss). Epiillumination was achieved with a 100 W mercury lamp (model 770; Opti-Quip, Inc., Highland Mills, NY) with fluorescence filters for FITC (excitation, 450-490 nm; emission 515-545 nm) or

Rhodamine (excitation, 525-550 nm; emission 580-635 nm). Images of the tumors were acquired with a 35 mm camera (HFX-DX; Nikon, Melville, NY).

Particle extravasation. The entire area of the tumor was scanned for extravasation of stealth liposomes or latex beads. The criteria for extravasation was the presence of fluorescence in the interstitial space in 5 or more regions of the tumor 24 hours after injection. Normal tissue surrounding the tumor implant was also examined for extravasation. Four animals bearing the tumor of interest were injected with each size of liposome/latex bead. The pore cutoff size was determined as the range between the largest particle size that could extravasate and the smallest size that could not extravasate, as described previously [10].

3.3 Results and Discussion

Many tumor types were investigated for their capacity to grow in the dorsal chamber. Not all tumors are capable of growing in this site even though they may grow subcutaneously. In most cases, there was a palpable mass within 3 weeks of transplanting a tumor chunk into the flank of SCID mice. The criteria for growth in the dorsal chamber were vascularization and increase in tumor mass of the transplanted tumor piece within a 14 to 20 day period. Examples of tumor growth are illustrated in Appendix C (Figures C-1, C-2, C-3). Twenty-one tumors were investigated; of these 8 were found to grow in the dorsal chamber preparation (Table 3-2). The results reveal that tumors of neuroectodermal glial cell origin do not grow in the dorsal chamber even though they could be passaged subcutaneously.

The tumors investigated for pore cutoff size contained one human tumor and six murine tumors. LS174T is the Trypsin variant of LS-180 which was isolated from a 58-year old woman with Dukes' type B colon adenocarcinoma [28]. The other tumors are spontaneously derived murine tumors. HCa-1 is a spontaneously developed hepatic carcinoma syngeneic to C3Hf/Kam mice. MCa IV is a spontaneously developed mammary carcinoma syngeneic to C3Hf/Kam mice.

Shionogi was a spontaneously developed mammary carcinoma initially androgen independent, but when sequentially passaged in male and female mice it transformed into an androgen-dependent tumor with similarities to other androgen target tissues [29]. The gross morphology of the vasculature varied and was characteristic for a given tumor (Figure C-4).

Table 3-2. Tumor Growth in the Dorsal Chamber

Tumor Type	N	Growth	Used for
MCa IV(mouse mammary carcinoma)	---	14 days	dorsal chamber cranial window
Shionogi (murine androgen dependent mammary carcinoma)	---	14 days	dorsal chamber
HCa I (murine hepatocarcinoma)	3	14 days	dorsal chamber
LS174T (human colon adenocarcinoma)	---	14 days	dorsal chamber cranial window
ST-Melanoma	2	16 days	dorsal chamber
ST-4 (anaplastic, murine origin)	3	24 days	dorsal chamber
ST-8 (anaplastic, murine origin)	2	14 days	dorsal chamber cranial window
ST-12 (anaplastic, murine origin)	3	14 days	dorsal chamber
Sa I (mouse sarcoma)	3	no growth	
Sa II (mouse sarcoma)	3	no growth	
ST-1 (anaplastic, murine origin)	3	no growth	
ST-2 (anaplastic, murine origin)	3	no growth	
ST-10 (anaplastic, murine origin)	3	no growth	
54A (human lung carcinoma)	4	no growth	
OCa I (murine ovarian carcinoma)	2	no growth	
OCa II (murine ovarian carcinoma)	2	no growth	
ZR75 (human estrogen dependent adenocarcinoma)	6	no growth	
PC-3 (human prostatic cancer)	4	no growth	
FSa II (murine fibrosarcoma)	6	overgrowth	
HGL21 (human glioblastoma)	4	no growth	cranial window
U87 (human glioblastoma)	4	no growth	cranial window

Tumors were investigated for their exclusion size using different sized liposomes. The criterion for extravasation was the presence of fluorescence in the interstitial space in 5 or more regions of the tumor 24 hours after injection as discussed in the Methods. Four animals bearing the tumor of interest were injected with each size of liposome/latex bead. It was previously shown that extravasation of latex beads is similar to liposomes of the same size even though they are more rigid [10]

Figure C-5 is a representative series of images captured for the MCaIV tumor showing decreased extravasation with increased particle size. There was no extravasation in normal tissue for any tumor at any liposome size. The majority of tumors exhibit a pore cutoff size between 400 and 780 nm (Figure 3-2). However, MCa IV had a pore cutoff size of between 1.2 and 2 μm.

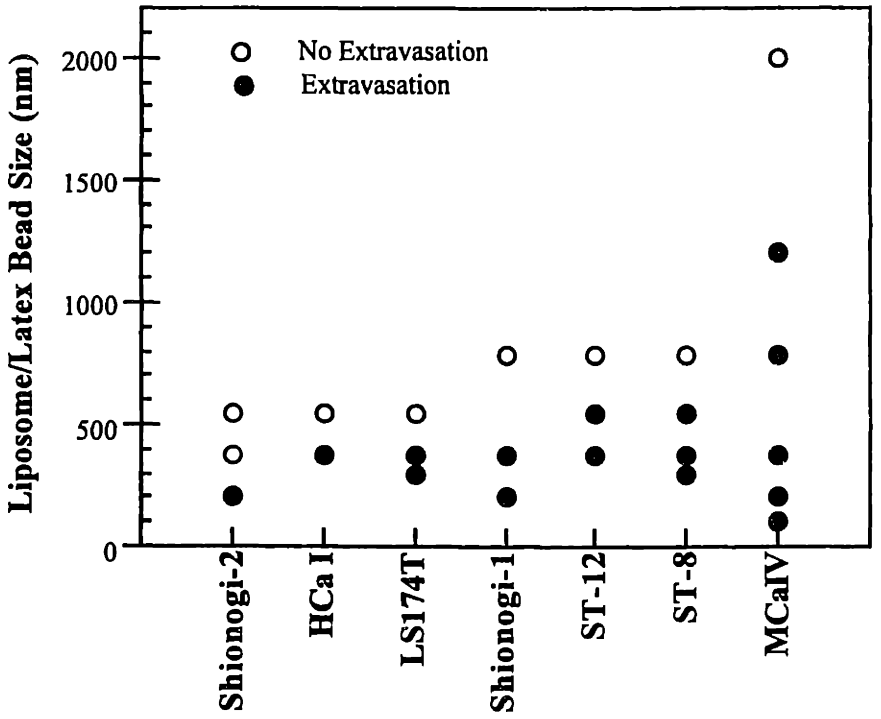

Figure 3-2. Tumor pore cutoff sizes. The filled circles indicate that significant extravasation was seen at those liposome/latex bead size. The open circles indicate no extravasation at those liposome/latex bead size. Four animals were used for each data point. At least five locations in each tumor were observed for fluorescence.

In 1986 Heuser et al found differential macromolecular leakage of FITC-rat serum albumin (~7 nm diameter) in Walker 256 carcinoma and a rat chondrosarcoma [30]. We did not specifically study the differential extravasation of the liposomes, but qualitatively noted that certain areas within the tumor exhibited greater fluorescence than others. All vessels were perfused, and there was no necrosis at sites of high fluorescence or low fluorescence.

All tumors exhibited extravasation of liposomes greater than 200 nm. This result provides no insight into the physical nature of the structure. It is generally accepted that the vesicle diameter

is between 50-70 nm [5, 31-36]. The size at which extravasation is seen is on the order of 10 times larger than the reported vesicle diameter. Transendothelial channel diameters are on the same order of magnitude as vesicles, with VVOs being slightly larger at ~100 nm [4, 31, 32, 37, 38]. This is still 5 times smaller than the pore cutoff size for the majority of tumors studied. Observed diameters of fenestrae are approximately 60 nm [17, 39].

As is seen for MCaIV (Figure C-5), the extravasation pattern for small diameter liposomes is very diffuse. As the particle size increases, the extravasation pattern becomes more focal until there is no extravasation of latex beads. Confluent monolayers of wounded endothelial cells showed enhanced uptake of 5 μm polystyrene beads [40]. This is proposed to be the result of increased proliferation and migration of endothelial cells at the wound edge. If phagocytosis were the primary pathway we would expect to see extravasation independent of the particle size, a diffuse pattern indicating random phagocytosis by endothelial cells, and more extravasation at the outer periphery of the tumor where potentially more endothelial cells are proliferating and migrating. We do not observe any of these patterns in the seven tumors studied.

The interendothelial junction may become larger in response to released cytokines. The gaps can be up to 1 μm wide [41]. Widened interendothelial junctions have been found in tumor endothelium [17, 39, 42-44]. Our results indicate that the macromolecular pathway is not via vesicles, transendothelial channels (VVOs), fenestrae or phagocytosis in the tumors studied. The pore cutoff size in this study can only be due to the widened interendothelial junctions or transendothelial open gaps due to the size and pattern of extravasation observed.

3.4. Conclusion

The hyperpermeable nature of tumor microcirculation is well-documented [7, 26, 45]. This study demonstrated that tumors pore cutoff sizes are tumor dependent, and that the majority of tumors exhibited a pore cutoff size between 380 and 780 nm. The primary mechanism for particle

transvascular transport based on the observed pore cutoff size in this functional assay is via widened interendothelial junctions or transendothelial open junctions.

This work provides a fundamental basis for the subsequent studies on the modulation of the pore cutoff size. The structural morphology of tumor microvessels can be modulated by a wide variety of cytokines, angiogenic growth factors, and enzymes. Any change in the host local microenvionrment or the tumor milieu may affect the permeability or the characteristic pore cutoff size of the tumor.

3.5. References

1. Machy, P. and L. Leserman, Liposomes in Cell Biology and Pharmacology. 1987, London: John Libbey and Company Ltd.

2. Jain, R., Delivery of molecular medicine to solid tumors. Science. **271**: 1079-1080 (1996).

3. Curry, F., Determinants of capillary permeability: A review of mechanisms based on single capillary studies in the frog. Circulation Research. **59**(4): 367-380 (1986).

4. Feng, D., J. Nagy, J. Hipp, H. Dvorak, and A. Dvorak, Vesiculo-vacuolar organelles and the regulation of venule permeability to macromolecules by vascular permeability factor, histamine, and serotonin. Journal of Experimental Medicine. **183**: 1981-1986 (1996).

5. Palade, G. and A. Milici, Vascular Endothelium: role in albumin transport. Molecular mechanisms in cell growth and differentiation. **2**: 223-247 (1991).

6. Gerlowski, L. and R. Jain, Microvascular permeability of normal and neoplastic tissues. Microvascular Research. **31**: 288 - 305 (1986).

7. Dvorak, H., J. Nagy, J. Dvorak, and A. Dvorak, Identification and characterization of the blood vessels of solid tumors that are leaky to circulating macromolecules. American Journal of Pathology. **133**(1): 95-109 (1988).

8. Poste, G., C. Bucana, A. Raz, P. Bugelski, R. Kirsh, and I. Fidler, Analysis of the fate of systemically administered liposomes and implications for their use in drug delivery. Cancer Research. **42**: 1412-1422 (1982).

9. Yuan, F., M. Leunig, S. Huang, D. Berk, D. Papahadjoupolos, and R. Jain, Microvascular permeability and interstitial penetration of sterically stabilized (Stealth) liposomes in a human tumor xenograft. Cancer Research. **54**: 3352-3356 (1994).

10. Yuan, F., M. Dellian, D. Fukumura, M. Leunig, D. Berk, V. Torchillin, and R. Jain, Vascular permeability in a human tumor xenograft: Molecular size dependence and cutoff size. Cancer Research. **55**: 3752-3756 (1995).

11. Papahadjopoulos, D., T. Allen, A. Gabizon, E. Mayhew, K. Matthay, S. Huang, K. Lee, M. Woodle, D. Lasic, C. Redemann, and F. Martin, Sterically stabilized liposomes: Improvements in pharmacokinetics and antitumor therapeutic efficacy. Proceedings of the National Academy of Sciences-USA. **88**: 11460-11464 (1991).

12. Warren, B., The ultrastructure of the microcirculation of the advancing edge of Walker 256 carcinoma. Microvascular Research. **2**: 443-453 (1970).

13. Deane, B. and P. Lantos, The vasculature of experimental brain tumors. Journal of the Neurological Sciences. **49**: 67-77 (1981).

14. Hirano, A. and H. Zimmerman, Fenestrated blood vessels in a metastatic renal carcinoma in the brain. Laboratory Investigation. **26**(4): 465-468 (1972).

15. Hirano, A. and T. Matsui, Vascular structures in brain tumors. Human Pathology. **6**: 611-621 (1975).

16. Coomber, B., P. Stewart, K. Hayakawa, C. Farrell, and R.D. Maestro, Quantitative morphology of human glioblastoma multiforme microvessels: structural basis of blood-brain barrier defect. Journal of Neuro-Oncology. **5**: 299-307 (1987).

17. Roberts, W. and G. Palade, Neovasculature induced by vascular endothelial growth factor is fenestrated. Cancer Research. **57**: 765-772 (1997).

18. Kohn, S., D. Front, and I. Nir, Blood-brain barrier permeability of human gliomas as determined by quantitation of cytoplasmic vesicles of the capillary endothelium and scintographic findings. Cancer Investigation. **7**(4): 313-321 (1989).

19. Roy, S. and C. Sarkar, Ultrastructural study of micro-blood vessels in human brain tumors and peritumoral tissue. Journal of Neuro-Oncology. **7**: 283-294 (1989).

20. Silbergeld, D. and F. Ali-Osman, Isolation and characterization of microvessels from normal brain and brain tumors. Journal of Neuro-Oncology. **11**: 49-55 (1991).

21. Dinda, A., C. Sarkar, S. Roy, K. Kharbanda, M. Mathur, A. Khosla, and A. Banerji, A transmission and scanning electron microscopic study of tumoral and peritumoral microblood vessels in human gliomas. Journal of Neuro-Oncology. **16**: 149-158 (1993).

22. Lim, L. and J. Gibbins, Immunohistochemical and ultrastructural evidence of a modified in the giant cell granuloma of the jaws. Oral and Maxillofacial Pathology. **79**(2): 190-198 (1995).

23. Coomber, B., P. Stewert, E. Hayakawa, C. Farrell, and R.D. Maestro, A quantitative assessment of microvessel ultrastructure in C6 astrocytoma spheroids transplanted to brain and to muscle. Journal of Neuropathology and Experimental Neurology. **47**(1): 29-40 (1988).

24. Erroi, A., M. Bassetti, A. Spada, and G. Giannattasio, Microvasculature of human micro- and macroprolactinomas. Neuroendocrinology. **43**: 159-165 (1986).

25. Underwood, J. and I. Carr, The ultrastructure and permeability characteristics of the blood vessels of a transplantable rat sarcoma. Journal of Pathology. **107**: 157-166 (1972).

26. Leunig, M., F. Yuan, M. Menger, Y. Boucher, A. Goetz, K. Messmer, and R. Jain, Angiogenesis, microvascular architecture, microhemodynamics, and interstitial fluid pressure

during early growth of human adenocarcinoma LS174T in SCID mice. Cancer Research. **52**: 6553-6560 (1992).

27. Goodall, C., A. Sanders, and P. Shubik, Studies of vascular patterns in living tumors with a transparent chamber inserted in hamster cheek pouch. Journal of the National Cancer Institute. **35**: 497-521 (1965).

28. Tom, B., L. Rutzky, R. Oyasu, J. Tomita, D. Goldenberg, and B. Kahan, Human colon adenocarcinoma cells II. Tumorigenic and organoid expression in vitro. Journal of the National Cancer Institute. **58**(5): 1507-12 (1976).

29. Minesita, T. and K. Yamaguchi, An androgen-dependent tumor derived from a hormone-independent spontaneous tumor of a female mouse. Steroids. **4**: 815-830 (1964).

30. Heuser, L. and F. Miller, Differential macromolecular leakage from the vasculature of tumors. Cancer. **57**: 461-464 (1986).

31. Bundgaard, M., J. Frøkjaer-jensen, and C. Crone, Endothelial plasmalemmal vesicles as elements in a system of branching invaginations from the cell surface. Proceedings of the National Academy of Sciences. **76**(12): 6439-6442 (1979).

32. Clough, G. and C. Michel, The role of vesicles in the transport of ferritin through frog endothelium. Journal of Physiology. **315**: 127-142 (1981).

33. Michel, C., The Transport of Albumin: A critique of the vesicular system in transendothelial transport. American Review of Respiratory Disease. **146**: s32-s36 (1992).

34. Predescu, D. and G. Palade, Plasmalemmal vesicles represent the large pore system of continuous microvascular endothelium. American Journal of Physiology. **265**: H725-H733 (1993).

35. Predescu, D., R. Horvat, S. Predescu, and G. Palade, Transcytosis in the continuous endothelium of the myocardial microvasculature is inhibited by N-ethylmaleimide. Proceedings of the National Academy of Sciences - USA. **91**: 3014-3018 (1994).

36. Saucan, L. and G. Palade, Membrane and secretory proteins are transported from the golgi complex to the sinusoidal plasmalemma of hepatocytes by distinct vesicular carriers. Journal of Cell Biology. **125**(4): 733-741 (1994).

37. Kohn, S., J. Nagy, H. Dvorak, and A. Dvorak, Pathways of macromolecular tracer transport across venules and small veins. Laboratory Investigation. **67**(5): 596-607 (1992).

38. Q-Hong, J. Nagy, D. Senger, H. Dvorak, and A. Dvorak, Ultrastructural localization of vascular permeability factor/vascular endothelial growth factor (VPF/VEGF) to the abluminal plasma membrane and vesiculovacuolar organelles of tumor microvascular endothelium. Journal of Histochemistry and Cytochemistry. **43**(4): 381-389 (1995).

39. Roberts, W. and G. Palade, Increased microvascular permeability and endothelial fenestration induced by vascular endothelial growth factor. Journal of Cell Science. **108**: 2369-2379 (1995).

40. Ryan, U., The endothelial surface and responses to injury. Federation Proceedings. **45**: 101-108 (1986).

41. Majno, G. and G. Palade, Studies on inflammation 1. The effect of histamine and serotonin on vascular permeability: an electron microscopic study. Journal of Biophysics Biochemistry and Cytology. **11**: 571-605 (1961).

42. Dejana, E., M. Corada, and M. Lampugnani, Endothelial cell-to-cell junctions. FASEB Journal. **9**: 910-918 (1995).

43. Neal, C. and C. Michel, Transcellular Gaps in microvascular walls of frog and rat when permeability is increased by perfusion with the ionophore A23187. Journal of Physiology. **488**(2): 427-437 (1995).

44. Tanaka, Y., Y. Toki, T. Sakane, T. Nadai, H. Sezaki, and S. Yamashita, Characterization of drug transport through tight-junctional pathway in Caco-2 monolayer: Comparison with isolated rat jejunum and colon. Pharmaceutical Research. **12**(4): 523-528 (1995).

45. Yuan, F., M. Leunig, D. Berk, and R. Jain, Microvascular permeability of albumin, vascular surface area, and vascular volume measured in human adenocarcinoma LS174T using dorsal chamber in SCID mice. Microvascular Research. **45**: 269-289 (1993).

Chapter 4.
PORE CUTOFF SIZE CORRELATION WITH MICROVESSEL PERMEABILITY TO BOVINE SERUM ALBUMIN

4.1 Motivation and Background

Permeability depends on the physicochemical properties of the molecule being studied as well as the physiological and physicochemical properties of the barrier under study. For example, properties which influence the uptake of nanoparticles or macromolecules include tumor vascular volume, vascular permeability, and blood flow rate. Tumor microvessels are less permselective than normal tissue vessels [1-7]; known exceptions to this include certain brain tumors [4]. Vascular permeability may depend on the following: 1) tumor type [4, 8], 2) tumor size [9] or growth rate of the tumor, 3) vessel location within the tumor, 4) tumor's mechanism for maintaining its vascular wall structure, and 5) release and circulation of various cytokines, growth factors, and other controls of tumor microenvironment.

Previous measurement in LS174T implanted in the dorsal chamber of permeability to 90 nm liposomes indicated that it was 16% of that of Rho-BSA [5]. In a later study it was shown that the effective vascular permeability does not depend on molecular weight of the test molecule [6] which is in contrast to what is found in normal microvessels. Previous results (Chapter 3) indicate that the maximal sized particle that a vessel will allow to extravasate varies across a series of tumor types, evidence that each tumor has a characteristic pore cutoff size.

In this study, permeability measurements were performed on tumors with a range of pore cutoff sizes implanted into SCID mice. We measured the average effective vascular permeability to bovine serum albumin (BSA) using quantitative fluorescent microscopy. The objective of this study was to investigate whether the pore cutoff size influences transport of a test molecule. We hypothesize that there will be no difference in the permeability across tumor microvessels because the radius of albumin is much less than the radius of the pores.

4.2 Materials and Methods

Dorsal Chamber Implantation. The method used is described in Chapter 3.

Tumor Implantation. The cell lines studied were MCaIV, HCa-1, and ST-8. Tumor implantation is described in Chapter 3.

Liposome Preparation. Liposomes were prepared as described in Chapter 3.

Microscopy. The experimental procedure was previously described [3]. Briefly, animals bearing the dorsal chamber were anesthetized by intramuscular injection of 0.3 μl of anesthesia (9 parts saline: 1 part ketamine: 0.1 parts Xylazine). The tail vein of the animal was cannulated with a 30G needle catheter connected to a syringe containing 0.15 ml of Tetramethylrhodamine-labeled bovine serum albumin (Rho-BSA; Molecular Probes, Eugene OR). Rho-BSA was prepared as in Fukumura [10]. The animal was mounted on the microscope stage (Axioplan, Zeiss) and observed using a 20x objective (LD Achroplan, Zeiss) and an intravital fluorescence microscope (Axioplan, Zeiss, Oberkochen, Germany) equipped with a fluorescence filter for Rhodamine (excitation, 525-550 nm; emission 580-635 nm), an intensified CCD video camera (C2400-88, Hamamatsu Photonics K.K., Hamamatsu, Japan), a photomultiplier (9203B; EMI, Rockaway, NJ), and a S-VHS videocassette recorder (SVO-9500MD, Sony).

In each animal, an image of the vasculature was recorded on video tape for off-line analysis of vessel diameter and length, and the background intensity was measured under epifluorescence illumination (100 W mercury lamp, model 770; Opti-Quip, Inc., Highland Mills, NY). A bolus injection of Rho-BSA was given via the tail vein (0.15 ml over 20 seconds). The fluorescence intensity was measured intermittently for 20 minutes, the time interval for each observation was 10 seconds. This was to avoid any photochemical toxicity to the endothelial cells by the Rho-BSA [3].

Microvascular Permeability Estimation. The complete derivation is provided in Yuan et al [3] and in Appendix D. The equation to estimate the effective microvascular permeability (P) is:

$$P = (1 - H_{Tm})\frac{V_{ves}}{S}\left(\frac{1}{I_0 - I_b}\frac{dI}{dt} + \frac{1}{K}\right) \tag{4-1}$$

where I is the average fluorescence intensity of the entire image, I_0 is the fluorescence intensity immediately after the filling of all vessels with the fluorescent tracer, I_b is the background tissue fluorescence intensity. H_{Tm} is the average hematocrit of microvessels and was assumed to be 19% [11]. The time constant of plasma clearance, K, was 9.1×10^3 seconds [5]. V_{ves} and S are the total volume and surface area of vessels within the volume of measurement respectively. The ratio is determined by:

$$\frac{S}{V_{ves}} = \sum_{n=1}^{M} 4d_n L_n \Big/ \sum_{n=1}^{M} d_n^2 L_n \tag{4-2}$$

where d_n and L_n are the diameter and length of the n^{th} vessel, and M is the total number of vessels on the tumor surface within the image before injection of Rho-BSA.

4.3 Results and Discussion

The transvascular transport of macromolecules is a combination of diffusive and convective forces which can be described by the Patlek equation [1]:

$$J_s = J_v(1 - \sigma_s)\left[\frac{C_p - C_{\text{int}}e^{-Pe}}{1 - e^{-Pe}}\right] \tag{4-3}$$

$$J_v = L_p S\left[\left(P_p - P_{\text{int}}\right) - \sigma\left(\pi_p - \pi_{\text{int}}\right)\right] \tag{4-4}$$

$$Pe = \frac{J_v(1-\sigma_s)}{PS} \qquad (4\text{-}5)$$

Where J_S is the solute flux (moles/s), J_V is the fluid volume flux (cm^3/s), σ_S is the solute reflection coefficient, c_p, c_{int} are the plasma concentration and interstitial concentration of solute respectively. The expression in brackets is a ratio of convective to diffusional transport. The fluid flux (equation 4-4) is described by a balance of hydrostatic (P) difference between the capillary (P_p) and interstitial space(P_{int}) and colloid osmotic (π) difference between the plasma osmotic pressure (π_p) and the interstitial osmotic pressure (π_{int}) modified by the hydraulic conductivity, L_p ($cm^3/s/dyne$), and capillary surface area, S (cm^2). The reflection coefficient, σ, ranges from permeability equal to water ($\sigma = 0$) to complete impermeability ($\sigma = 1$). The Peclet number (Pe) is ratio of convective transport of the solute and diffusive transport of the solute.

When diffusive transport dominates the Pe number becomes small and the solute flux reduces to

$$J_s = PS(C_p - C_{int}) \qquad (4\text{-}6)$$

Convection may be the dominant transvascular transport mechanism in normal microvessels, but within tumors, diffusion remains dominant transport mechanism [12-14]. This is due to the high interstitial fluid pressures [13] and the low oncotic pressures [15]. In addition, convection is expected to contribute minimally to the transport in these experiments because the tumor is sandwiched between the host striated skin muscle layer and the coverslip [6]. Therefore, the effective microvascular permeability (P) measured depends primarily on diffusive transport but also incorporates the insignificant component of convection.

The effective microvascular permeability (P) to Rho-BSA was measured in 3 tumor cell lines transplanted in SCID mice, HCa-I, MCa IV, and ST-8. The tumors selected for this study spanned the entire range of pore cutoff sizes (Figure 3-2). HCa-I was specifically chosen because

its pore cutoff size was identical to LS174T (pore cutoff size is between 400 and 600 nm). The permeability of LS174T was determined in a previous study [5]. All tumors showed hyperpermeability to Rho-BSA (Table 4-1). The permeabilities were not statistically different from each other (ANOVA). This implies that Rho-BSA transport through microvessel walls is independent of the pore cutoff size.

Table 4-1. Mean Effective Microvascular Permeability to BSA

Tumor Cell Line (N)[a]	Pore Cutoff Size (nm)	Permeability (x 10^7 cm/s)
HCa-I (5)	400 - 550	2.069 ± 1.44 (1.60 - 3.99)[b]
LS174T (6)[c]	400 - 600	1.24 ± 0.45 (0.56 - 1.67)
ST-8 (5)	550 - 780	3.73 ± 3.34 (1.67 - 9.28)
MCaIV (8)[d]	1200 - 2000	2.5 ± 1.5 (1.2 - 5.1)

[a] N, the number of animals
[b] Mean ±SD (range)
[c] [5]
[d] [10]

The effective microvascular permeability minimizes intratumor vascular heterogeneity. There was significant heterogeneity among individual microvessels within the tissue volume. For example, a permeable vessel could be next to an impermeable vessel. In addition to site heterogeneity, there is also temporal heterogeneity in the permeability of a microvessel. Single vessel perfusion measurement of permeability is more direct and accurate. This technique was utilized on LS174T tumors implanted into dorsal chambers of SCID mice [12]. This study reported that the convective transport contribution to vascular permeability is unlikely to be a dominant mode of transport.

Normal tissue microvessel permeability was not measured because 1) the permeability of normal tissues is at the limit of resolution of the effective microvascular permeability technique, and 2) the permeability would be a sum of the various tissues in the chamber (dermis, epidermis, subcutaneous, and striated muscle tissues) with different vascular patterns and thus would not be a meaningful parameter.

The primary factor governing transcapillary transport is the molecular size of the solvent filled channel. Additional factors important to transcapillary transport are the molecular shape, flexibility, and charge of the molecule and the pore. The partitioning coefficient of the macromolecule into the pore depends on the ratio of the particle radius to pore radius. For a spherical particle in a cylindrical pore, the partitioning is described by [16]:

$$\phi = \left(1 - \frac{r_s}{r_p}\right)^2 \tag{4-7}$$

where Φ is the partitioning coefficient, r_s and r_p are the solute radius and pore radius respectively. BSA is assumed to have the hydrodynamic characteristics of a solid particle. We assume a radius of 3.5 nm for albumin [6]. The r_s/r_p for the four tumors above ranged from 0.0035 - 0.035. The following equation was used to estimate the diffusional hindrance factor, K_d for BSA [17]:

$$K_d = 1 - 2.1044\lambda + 2.089\lambda^3 - 0.948\lambda^5 \tag{4-8}$$

where

$$\lambda = \frac{r_{solute}}{r_{pore}} \tag{4-9}$$

Utilizing $\lambda = 0.035$, pore theory predicts that the effectivie diffusivity is 86% of the value in free solution. Thus, there was no significant hindrance to diffusion of BSA through the pores.

Serum albumin plays an important role in maintaining the oncotic pressure difference between the vascular and interstitial compartments. Serum albumin may enhance or inhibit transcapillary exchange. Albumin binds to the endothelial surface and reduces the transvascular flux of water, solutes, and macromolecules and it acts as a carrier protein for transport of many small ligands [18]. The mechanism of its transport through the vessel wall remains controversial.

Inflammation increases microvascular permeability. Most chemical mediators of inflammation cause increased vascular permeability by widening the intercellular junctions [19-21]. Thus, the primary pathway for macromolecules was thought to be through the interendothelial junctions. However, recent work suggests that vesicles play a crucial role in albumin transport [22, 23]. Recently, the protein responsible, albondin, was isolated [18]. This protein is thought to be responsible for about 50% of the transvascular transport of albumin [18]. We know of no studies elucidating the presence of albondin in tumor endothelium, but this could play a role in the tumor setting.

VEGF is secreted by a wide variety of cultured, transplanted, and primary human tumors [24-26]. VEGF is thought to aid the angiogenic process by inducing endothelial proliferation [27-30]. The same molecule is also known as VPF (vascular permeability factor) [28, 30]. On a molar basis it increases the vascular permeability 50,000 times that of histamine [28, 30, 31]. This transient hyperpermeability is not blocked by antihistamines or other inhibitors of inflammatory mediators [24].

Tumors secrete VEGF [24, 32] which has been shown to increase the number of transendothelial channels (or VVOs) [33], induce fenestrations and widen interendothelial junctions [34, 35]. Treatment of established tumors with anti-VEGF antibody lowers their vascular permeability [36], implicating the important influence of VEGF on tumor microvascular permeability.

Previous studies indicate that acute treatment with bFGF does not modify vascular permeability, whereas topical treatment with VEGF does transiently increase vascular permeability within 10 minutes [34]. Elvex pellets containing more than 50 ng of VEGF led to angiogenesis and these vessels had open junctions and fenestrations (~60 nm) when implanted subcutaneously [35]. Even VEGF pellets which did not induce vessel growth produced fenestrae and open interendothelial junctions in adjacent tissue and increased permeability as suggested by the leakage of carbon black. Elvax pellets containing 0.5-2 μg bFGF pellets also stimulated fenestrae and open interendothelial junctions. In contrast, VEGF and bFGF collagen gels (containing 60 μg

growth factor) implanted in the cranial window and dorsal chamber did not show increased permeability to albumin over matched controls [37].

Naturally-occurring fenestrated endothelium does not demonstrate increased albumin permeability over continuous endothelium [38]. However, the glycocalyx or the basement membrane structure may contribute to the permselectivity of the fenestrated endothelium [38]. It is well known that the basement membrane is either absent or discontinuous in tumors (Chapter 2). Whether VEGF modifies the glycocalyx is unknown.

In the present study, we found that the pore cutoff size of MCaIV is much larger than that of U87 in the cranial window (to be discussed in Chapter 6). The permeability to BSA of U87 (3.8×10^{-7} cm/s) is roughly 3 times that of MCaIV (1.9×10^{-7} cm/s) in the cranial window [4]. This discrepancy could be explained by the presence of receptor-mediated transport of albumin in U87.

4.4 Conclusions

In conclusion, we found no correlation of the tumor microvessel pore cutoff size using permeability to Rho-BSA as a probe. The transport of Rho-BSA is not hindered because $r_s/r_p \ll 1$ in the tumors studied. This result does not exclude the possibility that albumin is transported by other methods, such as vesicles and receptor-mediated transport.

4.5 References

1. Jain, R., Transport of molecules across tumor vasculature. Cancer and Metastasis Reviews. **6**: 559-593 (1987).

2. Gerlowski, L. and R. Jain, Microvascular permeability of normal and neoplastic tissues. Microvascular Research. **31**: 288 - 305 (1986).

3. Yuan, F., M. Leunig, D. Berk, and R. Jain, Microvascular permeability of albumin, vascular surface area, and vascular volume measured in human adenocarcinoma LS174T using dorsal chamber in SCID mice. Microvascular Research. **45**: 269-289 (1993).

4. Yuan, F., H. Salehi, Y. Boucher, U. Vasthare, R. Tuma, and R. Jain, Vascular permeability and microcirculation of gliomas and mammary carcinomas transplanted in rat and mouse cranial windows. Cancer Research. **54**: 4564-4568 (1994).

5. Yuan, F., M. Leunig, S. Huang, D. Berk, D. Papahadjoupolos, and R. Jain, Microvascular permeability and interstitial penetration of sterically stabilized (Stealth) liposomes in a human tumor xenograft. Cancer Research. **54**: 3352-3356 (1994).

6. Yuan, F., M. Dellian, D. Fukumura, M. Leunig, D. Berk, V. Torchillin, and R. Jain, Vascular permeability in a human tumor xenograft: Molecular size dependence and cutoff size. Cancer Research. **55**: 3752-3756 (1995).

7. Wu, N., B. Klitzman, G. Rosner, D. Needham, and M. Dewhirst, Measurement of Material Extravasation in Microvascular Networks Using Fluorsescence Video-Microscopy. Microvascular Research. **46**: 231-253 (1993).

8. Sands, H., P. Jones, S. Shah, D. Palme, R. Vessella, and B. Gallagher, Correlation of vascular permeability and blood flow with monoclonal Antibody Uptake by Human Clouser and Renal Cell Xenografts. Cancer Research. **48**: 188 -193 (1988).

9. Blasburg, R., T. Kobayashi, C. Patlak, M. Shinohara, M. Miyoaka, J. Rice, and W. Shapiro, Regional blood flow, capillary permeability, and glucose utilization in two brain tumor models: Preliminary observations and pharmacokinetic implications. Cancer Treatment Reports. **65 (supplement 2)**: 3-12 (1981).

10. Fukumura, D., F. Yuan, M. Endo, and R. Jain, Role of nitric oxide in tumor microcirculation. American Journal of Pathology. **150**(2): 1-13 (1997).

11. Brizel, D., M. Klitzman, J. Cook, J. Edwards, G. Rosner, and M. Dewhirst, A comparison of tumor and normal tissue microvascular hematocrits and red cell fluxes in a rat window chamber model. International Journal Radiation Oncology Biology Physics. **25**: 269-276 (1993).

12. Lichtenbeld, H., F. Yuan, C. Michel, and R. Jain, Perfusion of single tumor microvessels: Application to vascular permeability measurement. Microcirculation. **3**(4): 349-357 (1996).

13. Boucher, Y., L. Baxter, and R. Jain, Interstitial pressure gradients in tissue-isolated and subcutaneous tumors: Implications for therapy. Cancer Research. **50**: 4478-4484 (1990).

14. Boucher, Y. and R. Jain, Microvascular pressure is the principal driving force for interstitial hypertension in solid tumors: Implications for vascular collapse. Cancer Research. **52**: 5110-5114 (1992).

15. Stohrer, M., Y. Boucher, M. Stangassinger, and R. Jain. Oncotic pressure in human tumor xenografts. in Proceedings of the 86th Annual Meeting of the American Association for Cancer Research. 1995. Toronto, Ontario:

16. Deen, W., Hindered transport of large molecules in liquid-filled pores. AIChE Journal. **33**(9): 1409-1425 (1987).

17. Anderson, J. and J. Quinn, Restricted transport in small pores. A model for steric exclusion and hindered particle motion. Biophysical Journal. **14**: 130 (1974).

18. Schnitzer, J. and P. Oh, Albondin-mediated capillary permeability to albumin. Journal of Biological Chemistry. **269**(8): 6072-6082 (1994).

19. Cotran, R., V. Kumar, and S. Robbins, Robbins' Pathologic Basis of Disease. 4 ed. 1989, Philadelphia: WB Saunders Company.

20. Majno, G. and G. Palade, Studies on inflammation 1. The effect of histamine and serotonin on vascular permeability: an electron microscopic study. Journal of Biophysics Biochemistry and Cytology. **11**: 571-605 (1961).

21. Majno, G., S. Shea, and M. Levethal, Endothelial contraction induced by histamine-type mediators. Journal of Cell Biology. **42**: 647-672 (1969).

22. Lum, H. and A. Malik, Regulation of vascular endothelial barrier function. American Journal of Physiology. **267**: L223-L241 (1994).

23. Schnitzer, J., W. Carley, and G. Palade, Albumin interacts specifically with a 60 kDa microvascular endothelial glycoprotein. Proceedings of the National Academy of Sciences. **85**: 6773-6777 (1988).

24. Senger, D., S. Galli, A. Dvorak, C. Perruzza, V. Harvey, and H. Dvorak, Tumor cells secrete a vascular permeability factor that promotes accumulation of ascites fluid. Science. **219**: 983-985 (1983).

25. Senger, D., D. Connolly, C. Perruzza, D. Alsup, R. Nelson, R. Leimgruber, J. Feder, and H. Dvorak, Purification of a vascular permeability factor (VPF) from tumor cell conditioned medium. Federation Proceedings. **46**: 2102 (1987).

26. Berse, B., L. Brown, L.V.D. Water, H. Dvorak, and D. Senger, Vascular permeability factor (vascular endothelial growth factor) gene is expressed differentially in normal tissues, macrophages, and tumors. Molecular Biology Cell. **3**: 211-220 (1992).

27. Leung, D., G. Cachianes, W. Kuang, D. Goeddel, and N. Ferrara, Vascular endothelial growth factor is a secreted angiogenic mitogen. Science. **246**: 1306 (1989).

28. Dvorak, H., L. Brown, M. Detmar, and A. Dvorak, Vascular permeability factor/Vascular endothelial growth factor, microvascular hyperpermeability, and angiogenesis. American Journal of Pathology. **146**(5): 1029-1039 (1995).

29. Gospodarowicz, D., J. Abraham, and J. Schilling, Isolation and characterization of a vascular endothelial cell mitogen produced by pituitary-derived folliculostellate cells. Proceedings of the National Academy of Science. **86**: 7311-7315 (1989).

30. Senger, D., L. Brown, K. Claffey, and H. Dvorak, Vascular permeability factor, tumor angiogenesis and stroma generation. Invasion Metastasis. **14**: 385-394 (1994-95).

31. Senger, D., D. Connolly, L.V.D. Water, J. Feder, and H. Dvorak, Purification and NH_2-terminal amino acid sequence of guinea pig tumor-secreted vascular permeability factor. Cancer Research. **50**: 1774-1778 (1990).

32. Q-Hong, J. Nagy, D. Senger, H. Dvorak, and A. Dvorak, Ultrastructural localization of vascular permeability factor/vascular endothelial growth factor (VPF/VEGF) to the abluminal

plasma membrane and vesiculovacuolar organelles of tumor microvascular endothelium. Journal of Histochemistry and Cytochemistry. **43**(4): 381-389 (1995).

33. Feng, D., J. Nagy, J. Hipp, H. Dvorak, and A. Dvorak, Vesiculo-vacuolar organelles and the regulation of venule permeability to macromolecules by vascular permeability factor, histamine, and serotonin. Journal of Experimental Medicine. **183**: 1981-1986 (1996).

34. Roberts, W. and G. Palade, Increased microvascular permeability and endothelial fenestration induced by vascular endothelial growth factor. Journal of Cell Science. **108**: 2369-2379 (1995).

35. Roberts, W. and G. Palade, Neovasculature induced by vascular endothelial growth factor is fenestrated. Cancer Research. **57**: 765-772 (1997).

36. Yuan, F., Y. Chen, M. Dellian, N. Safabakhsh, N. Ferrara, and R. Jain, Time-dependent vascular regression and permeability changes in established human tumor xenografts induced by an anti-vascular growth factor/vascular permeability factor antibody. Proceedings of the National Academy of Science-USA. **93**: 14765-14770 (1996).

37. Dellian, M., B. Witwer, H. Salehi, F. Yuan, and R. Jain, Quantitation and physiological characterization of angiogenic vessels in mice. American Journal of Pathology. **149**: 59-71 (1996).

38. Levick, J. and L. Smaje, An analysis of the permeability of a fenestrae. Microvascular Research. **33**: 233-256 (1987).

Chapter 5.

MODULATION OF THE PORE CUTOFF SIZE VIA HORMONE WITHDRAWAL

5.1 Motivation and Background

New blood vessel growth in the microcirculation of the tumor is required if the tumor is to grow beyond a few millimeters. Angiogenesis is a complex biological process which is fundamental to reproduction, development, and tissue repair. It is commonly thought to occur as a result of endothelial sprouting, involving the release of several growth factors working in concert to cause digestion of the extracellular matrix, endothelial cell proliferation, endothelial cell migration, and endothelial cell differentiation [1]. Another mode of tumor angiogenesis is intussusceptive microvascular growth. This process is characterized by the formation of small intervascular tissue structures inside the blood vessels that subsequently grow [2].

The normal turnover rate of the endothelium is relatively low [3]. The factors that permit the disturbance of the quiescent state are not clearly delineated. In certain normal conditions, proliferation is halted (i.e. wound healing, corpus luteum formation) at the appropriate time. This is also not understood. It is well understood that in the development of a tumor mass, neovascularization is the result of angiogenic factors secreted by the tumor cells and host cells [4]. These angiogenic factors may have independent, synergistic, stimulatory, or inhibitory effects [5, 6]. In addition, different tumors induce angiogenesis via different growth factors [7, 8]

Vascular targeting, which would damage the vessels feeding the tumor, could potentially reduce the tumor burden indirectly by starving it or leading to cellular states which are more responsive to current treatments. Very few studies have been conducted which look at vascular changes after treatment.

One could study growth and regression in the same tumor cell line with a hormone-dependent tumor, in which regression can be achieved by hormone ablation. This is a relevant model because 1) breast cancer is the most frequent malignancy among women, with an estimated

422,000 new cases annually in developed countries and more than 60% of human breast cancers are estrogen responsive [9], and 2) in 1994, prostate cancer became the most common cancer in males in the United States; more prevalent than lung cancer. Androgen deprivation leads to remission in approximately 50% of prostatic cancer patients. Remission lasts for a median time period of 1 year in metastatic disease and is followed by progression of the disease.

The role of hormones in the growth process of tumors is complex. It is hypothesized that the actions of steroids are modulated by locally acting peptides. Growth stimulation by estrogen in vitro is accompanied by an increase in growth stimulatory TGFα and IGF-II production [10]. The production of bFGF in prostate cancer cell lines is variable [10]. Hormone independent tumors constitutively produce growth factors. It has been suggested that either the increased production of growth factors or the decreased production of inhibitory factors may be indirectly associated with transformation from normal to malignant states.

Studies on the quantification of angiogenesis in breast cancer have shown that levels of growth factor can be used as an independent prognostic factor [11]. VEGF, bFGF, TGF-β1, PDGF, and placenta growth factor were found to be expressed within human primary breast cancers [11-13]. In addition, it was found that VEGF and VEGF receptor expression is spatially and temporally correlated with hormonally regulated tissues which stimulate angiogenesis [13]. Treatment of tumors with anti-VEGF antibody resulted in time-dependent decreased permeability [14]. These same tumors also demonstrated vessel regression after treatment with the antibody [14].

Similar to tumor microvessel permeability, we hypothesize that the pore cutoff size is altered during growth and regression of tumors with concurrent microvascular remodeling and differential expression of various growth factors. Implantation of a hormone-dependent tumor provides the opportunity to conduct an in situ investigation into the changes in the functional transvascular gaps during tumor growth and hormone-ablation induced regression.

5.2 Materials and Methods

Dorsal Chamber Implantation. The method used is described in Chapter 3.

Tumor Implantation. Shionogi cells were kindly provided by M. E. Gleaze, Division of Urology, University of British Columbia, Vancouver, Canada and passaged in vivo in our laboratory. Implantation is described in Chapter 3. All experiments were performed within 10 to 20 days after implantation.

Orchiectomy. Animals in a given cohort were divided into two groups. Half of the animals were orchiectomized, the other half underwent sham operations. Animals were anesthetized with 0.25 ml of anesthesia (9 parts saline: 1 part ketamine: 0.1 parts Xylazine) intramuscularly. Prior to surgery the scrotum was shaved, and a 1 mm vertical incision was made across the scrotum. The testes were exposed by blunt dissection of the superficial fascia. The testis and epididymis were removed bilaterally and the incision was closed with 3 interrupted sutures (5-0 nylon). Sham operated animals underwent the same procedure except for removal of the testis and epididymis. All surgical procedures were performed under aseptic conditions in a specific germ free environment. During surgery the body temperature of the animals was kept constant at 36 - 37 °C by means of a heating pad.

Liposome Preparation. Liposomes were prepared as described in Chapter 3. In some cases, the fluorescent label used was fluorescein isothiocyanate (FITC).

Microscopy. The experimental setup is described in Chapter 3.

Particle Extravasation. This procedure is described in Chapter 3.

5.3 Results and Discussion

Shionogi Carcinoma 115 (Shionogi) is an androgen-dependent mouse mammary tumor, which was established in 1964 [15]. Shionogi cells have androgen receptors, exhibit androgen responsiveness, and secrete androgen-induced growth factor (AIGF), a member of the fibroblast growth factor family. Androgen removal results in complete tumor regression if androgen ablation is initiated while the tumor is small. Partial size decrease results when androgen is cut off in medium to large size tumors. Results of DNA studies show fragmented DNA characteristic of apoptosis after 96 hours and decreased expression of G_1-specific genes 3 to 4 days after androgen ablation. Apoptosis, or programmed cell death, involves a cascade in which the cells undergo an epigenetic reprogramming, which leads to double-strand fragmentation of their DNA followed by cellular fragmentation into apoptic bodies. There is a decreased production of secreted proteins and an increase of a variety of new gene products which leads ultimately to DNA fragmentation. The cell itself is fragmented into apoptic bodies after DNA fragmentation [16].

Shionogi tumors exhibit differential levels of androgen responsiveness; androgen-dependent, -independent, and -suppressed. This heterogeneity is even more complicated in situ. Recently, it was shown that Shionogi tumors exhibit variable proliferation response to various growth factors such as bFGF, aFGF, EGF, and TGFβ [17]. All of the above studies were conducted in tissue culture which would not yield any information on the local concentration of the secreted gene products and other events that arise in situ after hormone ablation. Furthermore, vascular changes could not be studied.

In this study, microvascular growth and regression were followed for a maximum of 27 days. Initial vascularization was vigorous and occurred within ten days. Prior to 7 days the vascular pattern was composed of very thin spidery vessels. Orchiectomy was performed on days 10 or 12, determined by the rate of vascularization of the cohort. All animals within a cohort underwent surgery on the same day. Figure F-1 shows the differing size of tumor mass and

vascular pattern of growing and regressing tumors. The tumor tissue regression correlated well with in vitro results [16-19]. Vessel rarefaction is evident in the regressing tumors.

The pore cutoff size range determined for this tumor was between 200 and 380 nm on day 12 (Chapter 3). Pore cutoff size measurements were made 2 days prior to surgery, the day of surgery, 2 days after surgery, 4 days after surgery, and 6 days after surgery (different cohorts of animals were used for each time point and each particle size). It was determined that the growth of the tumor had no effect on the pore cutoff size once the tumor was vascularized (Figure 5-1A). An immediate and significant impact on the pore cutoff size was observed 48 hours after orchiectomy. The pore cutoff size within 48 hours was less than 100 nm (Figure 5-1B). FITC-Bovine Serum Albumin (FITC-BSA) did not extravasate in orchiectomized animals after 48 hours.

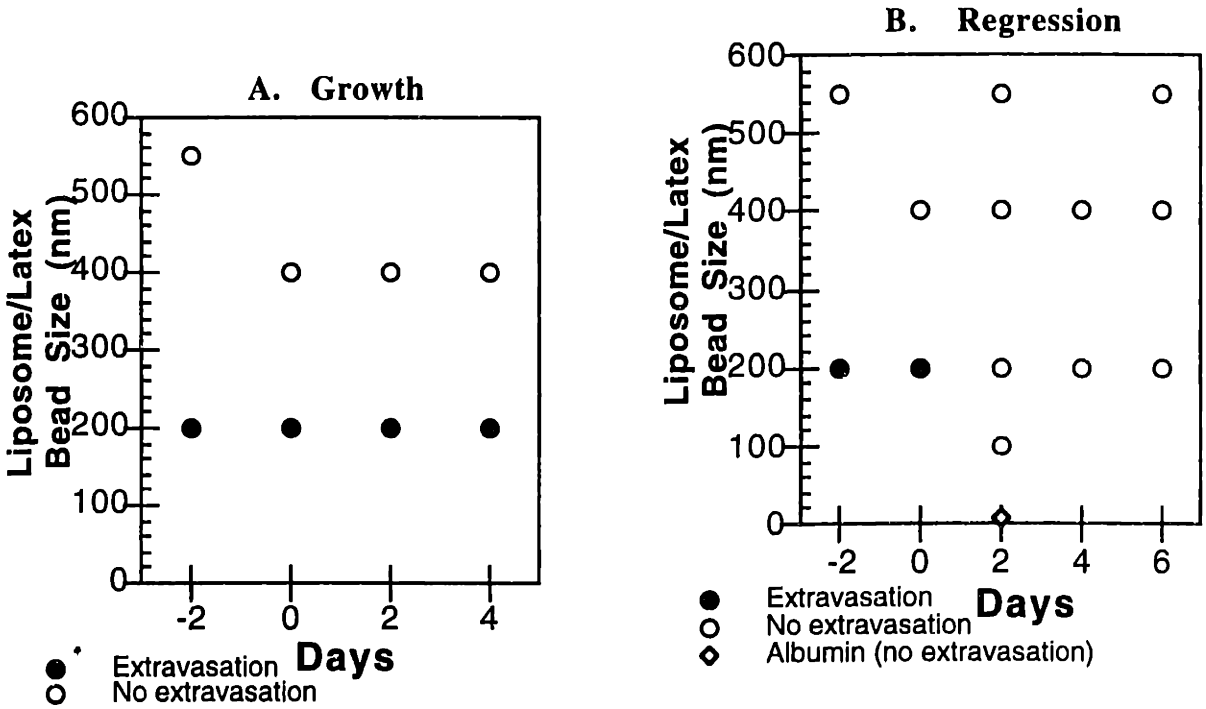

Figure 5-1. The Modulation of the Tumor Pore Cutoff Size with Growth and Regression. A: The growth response of Shionogi tumor in the dorsal chamber; Day 0 indicates the day of sham operation B: The regression response of Shionogi tumor in the dorsal chamber; Day 0 indicates the day of orchiectomy

The results for growth are interesting due to the fact that throughout the 20 day period the tumor mass is growing and the vasculature is continuously modified (Figure F-1). Data could not be collected prior to 8 days because there was no flow in a sufficient number of capillary sprouts to perform the experiments. This is in agreement with previous studies investigating the changing vascular microarchitecture in LS174T tumors transplanted in the dorsal chamber [20]. The continuous rearrangement of the blood vessels does not lead to any change in the pore cutoff size.

We observed subsequent changes in the va cular pattern after androgen ablation (Figure F-1). Vascular regression was observed concomitant with androgen ablation. Whether this is a direct effect of androgen on the endothelial cells, or an indirect effect resulting from reduced levels of VEGF remains unclear. Shionogi cells undergo apoptosis with androgen withdrawal (unpublished data). Furthermore, VEGF has been shown to be regulated by hormonal levels [13]. The treatment of tumors with anti-VEGF antibody induces regression of preformed vessels in solid tumors [14] similar to what we found with hormone withdrawal. This indicates that hormone ablation may be an anti-vascular therapy.

The treatment of tumors with anti-VEGF antibody induces decreased vascular permeability of preformed vessels in solid tumors [14]. The hormonal milieu as a specific component of the microenvironment, has been shown to regulate angiogenesis in hormone dependent mammary carcinomas [21]. We show here that the hormone milieu has a significant affect on the functional structure of the tumor microvascular endothelium.

5.4 Conclusions

The study indicates that changes in the local microenvironment lead to a dramatic change in the one vascular parameter studied. The growth and maintenance of tumor vasculature requires the constant stimulation of the necessary factors. Inhibiting one stimulatory factor (testosterone in this study) can significantly affect the continued stability of the entire tumor mass. Investigation of other morphological parameters such as vascular density, tumor size, and permeability changes with growth and regression are necessary. In addition, measurement of time course of change in

mRNA and protein levels of VEGF and testosterone may prove useful in understanding the underlying mechanism for the observed vascular and tumor regression.

Importantly, we show that hormone ablation significantly decreased the transvascular transport of other therapeutic agents one might want to deliver in combined or subsequent therapies. Thus, strategies utilizing chemotherapy, immunotherapy, and gene therapy may need to be used prior to initiating hormone ablation or other forms of antiangiogenic therapies.

5.5 References

1. Bicknell, R. and A. Harris, Novel growth regulatory factors and tumor angiogenesis. European Journal of Cancer. **27**(6): 781-785 (1991).

2. Patan, S., L. Munn, and R. Jain, Intussusceptive microvascular growth in human colon adenocarcinoma xenograft: A novel mechanism of tumor angiogenesis. Microvascular Research. **51**: 260-272 (1996).

3. Hobson, B. and J. Denekamp, Endothelial proliferation in tumours and normal tissues: continuous labelling studies. British Journal of Cancer. **49**: 405-415 (1984).

4. Fidler, I. and L. Ellis, The implications of angiogenesis for the biology and therapy of cancer metastasis. Cell. **79**: 185-188 (1994).

5. Denekamp, J., Review article: Angiogenesis, neovascular proliferation and vascular pathophysiology as targets for cancer therapy. British Journal of Radiology. **66**(783): 181-196 (1993).

6. O'Reilly, M., L. Holmgren, Y. Shing, C. Chen, R. Rosenthal, M. Moses, W. Lane, Y. Cao, E. Sage, and J. Folkman, Angiostatin: A novel angiogenesis inhibitor that mediates the suppression of metastases by a Lewis lung carcinoma. Cell. **79**: 315-328 (1994).

7. Kandel, J., E. Bossy-Wetzel, F. Radvanyi, M. Klagsbrun, J. Folkman, and D. Hanahan, Neovascularization is associated with a switch to the export of bFGF in the multistep development of fibrosarcoma. Cell. **66**: 1095-1104 (1991). .

8. Kim, K., B. Li, J. Winer, M. Armanini, N. Gillett, H. Phillips, and N. Ferrara, Inhibition of vascular endothelial growth factor-induced angiogenesis suppresses tumour growth in vivo. Nature. **362**: 841-844 (1993).

9. Harris, J., M. Morrow, and L. Norton, Malignant Tumors of the Breast, in Cancer:Principles & Practice of Oncology, V. DeVita, Editor. 1997, JB Lippincott: Philadelphia.

10. Waxman, J., A. Stubb, and H. Pandha, The biological basis for the treatment of prostate cancer, in Molecular Endocrinology of Cancer, J. Waxman, Editor. 1996, Cambridge University Press: New York. p. 305-317.

11. Relf, M., S. LeJeune, P. Scott, S. Fox, K. Smith, R. Leek, A. Moghaddam, R. Whitehouse, R. Bicknell, and A. Harris, Expression of the angiogenic factors vascular endothelial growth factor, acidic and basic fibroblast growth factor, tumor growth factor b-1, platelet-derived endothelial cell growth factor, placenta growth factor, and pleiotrophin in human primary breast cancer and its relation to angiogenesis. Cancer Research. **57**: 963-969 (1997).

12. Brown, L., B. Berse, R. Jackman, K. Tognazzi, E. Manseau, D. Senger, and H. Dvorak, Expression of vascular permeability factor (vascular endothelial growth factor) and its receptors in adenocarcinomas of the gastrointestinal tract. Cancer Research. **53**: 4727-4735 (1993).

13. Shweiki, D., A. Itin, G. Neufeld, H. Giay-Goren, and E. Keshet, Patterns of expression of vascular endothelial growth factor and VEGF receptors in mice suggest a role in hormonally regulated angiogenesis. Journal of Clinical Investigation. **91**: 2235-2243 (1993).

14. Yuan, F., Y. Chen, M. Dellian, N. Safabakhsh, N. Ferrara, and R. Jain, Time-dependent vascular regression and permeability changes in established human tumor xenografts induced by an anti-vascular growth factor/vascular permeability factor antibody. Proceedings of the National Academy of Science-USA. **93**: 14765-14770 (1996).

15. Minesita, T. and K. Yamaguchi, An androgen-dependent tumor derived from a hormone-independent spontaneous tumor of a female mouse. Steroids. **4**: 815-830 (1964).

16. Furuya, Y., J. Isaacs, and J. Shimazaki, Induction of programmed death/apoptosis in Androgen-dependent mouse mammary tumor cell line (Shionogi carcinoma 115) by androgen withdrawal. Japanese Journal of Cancer Research. **86**: 1159-1165 (1995).

17. Yamaguchi, T., K. Kawamoto, N. Uchida, and S. Watanabe, Three cell lines showing androgen-dependent, -independent, and -suppressed phenotypes, established from a single tumor of androgen-dependent shionogi carcinoma 115. In Vitro Cell and Development Biology. **28A**: 245-254 (1992).

18. Koga, M., S. Kasayama, K. Matsumoto, and B. Sato, Molecular mechanism of androgen-dependent growth in transformed cells. Pathway from basic science to clinical application. Journal of Steroid Biochemistry and Molecular Biology. **54**(1/2): 1-6 (1995).

19. Akakura, K., N. Bruchovsky, S. Goldenberg, P. Rennie, A. Buckley, and L. Sullivan, Effects of intermittent androgen suppression on androgen-dependent tumors. Cancer. **71**: 2782-2790 (1993).

20. Leunig, M., F. Yuan, M. Menger, Y. Boucher, A. Goetz, K. Messmer, and R. Jain, Angiogenesis, microvascular architecture, microhemodynamics, and interstitial fluid pressure during early growth of human adenocarcinoma LS174T in SCID mice. Cancer Research. **52**: 6553-6560 (1992).

21. Gagliardi, A. and D. Collins, Inhibition of angiogenesis by antiestrogens. Cancer Research. **53**: 533-535 (1993).

Chapter 6.
MODULATION OF THE PORE CUTOFF SIZE BY THE HOST MICROENVIRONMENT

6.1 Motivation and Background

Most cancer deaths are due to metastases that are resistant to conventional therapy [1]. A better understanding of the complex interactions between metastatic cells and host factors can provide a biological foundation for the design of more effective therapy and optimized delivery of existing agents. Recent evidence indicates that the organ microenvironment can influence the biology of cancer growth and metastasis in the following ways:

1) Degradation of the collagen matrix: Cancer cells produce various collagenases and glycosidases that degrade the extracellular matrix [2-6]. The expression and level of these proteases are influenced by cytokines produced by various tissues [4].

2) Growth factors: Autocrine or paracrine growth factors that control repair of tissues are tissue specific. Metastatic cells may usurp these for use to allow them to survive and grow preferentially within a particular tissue environment. Alternatively, organ specific growth factors may suppress growth of implanted tumors [7]. In addition, the influence of the local microenvironment may alter tumor cell regulation of various growth factors [7, 8].

3) Response to chemotherapy: It is a well-known clinical experience that metastases in different tissues exhibit different responses to chemotherapeutic agents [9]. Lymph node and skin metastases are more sensitive to chemotherapy than lung and bone metastases in women with breast cancer [10]. In addition, various murine models indicate that the tumor transplant site influences the tumor response to chemotherapeutics [9, 11-14].

4) Angiogenesis: Numerous known factors affect the initiation, rate, and maintenance of tumor vascularization [15, 16]. The extent of vascularization in and around tumors is dependent on the balance of the endogenous stimulating (e.g. bFGF) and inhibiting molecules (e.g. angiostatin). The level of growth factor and the level of growth factor receptor expression are both

important. For example, levels of bFGF expression are modulated by the organ site in human renal cell carcinoma transplants [8]. Murine experiments corroborate this data [12, 17-20]. The organ microenvironment, with its native inhibitors and inducers of angiogenesis, can profoundly affect angiogenesis.

The objective of this study was to investigate to what extent the local microenvironment affects the tumor pore cutoff size. The two sites chosen were striated skin muscle and pia mater. We hypothesize that the pore cutoff size in these two tumors will reflect the different characteristics of the host microvasculature. Chapter 3 established that each tumor had a characteristic pore cutoff size in the dorsal chamber. In Chapter 5 we showed that the removal of a growth stimulant caused a rapid and significant change in the pore cutoff size. Here, we extend those findings to implicate modulation of the pore cutoff size by the host microenvironment.

6.2 Materials and Methods

Dorsal Chamber Implantation. The method of implantation is described in Chapter 3.

Cranial Window Implantation. The method was previously described in Yuan et al [21]. Briefly, all experiments were performed in SCID mice, bred and maintained in a specific pathogen germ free environment in the Steele Laboratory. For the surgical implantation of the window, animals (25 - 30 g body weight) were anesthetized by intramuscular injection of 0.3 µl of anesthesia (9 parts saline: 1 part ketamine: 0.1 parts Xylazine). Prior to window implantation, the frontal and parietal region of the skull was shaved and washed with ethanol. The head of the animals was fixed by a stereotactic apparatus. A longitudinal incision of the skin was made between the occiput and forehead. This cut was enlarged by two half circular cuts to reveal the bony skull. The periosteum was carefully removed to the temporal crests. A 7-mm circle was drawn over the frontal and parietal regions of the skull (Figure 6-1). A groove was made in the circle with a high-speed air-turbine drill (CH4201S; Champion Dental Products, Placentia, CA)

with a 0.5 mm diameter burr tip. The groove depth was increased by cautious and continuous drilling. Cold saline was applied during the drilling process to avoid thermal injury of the cortical regions. Once the bone flap appeared loose, it was separated from the dura mater with a blunt microblade. After removal of the bone flap, the dura mater underneath was kept moist with saline-soaked pieces of gelfoam. All superficial bleeding was stopped before proceeding. A nick in the dura mater was made above a relatively avascular area of the brain. Iris microscissors were passed through the nick. The dura and arachnoid membranes were completely removed from the surface of both hemispheres, leaving the saggital sinus intact (Figure 6-2). The window was closed with a 8-mm coverslip by adhering it to the bone with a histocompatible cyanoacrylate glue. The total time for the surgical procedure was 45 minutes. All surgical procedures were performed under aseptic conditions in a specific germ free environment. During surgery the body temperature of the animals was kept constant at 36 - 37°C by means of a heating pad. Animals were observed for recurrent bleeding for a period of 24 hours.

Tumor Implantation. The cell lines studied were MCa IV, HCa-1, Shionogi (kindly provided by M. E. Gleaze, Division of Urology, University of British Columbia, Vancouver, Canada), ST-8 (kindly provided by Dr. L. Gerweck and T. Syed, Radiation Oncology, Massachusetts General Hospital, Boston), and U87. The implantation into the dorsal chamber was described in Chapter 3. The glass coverslip of the cranial window was carefully removed after 24 hours and a piece of tumor was placed at the center of the window. The window was closed again with a new 8-mm coverslip by adhering it to the bone with a histocompatible cyanoacrylate glue. Experiments were performed 7 days after implantation in the cranial window for all tumors but U87. U87 required a 14 -20 day growth period before significant vasculature appeared.

Liposome Preparation. Liposomes were prepared as described in Chapter 3.

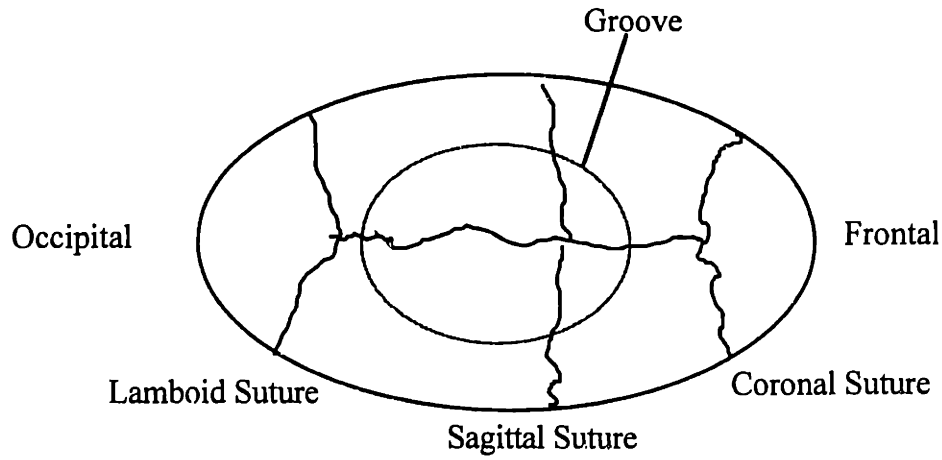

Figure 6-1. Location of the cranial window

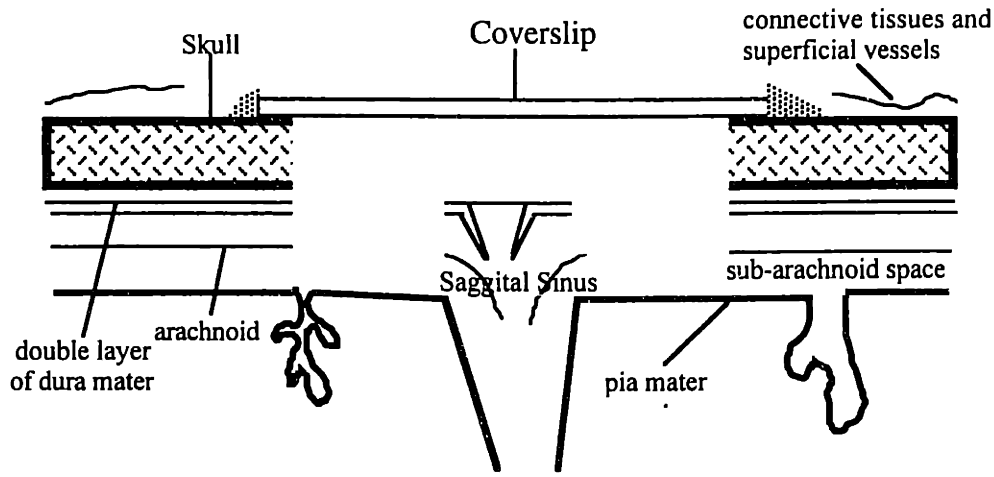

Figure 6-2 Tissue structures within the cranial window

Microscopy. Animals bearing a dorsal chamber or cranial window were anesthetized as described above. Liposomes or latex beads (2 μl) were injected into the tail vein of the mouse. The extravasation of the particles was observed 24 hours after injection. For observation, the animals were anesthetized as described above and immobilized in a polycarbonate tube (dorsal chamber) or stereotactic apparatus (cranial window). The rest of the experimental setup is the same as described in Chapter 3.

Particle Extravasation. This procedure is described in Chapter 3.

6.3 Results and Discussion

All of the tumors transplanted grew in the cranial window. These growth results are in contrast to the results from transplantation into the dorsal chamber where we found that some tumors will not grow in the dorsal chamber even though they do grow subcutaneously (Table 3-2). All the tumors examined grew twice as fast in the cranial window compared to the dorsal chamber. Figure G-1 shows an overview of the cranial window preparation with both normal tissue and transplanted U87. FITC-dextran (2 million MW) was injected IV at the time of observation in order to visualize the vessels under epiillumination to ensure good perfusion of the tumor. Due to technical constraints the vessels could not be observed under transillumination. The presence of FITC-dextran did not interfere with the determination of extravasation. Animals injected with FITC-liposomes did not receive an injection of FITC-dextran.

Figure G-2 is a representative series of images captured for HCa I and MCa IV tumors illustrating extravasation of different particle sizes. Healing of the BBB following surgical manipulation was expected to occur within 7 -10 days [22]. The development of intact perfused vessels was expected to occur within 7 days [22]. There was no extravasation in normal tissue for any tumor and any liposome size. We saw vascular sprouts within the tumors early with maximal angiogenic response around day 7 for all tumors but U87.

All of the tumors exhibited microvessel hyperpermeability to nanoparticles in the cranial window (Figure 6-3). The microvessel endothelium within the tumors did not have the BBB endothelium characteristics. Widened interendothelial junctions have been observed in conditions such as brain trauma, osmotic stress, and hydrocephalus [23]. Fenestrations and widened interendothelial junctions have been observed under electron microscope [23, 24].

The microvasculature of the brain is lined by continuous nonfenestrated endothelium with tight junctions and little pinocytic vesicle activity [25]. This structure is called the blood-brain-barrier (BBB). While this barrier is assumed to be extremely impermeable it does not seem to be

impervious to invading tumor cells migrating into the brain parenchyma. Brain metastases develop in 10 - 40 % of all patients with solid tumors [26].

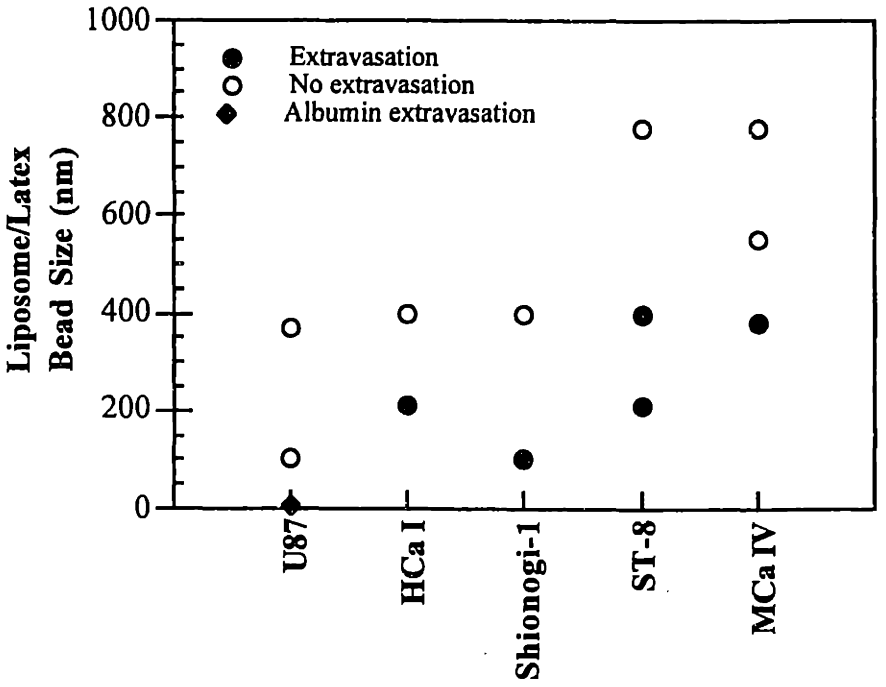

Figure 6-3. Tumor pore cutoff sizes in the cranial window. The permeability of U87 to BSA was established previously [21].

Metastasis to the central nervous system develop vasculature that mimics that of the tissue of origin [24]. The vasculature in the brain is impermeable to circulating macromolecules. Tumor invasion often leads to the breakdown of this barrier with a resultant cerebral edema which is extremely difficult to treat. Despite the proposed breakdown of the BBB, treatment of brain metastasis is much less effective than treatment of metastasis from the same tumor elsewhere [23].

Primary brain tumors and brain metastasis are resistant to most chemotherapeutic treatments [25]. It is thought that the BBB restricts the ability of the drugs to reach the interstitium. The integrity of the BBB is retained in some brain tumors [25] and altered in others [27, 28]. The discrepancies were thought to be due to different tumor types and different model systems. A more recent study indicates that the alterations to the BBB are due to location of the tumor lesions,

size of the lesion, and pattern of growth [29]. It has been shown that the blood-tumor barrier (BTB) is less selective than the BBB exhibiting differential areas of increase permeability and areas of impermeability [29, 30].

One of the more controversial regions in which to transplant tissue is in the brain due to the issue of maintenance of the BBB. CNS graft tissue suggests that the graft tissue determines the morphological and permeability characteristics of the newly developed blood vessels [22]. However, other experiments have demonstrated that it is the local host microenvironment that determines the transport barrier properties of the vasculature not the tissue of origin [31, 32]. This is an ongoing debate.

Because the host microenvironment varies among different organs [33], we expected to see a difference in the pore cutoff size at the two locations. The tumor pore cutoff sizes observed in the cranial window were smaller than those of the same tumor transplanted into the dorsal chamber (Figure 6-4). The cerebral microenvironment is continuing to form and regulate the BBB by secretion of various factors [31, 32]. The tumor is secreting specific cytokines, growth factors, and enzymes [34]. From our results we postulate that it is the balance between these two local tissue mechanisms that may lead to the observed pore cutoff size within the tumor microvessels. The normal striated skin muscle endothelium does not establish an extremely tight barrier as the BBB, therefore, it is possible that the lack of barrier forming factors leads to the formation of the larger pores in the dorsal chamber.

In a previous study the permeability of the microvasculature to BSA of various tumors implanted within the cranial window revealed hyperpermeability except for 1 tumor, HGL21 [35] (Table 6-1). In addition, the permeability of collagen gels containing VEGF or bFGF implanted in the dorsal chamber and the cranial window was investigated. It was found that the permeability in the cranial window was four times higher than in the dorsal chamber [36]. We found that U87 did not exhibit any significant increase in pore cutoff size whereas MCa IV did exhibit increased pore cutoff size. However, the permeability of U87 to BSA is greater than that found for MCa IV. This non-intuitive result accentuates the difference between the mechanisms contributing to the

permeability and the pore cutoff size of tumor microvessels. Therefore, a different balance may exist between host and tumor contribute to maintenance and induction of increased permeability and pore cutoff size.

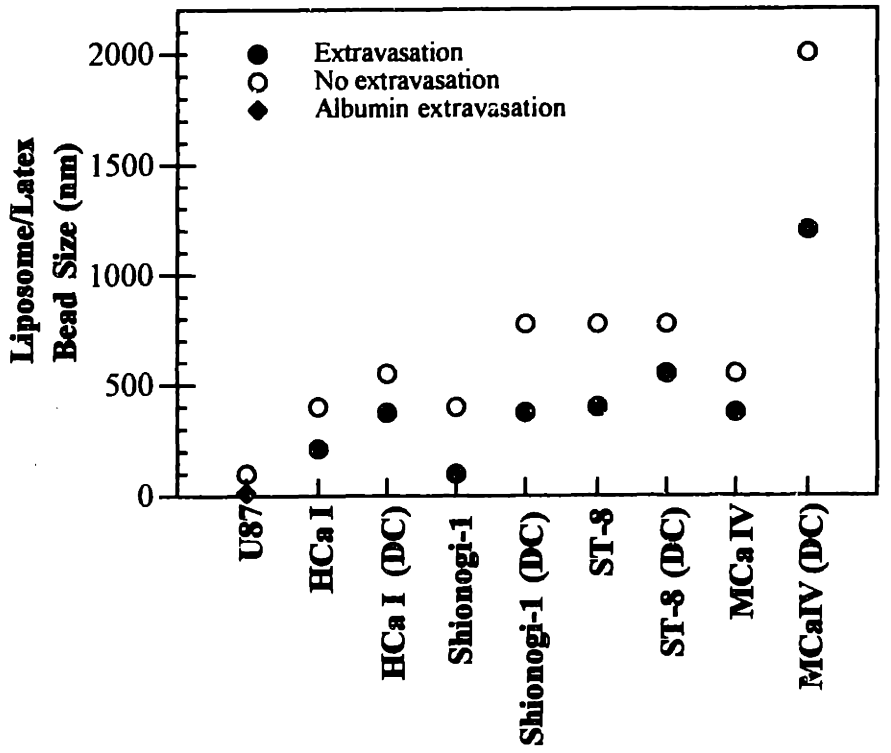

Figure 6-4. Modulation of tumor pore cutoff size with microenvironment. The cranial window result are plotted to the left of those obtained from dorsal chamber experiments.

Table 6-1. Vascular Permeability to BSA[a]

Tumor line	Permeability
MCaIV	1.9 ± 0.5 (1.9)[b] (1.3 - 2.5)[c]
U87	3.8 ±1.2 (4.3) (2.4-5.0)
HGL21	0.11 ± 0.05 (0.09) (0.05 - 0.19)

[a] from Yuan et al [35]
[b] mean ± SD (median)
[c] range

Only one tumor, ST-8, had a pore cutoff size on the same order of magnitude as that within the dorsal chamber. The competitive environment hypothesis may explain the lack of pore cutoff size difference in this tumor. Future studies into mRNA and protein levels of VEGF and its receptors in both locations may be useful in determining a potential mechanism.

6.4 Conclusions

This study showed that the local host microenvironment does play a role in determining tumor pore cutoff sizes. Both sites exhibit higher pore cutoff sizes than local host normal tissue microvessels. However, tumors implanted in the dorsal skinfold chamber had larger pore cutoff sizes than the same tumor implanted into the cranial window. The competitive environment hypothesis proposes that the host microenvironment and the tumor microenvironment compete in the establishment of the barrier structure of the tumor vessels. This seems to be rarely an all or none response as previously postulated with CNS graft studies [22, 31, 32]. The difference in the pore cutoff size is most likely due to the differential expression of various growth factors, upregulation or down regulation of their receptors, differential levels of various inhibitors, and the importance of degradative enzymes.

It is not unreasonable to expand this hypothesis to the differential response to chemotherapeutics seen in different metastatic sites. The resultant tumor vessels may be more of a mosaic in nature; exhibiting some of the characteristics of the site vessels and also some of the characteristics of the origin tissue vasculature. In addition, all tumors were hyperpermeable in the cranial window with the exception of a human glioma, HGL21 [35]. The BBB would not be expected to be a significant barrier to macromolecular or nanoparticle transport in most solid tumors.

6.5 References

1. Fidler, I., Modulation of the organ microenvironment for treatment of cancer metastasis. Journal of the National Cancer Institute. **87**(12): 1588-1592 (1995).

2. Liotta, L., U. Thogeirsson, and S. Garbisa, The role of collagenases in tumor cell invasion Cancer Metastasis Review. **1**: 277-288 (1982).

3. Nakajima, M. and T. Irimura, Heparanases and tumor metastasis. Journal of Cellular Biochemistry. **36**: 157-167 (1988).

4. Nakajima, M., K. Morikawa, A. Fabra, C. Bucana, and I. Fidler, Influence of organ environment on extracellular matrix degradative activity and metastasis of human colon carcinoma cells. Journal of the National Cancer Institute. **82**: 1890-1898 (1990).

5. Sloane, B. and K. Honn, Cysteine proteinases and metastasis. Cancer Metastasis Review. **3**: 249-263 (1984).

6. Woolley, D., Collagenolytic mechanisms in tumor cell invasion. Cancer Metastasis Review. **3**: 361-372 (1984).

7. Naito, S., A.v. Eschenbach, R. Giavazzi, and I. Fidler, Growth and metastasis of tumor cells isolated from a human renal cell carcinoma implanted into different organs of nude mice. Cancer Research. **46**: 4109-4115 (1986).

8. Singh, R., C. Bucana, M. Gutman, D. Fan, M. Wilson, and I. Fidler, Organ site-dependent expression of basic fibroblast growth factor in human renal cell carcinoma cells. American Journal of Pathology. **145**(2): 365-374 (1994).

9. Kjønniksen, I., K. Breistøl, and Ø. Fodstad, Site-dependent differences in sensitivity of LOX human melanoma tumors in nude rats to dacarbazine and mitosolomide, but not doxorubicin and cisplatin. Cancer Research. **52**: 1347-1351 (1992).

10. Slack, N. and I. Bross, The influence of site of metastasis on tumour growth and response to chemotherapy. British Journal of Cancer. **32**: 78-86 (1975).

11. Donelli, M., R. Russo, and S. Garatini, Selective chemotherapy in relation to the site of tumor transplantation. International Journal of Cancer. **32**: 78-86 (1975).

12. Dong, Z., R. Radinsky, D. Fan, R. Tsan, C. Bucana, C. Wilmanns, and I. Fidler, Organ-specific modulation of steady-state mdr gene expression and drug resistance in murine colon cancer cells. Journal of the National Cancer Institute. **86**(12): 913-920 (1994).

13. Furukawa, T., T. Kubota, M. Watanabe, T.-H. Kuo, M. Kitajima, and R. Hoffman, Differential chemosensitivity of local and metastatic human gastric cancer after orthotopic transplantation of histologically intact tumor tissue in nude mice. International Journa of Cancer. **54**: 397-401 (1993).

14. Wilmanns, C., D. Fan, C. O'Brian, C. Bucana, and I. Fidler, Orthotopic and ectopic organ environments differentially influence the sensitivity of mucin colon carcinoma cells to doxorubicin and 5-fluorouracil. International Journal of Cancer. **53**: 98 - 104 (1992).

15. Folkman, J. and M. Klagsbrun, Angiogenic factors. Science. **235**: 444-447 (1987).

16. Folkman, J., Angiogenesis in cancer, vascular, rheumatoid, and other diseases. Nature Medicine. **1**: 27-31 (1995).

17. Dvorak, H., L. Brown, M. Detmar, and A. Dvorak, Vascular permeability factor/Vascular endothelial growth factor, microvascular hyperpermeability, and angiogenesis. American Journal of Pathology. **146**(5): 1029-1039 (1995).

18. Brown, L., B. Berse, R. Jackman, K. Tognazzi, E. Manseau, D. Senger, and H. Dvorak, Expression of vascular permeability factor (vascular endothelial growth factor) and its receptors in adenocarcinomas of the gastrointestinal tract. Cancer Research. **53**: 4727-4735 (1993).

19. Brown, L., B. Berse, R. Jackman, K. Tognazzi, E. Manseau, H. Dvorak, and D. Senger, Increased expression of vascular permeability factor (vascular endothelial growth factor) and its receptors in kidney and bladder carcinomas. American Journal of Pathology. **143**(5): 1255-1262 (1993).

20. Q-Hong, J. Nagy, D. Senger, H. Dvorak, and A. Dvorak, Ultrastructural localization of vascular permeability factor/vascular endothelial growth factor (VPF/VEGF) to the abluminal plasma membrane and vesiculovacuolar organelles of tumor microvascular endothelium. Journal of Histochemistry and Cytochemistry. **43**(4): 381-389 (1995).

21. Yuan, F., H. Salehi, Y. Boucher, U. Vasthare, R. Tuma, and R. Jain, Vascular permeability and microcirculation of gliomas and mammary carcinomas transplanted in rat and mouse cranial windows. Cancer Research. **54**: 4564-4568 (1994).

22. Broadwell, R., H. Charlton, P. Ebert, W. Hickey, Y. Shirazi, J. Villegas, and A. Wolf, Allografts of CNS tissue possess a blood-brain barrier. Experimental Neurology. **112**(1): 1-28 (1991).

23. Coomber, B., P. Stewert, E. Hayakawa, C. Farrell, and R.D. Maestro, A quantitative assessment of microvessel ultrastructure in C6 astrocytoma spheroids transplanted to brain and to muscle. Journal of Neuropathology and Experimental Neurology. **47**(1): 29-40 (1988).

24. Hirano, A. and H. Zimmerman, Fenestrated blood vessels in a metastatic renal carcinoma in the brain. Laboratory Investigation. **26**(4): 465-468 (1972).

25. Schackert, G., R. Simmons, T. Buzbee, D. Hume, and I. Fidler, Macrophage infiltration into experimental brain metastases: occurence through an intact blood-brain barrier. Journal of the National Cancer Institute. **80**(13): 1027-1034 (1988).

26. Kornblith, P., M. Walker, and J. Cassady, Treatment of metastatic cancer to the brain, in Cancer, Principles, and Practice of Oncology, V. DeVita, S. Hellman, andS. Rosenberg, Editors. 1985, JB Lippincott: Philadelphia.

27. Stewart, P., K. Hayakawa, C. Farrell, and R.D. Maestro, Quantitative study of microvessel ultrastructure in human peritumoral brain tissue. Evidence for a blood-brain barrier defect. Journal of Neurosurgery. **67**(5): 697-705 (1987).

28. Coomber, B., P. Stewart, K. Hayakawa, C. Farrell, and R.D. Maestro, Quantitative morphology of human glioblastoma multiforme microvessels: structural basis of blood-brain barrier defect. Journal of Neuro-Oncology. **5**: 299-307 (1987).

29. Zhuang, R.-d., J. Price, T. Fujimaki, C. Bucana, and I. Fidler, Differential permeability of the blood-brain barrier in experimental brain metastases produced by human neoplasms implanted into nude mice. American Journal of Pathology. **141**(5): 1115-1124 (1992).

30. Jain, R., Transport of molecules across tumor vasculature. Cancer and Metastasis Reviews. **6**: 559-593 (1987).

31. Risau, W., Induction of blood-brain barrier endothelial cell differentiation. Annals of the New York Academy of Sciences. **633**: 405-419 (1991).

32. Stewart, P. and M. Wiley, Developing nervous tissue induces the formation of blood-brain barrier characteristics in invading endothelial cells: a study using quail chick transplantation chimeras. Developmental Biology. **84**: 183-192 (1981).

33. Fidler, I. and L. Ellis, The implications of angiogenesis for the biology and therapy of cancer metastasis. Cell. **79**: 185-188 (1994).

34. Senger, D., L. Brown, K. Claffey, and H. Dvorak, Vascular permeability factor, tumor angiogenesis and stroma generation. Invasion Metastasis. **14**: 385-394 (1994-95).

35. Yuan, F., M. Dellian, D. Fukumura, M. Leunig, D. Berk, V. Torchillin, and R. Jain, Vascular permeability in a human tumor xenograft: Molecular size dependence and cutoff size. Cancer Research. **55**: 3752-3756 (1995).

36. Dellian, M., B. Witwer, H. Salehi, F. Yuan, and R. Jain, Quantitation and physiological characterization of angiogenic vessels in mice. American Journal of Pathology. **149**: 59-71 (1996).

Chapter 7.
CHARACTERIZATION OF BASIC FIBROBLAST GROWTH FACTOR INTERACTION WITH HEPARIN IMMOBILIZED TO SEPHAROSE

7.1 Motivation

Basic fibroblast growth factor (bFGF) is one of the most potent known angiogenic factors [1-10]. It is sequestered by the extracellular matrix (ECM) and is released by exposure to heparan sulfate degrading enzymes, heparan sulfate, and heparin in active form [11] suggesting that the ECM is the storage site and bFGF is released in response to injury. There are various clinical settings in which vigorous revascularization is desired as well as those in which it is not. A quantitative in situ assay to characterize vascular response to chronic, sustained release of angiogenic factors is essential to understanding various angiogenic pathologies and for treatment in tissues with decreased perfusion.

Matrices developed for in vivo delivery of other drugs and adapted for delivery of bFGF (Table 7-1) fail because the polymer fabrication step significantly reduces the biological activity of the polypeptide. bFGF is not stabilized by disulfide bonds and is very sensitive to alterations in pH, temperature, and enzymatic cleavage.

Attempts to quantitate either the angiogenic or antiangiogenic response to a delivered agent in vivo are phenomenological [1, 3, 12, 18-25]. Extrapolation of the results to the in situ situation is not possible because quantitative information about release rates and transport resistances between the device and the blood vessels are lacking.

One system which has been utilized in angiogenic assays is the sucralfate-collagen system. This system immobilizes growth factors with affinity to heparin and provides a depot for sustained release. Confounding issues to the delivery of heparin affinity growth factors with this device are lack of knowledge of 1) the interaction of the growth factor with sucralfate, 2) the interaction of the growth factor with collagen , 3) the effect of sucralfate on the native tissue, 4) the duration of

growth factor activity, 5) the release rate of growth factor from device, 6) the transport of growth factor within collagen, and 7) the transport of growth factor within the tissue.

Table 7-1. Basic Fibroblast Growth Factor Delivery Matrices

Delivery Vehicle	Citation
Reconstituted Basement Membrane (Matrigel): consists of laminin, collagen IV, heparan sulfate, proteoglycan, and nidogen/entactin, and other connective tissue components	[12]
Alginate containing Heparin-Sepharose beads	[4, 5, 13, 14]
Polytetrafluoroethylene coated with collagen I or IV	[6]
Polytetrafluoroethylene (Gore Tex®) tubing with and without Hydroxypropylchitosan	[15]
Collagen gel containing Sucralfate	[3]
EDC cross-linked gelatin hydrogels	[2]
EVAc containing heparin-sepharose beads	[16]
"Biodegradable pellets"	[17]
Gelatin-Sepharose and Collagen IV-Sepharose	[1]
Polyester sponges	[18]
Polyvinyl foam coated with Elvax in a polyvinyl foam disc sealed with nitrocellulose filters	[19]

The important steps involved in bFGF-induced angiogenesis via sustained release of bFGF are 1) diffusion within and release from the device, 2) diffusion through peri-device acute or chronic inflammation tissue, where degradation of bFGF may occur, 3) diffusion through local tissue, where binding to ECM or cells, and/or degradation may occur, and 4) reaction with endothelial cells.

The heparin-sepharose-alginate system shows much promise in quantitative angiogenic inducement in vivo. This device consists of heparin-sepharose microbeads encapsulated in a biologically inert alginate gel (Figure 7-1). bFGF purportedly freely diffuses through the alginate and sepharose and becomes immobilized and stabilized by heparin. Advantages of this method are

the exploitation of the heparin binding property of bFGF, the lack of extreme processing steps [13], and the use of two materials that have been previously used in vivo. This system provides prolonged storage of bFGF and controlled release to specific sites in vivo.

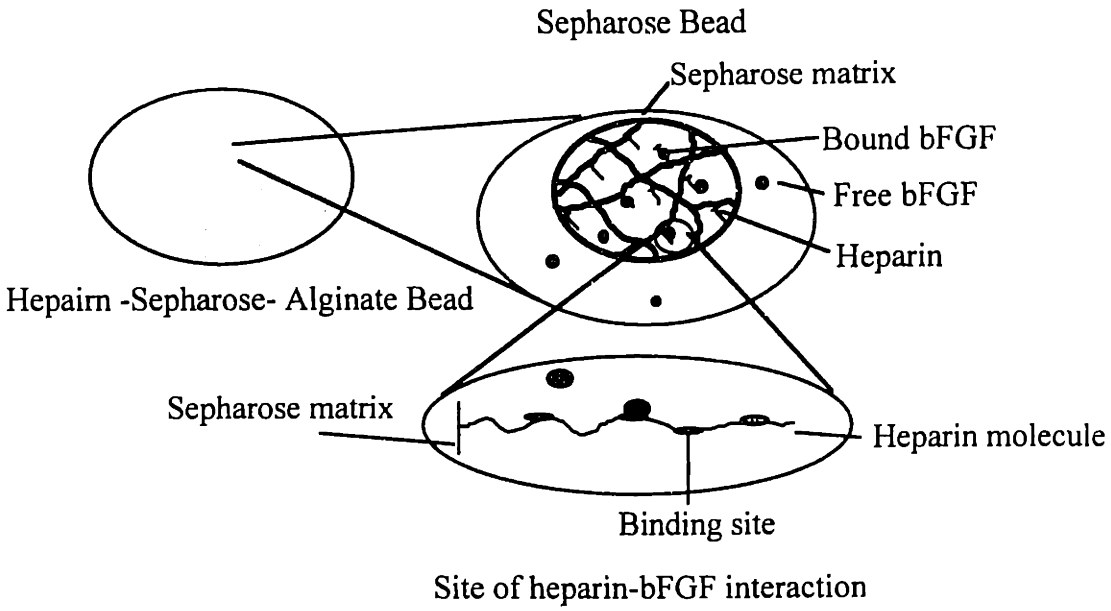

Figure 7-1. Calcium alginate microspheres. The alginate gel encapsulates the heparin-sepharose and sepharose microbeads.

The nature of the interaction between bFGF and immobilized heparin plays an important role in the release of bFGF from these devices. The effects of 1) reaction time, 2) bFGF:heparin ratios, and 3) bFGF affinity were investigated as a first step in the development of ta quantitative description of the bFGF heparin-sepharose interaction.

7.2 Model Formulation of bFGF Diffusion and Binding in Heparin-Sepharose Microbeads

bFGF incorporation into heparin-sepharose microbeads is achieved by movement from the bulk solution into the sepharose gel, diffusion through the sepharose gel, and specific binding to immobilized heparin within the gel. The expected behavior depends on the relative rates of diffusion and reaction. The model developed assumed a uniform distribution of heparin throughout a non-reactive sepharose gel. The sepharose microbeads were suspended in a well-

mixed solution of bFGF. The bFGF diffuses through the sepharose network and reacts wtih the heparin. The material balance within a homogeneous sphere is described by Fickian diffusion incorporating a reaction, "binding", term,

$$\varepsilon \frac{\partial C}{\partial t} = D_{gel} \nabla^2 C - (1-\varepsilon) \frac{\partial S}{\partial t} \qquad (7\text{-}1)$$

where C is the pore fluid concentration, D_{gel} is the diffusion coefficient of bFGF in the gel, S is the concentration of bound complex within the gel, and ε is the void fraction of the sepharose gel.

The diffusivity in the gel was calculated as [26],

$$D_{gel} = DK_d / \gamma \qquad (7\text{-}2)$$

where D is the molecular diffusivity (cm^2/sec) of the protein in water at 20 °C, γ is the tortuosity within the gel, and K_d accounts for the hindered diffusion effects. The following equation was used to estimate K_d for bFGF [27]:

$$K_d = 1 - 2.1044\lambda + 2.089\lambda^3 - 0.948\lambda^5 \qquad (7\text{-}3)$$

where

$$\lambda = \frac{r_{solute}}{r_{pore}} \qquad (7\text{-}4)$$

The following equation was used to estimate D for bFGF [28]:

$$D = 3.6 \times 10^{-5} (MW)^{-0.34} \qquad (7\text{-}5)$$

The radius of bFGF (MW 16,000) was estimated as 1.6 nm and the tortuosity was assumed to be 1 [26].

The equation for a reversible, rapid, monovalent linear reaction is:

$$\frac{\partial S}{\partial t} = k_{on} C R - k_{off} S \tag{7-6}$$

where k_{on} is the forward rate constant, k_{off} is the reverse rate constant, R is the concentration of binding sites in the gel.

The conservation equation describing the situation in the well-mixed fluid phase is:

$$V_{bulk} \frac{dC_{bulk}}{dt} = \frac{3V_{gel}\varepsilon}{r_{sphere}} \left(-D_{gel} \frac{\partial C}{\partial r}\Big|_{r=r_{sphere}} \right) \tag{7-7}$$

Initial and boundary conditions are:

$$\begin{aligned} &t = 0,\ S = C = 0,\ C_{bulk} = C_{bulk0} \\ &r = 0,\ dC/dr = 0 \\ &r = r_{sphere},\ -\varepsilon D_{gel} \frac{\partial C}{\partial r} = k_{m} \left[\frac{C}{\Phi} - C_{bulk} \right] \end{aligned} \tag{7-8}$$

The ratios of the binding reaction to diffusion process, the volume of fluid within the pores to the total volume of fluid, and the concentration within the pore to the bulk concentration provide information on the rate limiting step of the system [29]. The reported forward reaction constant for bFGF binding to heparin ranges from 1 x 10^6 $M^{-1}s^{-1}$ [30] to 0.9 x 10^8 $M^{-1}s^{-1}$ [31]. The diffusivity of bFGF in free solution is estimated to be on the order of 1.34 x 10^{-6} cm^2/sec . For most immobilization experiments the forward rate constants are large and the diffusivity is small, therefore the process is diffusion controlled [29].

The reaction is assumed to be at equilibrium,

$$S = \frac{CR_T}{K_D + C} \tag{7-9}$$

where R_T is the total concentration of binding sites in the device, K_D is the equilibrium dissociation constant of bFGF and heparin. R_T is the number of binding sites for bFGF on a heparin molecule. Substitution of equation (7-9) into equation (7-1) leads to the complete governing equation,

$$\frac{\partial C}{\partial t} = \left[\frac{D_{gel}}{\varepsilon \left[1 + \frac{(1-\varepsilon) R_T K_D}{(K_D + C)^2} \right]} \right] \nabla^2 C \tag{7-10}$$

The effective diffusivity is dependent on the total binding site concentration, the equilibrium dissociation constant, and the bFGF concentration within the pores, in addition to characteristics of the bFGF molecule itself:

$$D_{eff} = \frac{D_{gel}}{\varepsilon \left[1 + \frac{(1-\varepsilon) R_T K_D}{(K_D + C)^2} \right]} \tag{7-11}$$

7.3 Background

The following sections describe the important characteristics of the molecules and structures involved in the bFGF-immobilized heparin interaction.

7.3.1 Basic Fibroblast Growth Factor

In 1974, Gospodarowicz [32] isolated from the pituitary and the brain a factor found to stimulate 3T3 fibroblast proliferation, thus it was called fibroblast growth factor (FGF). It was not

until 1984 when Shing [33] found that heparin-sepharose affinity chromatography isolated and purified significant quantities of FGF. In 1985 Esch elucidated the primary protein structure of bFGF, and in 1986 the primary gene structure was elucidated by Abraham [34, 35]. bFGF belongs to the fibroblast growth factor family consisting of 8 structurally related proteins. These include acidic FGF (FGF-1), basic FGF (FGF-2), Keratinocyte growth factor, int-2, hst-Kaposi FGF, FGF-5, and FGF-6. aFGF and bFGF are the classical prototypes of this family. sharing between 30 and 55% primary amino acid sequence [36]. bFGF is 45% homologous to *hst*, an oncogene similar to Kaposi's sarcoma oncogene, and is 30% homologous to *int-2*, another oncogene. bFGF is a 16-25 kDa basic protein. As with all fibroblast growth factors, it exhibits unusually high affinity for heparin.

bFGF is found in a wide range of tissues (Table 7-2). It was hypothesized that bFGF might be important in regulating cells of the vascular system as these organs are heavily vascularized. It is found on cell surface membranes or in the ECM (Figure 7-2). Specific cell surface receptors are located on the target cells that respond to bFGF. bFGF binds with high affinity to these receptors. Once bound to these receptors bFGF can be dissociated by the addition of polyanionic compounds such as heparin, protamine, and suramine. There is a lower association with the ECM and with heparan sulfate proteoglycans (HSPGs) located on the surface of the cells.

Table 7-2. bFGF Location in Tissues and Cultured Cells

Tissues	Cultured Normal Cells	Cultured Tumor Cells
Brain	Corneal endothelial cells	Y-1 Adrenal cortex cells
Retina	Capillary endothelial cells	Osteosarcoma U2OS
Pituitary	Pituitary cells	Ewing's sarcoma
Kidney	Ovarian granulosa cells	Rhabdomyosarcoma
Placenta	Adrenal cortex cells	Melanoma
Corpus Luteum	Lens epithelial cells	Hepatoma (Sk HP-1)
Adrenal Glands	Uterine epithelial cells	Retinoblastoma
Immune System	Myoblasts	and others
Prostate	Retinal pigmented epithelial	
Bone	cells	
Cartilage	Vascular smooth muscle cells	
Chondrosarcoma	Astrocytes	
Melanoma	Osteoblasts	

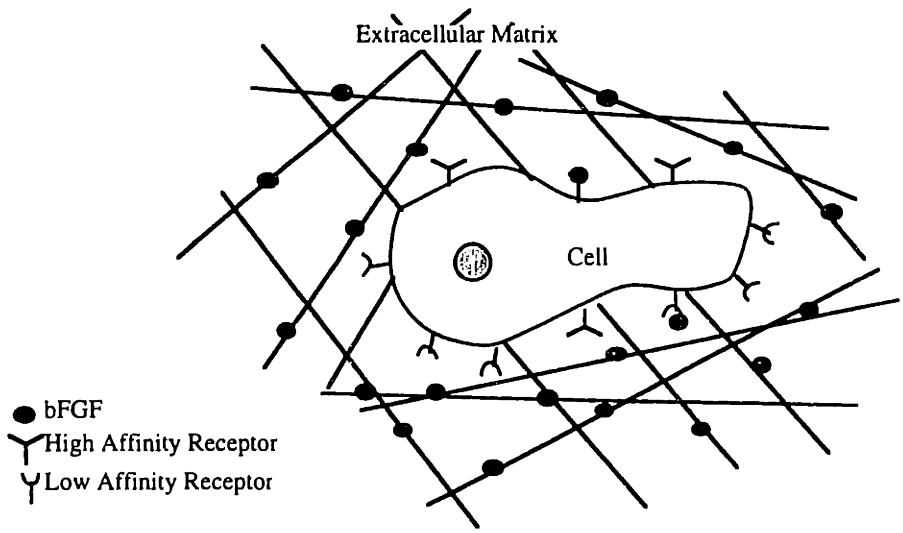

Figure 7-2. bFGF locations in situ

This binding leads to stabilization of the protein from the harsh environment of the extracellular milieu, especially from protease degradation. Extracellular matrix binding also provides an interesting method of stable storage of bFGF until the free form is required by cells. In fact, the ECM with its high concentration of HSPG has been implicated as a source of bFGF during inflammation [37]. bFGF also binds to sulfated GAGs in solution [38].

bFGF regulates a wide variety of physiological processes; development, regeneration, wound healing, and pathogenesis. bFGF has a role in most instances of neovascularization [39]. It is a reported mitogen for a wide variety of cells *in vitro* including endothelial cells, vascular smooth muscle cells, as well as neuronal cells (Table 7-3). bFGF acts on endothelial cells grown on a collagen matrix to promote migration and synthesis of plasminogen activators [40]. Less is known about its effects in vivo. It is one of the most potent angiogenic factors; picomolar quantities induce angiogenesis in vivo [41, 42].

Table 7-3. Cells with bFGF Modulated Proliferation

Endothelial cells-- capillary, large vessels, endocardium	Lens epithelial cells
Vascular smooth muscle cells	Adrenal cortex cells
Fibroblasts	Ovarian granulosa cells
Myoblasts	Prostatic epithelial cells
Chondrocytes	Melanocytes
Neuronal cells	Mesothelial cells
Glial and astroglial cells	Blastema cells
Corneal endothelial cells	Osteoblasts

7.3.2 Heparin

Heparin belongs to the family of glycosaminoglycans (GAG). Glycosaminoglycans are linear heteropolysaccharides possessing a characteristic repeating disaccharide unit usually consisting of alternating uronic acid and amino sugar residues. L-iduronic acid (IdoA) is the prevalent acid and N-sulfated D-glucosamine ($GlcNSO_3$) is the major amino sugar in heparin. Heparin is commonly represented by its major disaccharide units, a-1,4-linked L-iduronic acid 2-sulfate--D-glucosamine N,6-disulfate (IdoA-2S--$GlcNSO_3$-6S). (Figure 7-3). At physiological pH the three acid functional groups in heparin are fully dissociated to yield $-OSO_3^-$, $-NHSO_3^-$, and $-COO^-$.

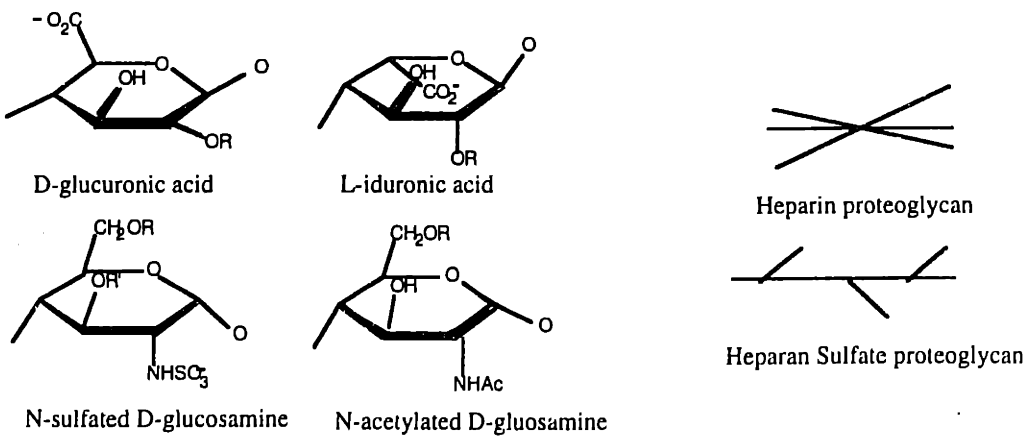

Figure 7-3. Structure of heparin and heparan sulfate proteoglycan

GAGs such as heparin bind to proteins to form proteoglycans and are integral components of basement membrane. They act in mediating processes such as cell adhesion, cell migration, and extracellular immobilization of growth factors. HSPG is a complex polysaccharide, containing many heparin-like residues. HSPG is implicated in retaining growth factors in the ECM, shuttling growth factors during paracrine signaling, and acting as an accessory receptor to promote binding of bFGF to high affinity receptors. Most of the extracellular bFGF is immobilized on HSPG and it is thought that HSPG potentiates the mitogenic activity of bFGF.

Commercially available heparin chains are the result of depolymerization of long native heparin chains. These chains are polydisperse in molecular weight (from 5000-25000 MW) due to the uneven distribution of particular saccharide sequences along the heparin chain and the length of the chain. Native heparin is composed of families of chains rather than a continuum of lengths [43]. In addition, differences in the primary structure of heparin; i.e. the nature of the uronic acid, the occurrence of substituted or unsubstituted glucosamine, the degree of sulfation, and the position of sulfation contribute to the polydispersity [44]. This polydispersity leads to difficulty in quantifying kinetic binding properties.

7.3.3 bFGF-Heparin Interaction

The heparin bFGF interaction is thought to impart stabilization of the bFGF against proteolytic, thermal, and pH-dependent degradation and denaturation [45-50]. The heparin binding site on bFGF and the bFGF binding site has been much investigated. Various techniques have been utilized; reductive methylation of aFGF lysine residues, bFGF deletion mutation analysis, synthetic peptide studies[39], x-ray crystallography [46, 47], and site directed mutagenesis [51]. The heparin binding sequence on bFGF is composed of 2 discontinuous sequences of positively charge amino acids [39]. These sequences are in the region of amino acids 24-68 and 93 - 120. In addition, the basic amino acids in the region of 115 - 129 are important for heparin affinity and receptor binding [39, 46, 47, 51].

In contrast to the determination of the binding sites on bFGF, the binding site on heparin has been much more elusive. Heparin is a strongly anionic polyelectrolyte molecule. Such interactions are influenced by protein/polysaccharide concentration ratios, protein/polysaccharide charge ratios, and the pH of the solution. Critical concentrations of sugar can lead to phase separations, resulting in mechanisms of self-association of the protein. It is postulated that there are three types of protein binding sites on the heparin molecule: 1) non-specific such as interactions with fibronectin, 2) electrostatic, and 3) specific such as the anti-thrombin III binding site (which is a hexasaccharide unit) and the linking sequence which links the glucosamine to a serine residue. Anti-thrombin III binds with high specific affinity to a pentasaccharide heparin sequence containing a 3-O-sulfate on the central glucosamine and several critical N- and O-sulfates on the other saccharides. It was hoped that the bFGF binding site would be similar to the anti-thrombin III site.

The goal of numerous studies was to elucidate the "minimal structural" requirements of heparin needed to interact with bFGF. The important structural properties are the number of saccharides, the saccharide sequence, and the sulfation pattern. There is some disagreement on the minimal length required to bind bFGF. Octasaccharides [52-54], 7 disaccharide units [55], decasaccharide [56], and tetrasaccharides [57] are all proposed. However, it is generally accepted that the minimal length required to bind to bFGF and to maintain its mitogenic activity is between a deca- and a dodecasaccharide. For example, 8-10 sugar residues are required to obtain 50 - 80% high affinity binding to CHO cells [57].

A different approach is to calculate the molecular weight of the binding site. Arakawa et al measured the bFGF binding site as approximately 2300 kDa, which is about equivalent to an octasaccharide [58]. Arakawa, et al, found between 6 -7 binding sites on 15,000 Da heparin and 2 sites on 5000 Da heparin. This differs from the result found by Mach et al for aFGF of a 250 kDa site [30]. Other investigators using site-directed mutagenesis of the bFGF molecule discovered a 4-5 monosaccharide binding site on 5000 MW heparin (~25 Å in length) [59]. Ten bFGF molecules bound to a 14-16 kDa heparin, which leads to a 1400 - 1600 kDa binding site [60].

The sugars that comprise this length of binding region are also important. The dominant structural unit (5 of 7 disaccharides) was IdoA(2-SO_3)α1,4 GlcNSO_3 [54, 55]. The clustering of 3-IdoA(2-SO_4)-containing disaccharide units and an unsulfated unsaturated hexuronic acid occupying the nonsaturated ends are important structural requirements [53, 54].

Sulfation patterns were investigated independently of the disaccharide structure. Initially, it was found that desulfation of heparin prevents the interaction with FGF [11]. Further studies revealed that the presence of N-sulfates is critical to the release of matrix-bound bFGF and that O-sulfation facilitated release but was not an absolute requirement [52, 57]. Maccarana et al showed that the GlcN 6-O-sulfate was not important [54]. The N- and the 2-O-sulfate groups were relevant and essential for bFGF binding but that the 6-O-sulfate groups were irrelevant [38, 55, 61]. However, this was recently contradicted when it was found that bFGF will bind to nonsulfated tetra- and tri- saccharide units [62]. bFGF can specifically recognize structural features of the nonsulfated carbohydrate backbone of heparin/heparan sulfate independent of ionic interactions with highly charged sulfate groups [62]. It is generally believed that the sulfate groups are essential for mitogenic activity.

The equilibrium binding constant for the bFGF-heparin interaction spans five orders of magnitude (Table 7-4). A possible explanation for this large range could be due to different experimental conditions. In conclusion, it is generally agreed that to obtain any biological activity of the immobilized bFGF there must be a larger heparin sequence such as an octomer [62] or dodecasaccharide [63]. The heparin must be sulfated to maintain activity but a specific complementary epitope is not required.

Table 7-4. Equilibrium Binding Constants for bFGF-Heparin Interaction

Method	K_D (nM)	Citation
Light Scattering	50	[30]
Plasmon Resonance	140	
Isothermal Titration Calorimetry	505 ± 227	[64]
	461 ± 357	
Competitive Binding in Solution	NA	[62]
Fluorescence Spectroscopy	0.4 - 0.7[a]	[65]
	0.8 - 1.8[b]	
Light Scattering	10	[58]
Isothermal Titration Calorimetry	470	[59]
	1300 ± 280	
Cell Binding (Bovine Capillary Endothelial Cells)	0.013 (high affinity) 0.76 (low affinity)	[31]
Cell Binding (Chinese Hamster Ovary Cells)	NA	[66]
Endothelial Cell Membrane "Cell"	610	[11]
Cell Binding (HOME)	.0422 (high affinity)	[67]
	0.922 (low affinity	
Light Scattering	NA	[50]
Isothermal Titration Calorimetry	470 ± 20	[68]

[a] acidic fibroblast growth factor
[b] basic fibroblast growth factor

7.3.4 Sepharose Gels

Cross-linked polysaccharides (such as agarose) are utilized extensively for gel filtration, adsorbents, and affinity columns. Agarose is a polysaccharide with high gelling ability that consists of alternating copolymer of 3-linked b-D-galactopyranose and 4-linked 3,6 - anhydro-α-L-galactopyranose residues [69]. Its physical structure is composed of "junction zones" or non-covalent cooperative binding of chains in an ordered conformation (Figure 7-4). The molecule forms a double-helix with 0.95 axial periodicity, 1.90 nm pitch of left-handed 3-fold helix, axial cavity of 0.45 nm (presumed to be occupied by water), chain density of 1.4 g/ml, mass/length 0.17e-13 g/cm. The helices are an extensive laterally aggregated composition of many chains (10-10^4) in a side-by -side assembly [70]. The chains are like long stiff rods. There are large voids, that vary in diameter up to 0.3 μm in sepharose 4B. The assembly is between 20-300 Å thick and the helix diameter equals 15 Å thick. Agarose activated with CNBr, then reacted with an excess of

an α–ω-diaminoalkane and cross-linked with glutaraldehyde (cross-linked agarose) exhibited a structure indistinguishable from those of uncross-linked agarose [69]. High salt increases the probability of empty gel areas, and decreases the distribution of the number of intersections. 4% agarose contains fibers of radius 1-15 nm with the number of helices/fiber approximately 1-200.

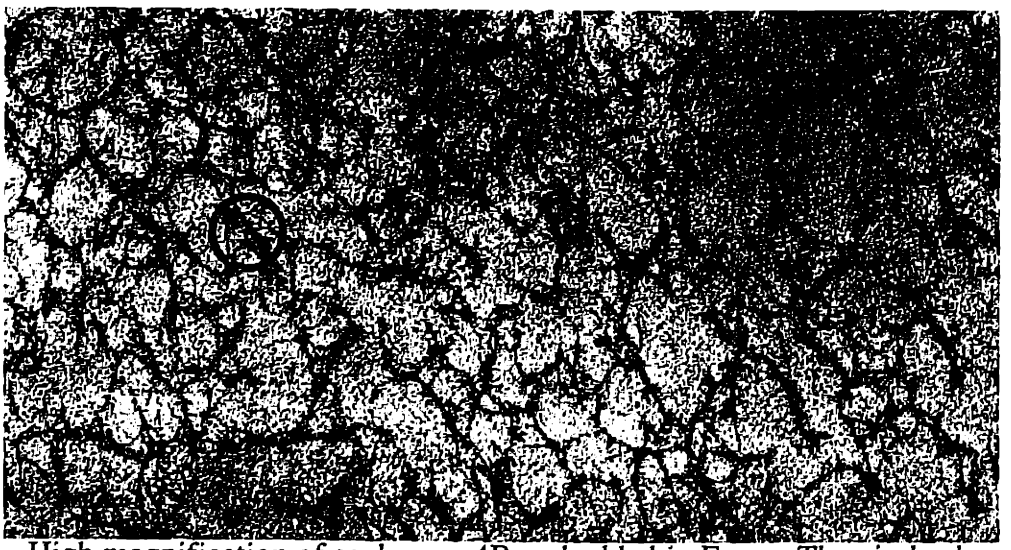

Figure 7-4. High magnification of sepharose 4B embedded in Epon. The circle shows the side-by-side assembly of thin filaments in the matrix framework (from Amsterdam [69]).

7.4 Materials and Methods

Materials. The source of materials was as follows: Sepharose CL-6B, and heparin immobilized on 4% agarose (heparin-agarose), heparin sodium salt Grade 1 from pig intestinal mucosa, Sigma Chemical Company (St. Louis, MO); Heparin-sepharose CL-6B, Pharmacia (Uppsala, Sweden); heparin sodium salt from porcine intestinal mucosa, Hepar Industries (Franklin, OH); Glycine, Mallinckrodt (Paris, KY); 1,9-Dimethyl-Methylene Blue (DMB), Aldrich Chemical Company (Milwaukee, WI); bFGF, R&D Systems (Minneapolis, MN); ^{125}I-bFGF (provided by Dr. M. Nugent); CNBr, Tris, $NaHCO_3$, sigmacote, Sigma Chemical Company (St. Louis, MO).

Binding assay. Heparin-sepharose, heparin-agarose, and sepharose microbeads were incubated with bFGF and ^{125}I-bFGF in siliconized (sigmacote) reaction vials pre-coated with albumin (5% albumin in normal saline). The desired total amount of heparin in 100 µl total volume was achieved by increasing the amount of heparin containing microbeads. In most of the incubation set-ups the volume percentage of solids was less than 0.6%. 0.1 µg of bFGF/^{125}I-bFGF (in a solution composed of 50 mM Tris, 1 mM CaCl2, 0.5% BSA) was added to each vial. The tubes were incubated at room temperature on an oscillating shaker to maintain gel suspension. The well-mixed reaction proceeded at room temperature for 2 hours at which time a sample volume of supernatant was removed for analysis (1272 CliniGamma gamma counter, LKB Nuclear). In addition, all ^{125}I-bFGF containing solutions were analyzed before and after incubation for free and protein associated radioactivity by trichloroacetic acid precipitation.

Trichloroacetic acid precipitation. For every microliter of sample, 1 microliter of a 10 mg/ml BSA solution, 2 microliters of KI (10 mM), 14 microliters of NaCl (150 mM), and 2.5 microliters of 100% TCA were added. The solution was vortexed, incubated at 4°C for 10 minutes, and then centrifuged for 3 minutes. The supernatant was removed and the radioactivity was assessed in the supernatant and the resuspended pellet (1272 Clinigamma gamma counter, LKB Nuclear).

Heparin-sepharose fragmentation. Swelled heparin-sepharose microbeads were ground in a volume of 1.5 ml of water for 3 minutes. Microscopically the majority of microbeads were in fragments, a minority of microbeads contained rough edges, deep cracks, or missing fragments. Heparin content was measured in the supernatant over the fragmented beads.

Sepharose activation. Sepharose activation by cyanogen bromide has been previously described [71]. Briefly, 1 g of wet Sepharose CL-6B was placed in a volume of 5 M potassium phosphate buffer (pH 11.9 at 10x dilution) dependent on the amount of activation desired (Table 7-

5). All solutions were diluted up to 2 ml with water and maintained at 4°C. Cyanogen bromide (1 g/ml in acetonitrile) was added slowly to the slurry and the solutions were stirred gently for 10 minutes. The activated sepharose was washed with water to pH 7; washed and resuspended in 0.1 M $NaHCO_3$.

Table 7-5. Activation Solution Volumes.

Activation	5M Potassium Phosphate Buffer	CNBr solution
High Activation	1.5 ml	600 µl
Medium Activation	0.3	120
Weak Activation	0.072	30

Covalent linkage of heparin to activated sepharose. Heparin coupling to activated sepharose has been previously described [72]. Suction dried activated gel was incubated with a heparin concentration of 10 mg/ml gel. The total volume was increased with 1 ml of 0.1 M $NaHCO_3$. The reaction mixture was stirred end-over-end for 16 hours at 4°C. A sample volume of the supernatant was removed for heparin content analysis. The gel was then sequentially washed with 0.01 M Tris-HCl in 0.15 M NaCl (pH 7.3), 1 M glycine (pH 8.5), and 0.01 M Tris-HCl in 0.15 M NaCl (pH 7.5).

Heparin Content Analysis. Heparin content in the sepharose gels was determined by the colorimetric DMB assay against a heparin standard [73]. Briefly 16 mg DMB was dissolved in 1 L water containing 3.04 g glycine , 2.37 g NaCl, and 95 ml 0.1 M HCl (pH 3.0, A_{525} = 0.31). The DMB reagent was made up fresh each month and stored in a brown bottle at room temperature. Two milliliters of DMB reagent was added to 100 µl of a standard heparin solution and the absorbance at 526 nm was measured within 1 minute (Beckman DU640 Spectrophotometer). Permeabolization in 0.1 N NaOH at 100°C for 16 hours liberated heparin from the sepharose gels. The resultant solution was neutralized to pH 7.0 by the addition of 0.1 N HCl. 100 µl of this solution was added to DMB reagent(2 ml) and the absorbance at 526 nm was measured.

7.5 Results and Discussion

The time dependence of incorporation of bFGF into heparin-sepharose microbeads is shown in Figure 7-5. Heparin-sepharose microbeads were incubated with bFGF for the indicated times. bFGF incorporation and release from heparin-sepharose microbeads is achieved by movement from the bulk solution into the sepharose, diffusion through the sepharose gel, and specific binding to immobilized heparin within the gel. The expected behavior depends on the relative rates of diffusion and reaction.

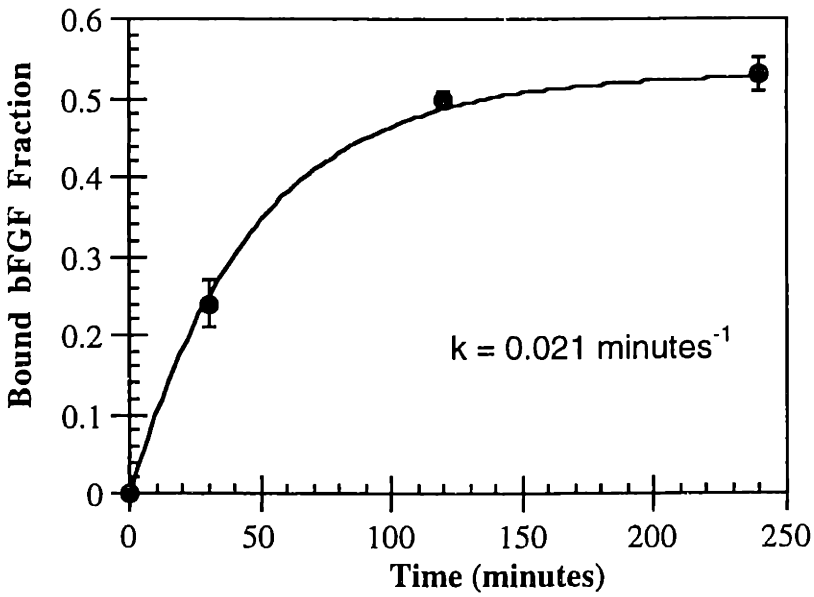

Figure 7-5. Equilibration of the bFGF-heparin-sepharose system. The total volume was 100 µl. Heparin-sepharose microbeads containing 2 mg/ml heparin were added such that the effective heparin concentration in the solution is 556 nM. The initial concentration of bFGF in solution was 62.5 nM. Data points represent the mean of triplicate vials ± standard deviations.

We can estimate the time for the diffusion process to reach equilibrium as $t \approx r^2/D_0$. The radius of a microbead is 45 µm and D_0 is on the order of 1.31 x 10^{-6} cm^2/sec, thus the characteristic time for diffusion is on the order of 15 seconds. However, as was predicted for our model, diffusion is also dependent on the total binding site concentration, the equilibrium dissociation constant, and the bFGF concentration within the pores. The time required for the

system to reach equilibrium was approximately 120 minutes. Based on this result, subsequent incubations were for 2 hours. The observed lumped rate constant was 0.02/minute.

The total amount of heparin available is 0.11 nmole and assuming that there are 6 - 7 binding sites for bFGF per heparin molecule [58] we predict that the heparin binding sites to bFGF ratio is approximately 100:1 in this experiment. If we assume that the concentration just within the pore is equivalent to the bulk concentration and using reported K_Ds from the literature, then Equation (7-9) predicts that 100% of the initial bFGF should be bound. A maximum of 50% of the bFGF was bound under the conditions of this experiment.

The diffusivity of bFGF in sepharose gels is dependent on the size, charge, and affinity of the bFGF molecule. The diffusivity in gels where the pore radius, the interfiber spacing, or other dimensions of the microstructure are comparable to the radius of the solute molecule is decreased, and the decrease is dependent on the molecular size. The exclusion size for sepharose microbeads is reported to be on the order of 4,000 kDa globular protein. Utilizing albumin as a test globular protein (MW 68,000 Da, Stokes-Einstein radius 3.5 nm) we obtain a pore radius of 206 nm (exclusion size x $r_{albumin}/MW_{albumin}$). This is only slightly different from 0.3 μm interfiber spacing reported by Amsterdam et al [69]. The Stokes-Einstein radius of bFGF was calculated by assuming that the diffusion coefficient is inversely proportional to the cube root of the molecular weight and the radius of albumin is 3.5 nm [28], is 1.6 nm. The potential decrease in pore size due to the presence of heparin within the interfiber spaces might decrease the pore size. The maximal attainable λ would be if a monolayer of heparin molecules were stretched to their full length of 30 nm. This is given by

$$\lambda_f = \lambda\left[1-4\lambda(1-\lambda)\right]^{-1/2} \qquad (7\text{-}12)$$

For the heparin-sepharose system thsi yeilds a λ_f of 0.20, which is sufficient to reduce the diffusion coefficient but not to cause pore blockage. However, it is unlikely that the heparin

molecules would be in the stretched out configuration. Thus, there should be no hindrance to diffusion of bFGF within the sepharose microbeads because $r_{pore} >> r_{bFGF}$.

One possible explanation for the decreased amount bound is that the amount of heparin per microbead is less than expected. Our own determination of the heparin in these microbeads using the DMB assay was 2.1±.02 mg/ml which is similar to Pharmacia's measurement (2 mg/ml).

To assess whether the binding we observed in the first experiment was simply due to nonspecific binding to sepharose we incubated bFGF with sepharose microbeads. Labeled bFGF was incubated with increasing volumes of sepharose microbeads. The amount of bFGF that binds to sepharose is negligible (Figure 7-6). Microbead volumes ranged from 10% to 42.5% and were incubated with ^{125}I-bFGF (no cold bFGF) for 1 hour. The amount of bFGF associated with sepharose is obtained by assuming that 4% of the microbead volume is composed of sepharose. The bound ratio for the highest concentration of microbeads was 1.7%. Nonspecific binding does not account for the amount of bFGF bound to heparin-sepharose microbeads.

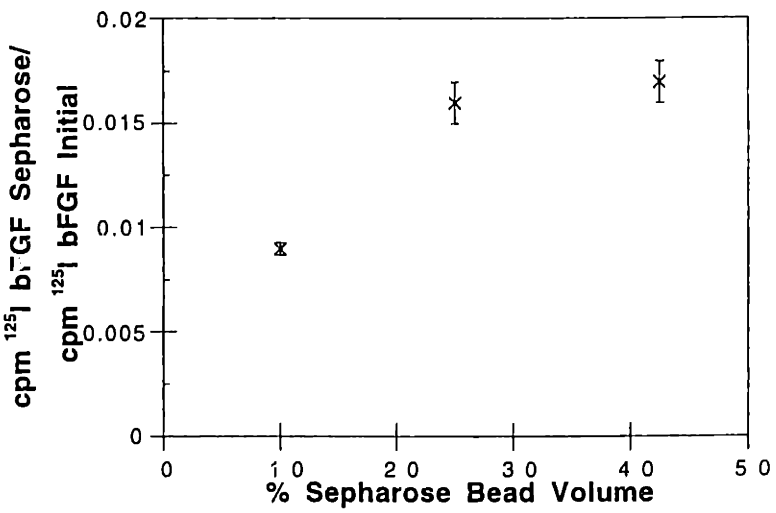

Figure 7-6. Nonspecific binding of ^{125}I-bFGF to sepharose microbeads. Data points represent the mean of triplicate vials ± standard deviations.

To asses the availability of heparin we investigated the binding of bFGF to a known volume of mechanically fragmented heparin-sepharose microbeads as compared to the same

volume of intact heparin-sepharose microbeads. We were concerned that heparin may be released from the sepharose as a result of the mechanical fragmentation. Heparin loss from the fragmented beads was negligible as determined by DMB assay of the solution over the fragmented microbeads. The concentration of heparin in this experiment was twice that of the initial experiment, but this did not affect the fraction of bFGF bound to intact beads. The difference of bound bFGF between fragmented and intact microbeads was not significant (Figure 7-7).

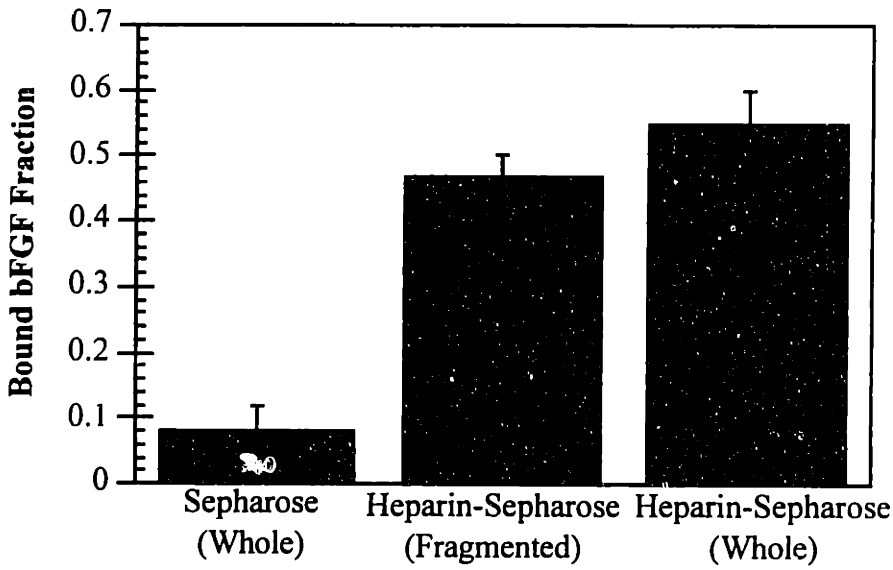

Figure 7-7. Heparin availability. 1111 nM Heparin and 62.5 nM bFGF were incubated in 100 µl for 2 hours. Each bar represents the mean of triplicate vials ± standard deviation.

There are four commonly used schemes for binding heparin to sepharose microbeads. These are 1) Carbodiimide; average amounts of heparin bound are 0.12-0.6 mg/ml wet gel [74], 2) Woodward's Reagent K; average amounts of heparin bound are 0.5 -3.1 mg/ml wet gel [75], 3) Sodium cyanoborohydride; average amounts of heparin bound are 2.9 mg/g wet gel [76], and 4) Cyanogen bromide; average amounts of heparin bound are 3.2 mg/ml wet gel [74].

The amount of heparin bound can be determined from a mass balance comparing the initial concentration with the final concentration in the incubate. There are approximately 7 different methods to test for glycosaminoglycan content (Table 7-6). This study utilized the DMB assay. DMB is a strongly metachromatic dye for the detection of sulfated glycosaminoglycans [77].

Table 7-6. Glycosaminoglycan (Heparin) Content Assays

Assay	Citation
Glucosamine-Elson Morgan	[78, 79]
Glucosamine-Ninhydrin	[80]
Uronic acid-Carbazole reaction	[79, 80]
Dye binding-Azure A	[80]
Dye binding-Orcinol	[81]
Dye binding-Toluidine Blue	[82]
Dye binding-Dimethylmethylene Blue	[73]
Elemental Analysis-Sulfur	[79]
Radiolabelling-^{14}C	[83]
Thrombin activity	[72, 84, 85]

In addition, we attempted to produce heparin-sepharose beads with increased heparin concentration within the beads themselves. Our results with preparing our heparin sepharose beads as well as a comparison of the DMB assay to Pharmacia's analysis of their heparin-sepharose product and Sigma's analysis of their heparin-agarose product is shown in Table 7-7. It has been shown that only one third of the amount transferred from the liquid to the gel phase remains bound after subsequent washes [79]. It is thought that this is due to heparin binding to 'brittle' parts of the gel beads and are easily lost during washing [79]. Therefore, the concentration of heparin in our microbeads, while low, is in agreement with predicted results.

Table 7-7. Heparin content within Gels

Activation Method	Heparin incubation (mg/ml gel)	post-wash Heparin (mg/ml gel)
High Activation (A)	12.81	3.63
Acetonitrile Activation (Ac)	11.08	1.07
Low Activation (C)	10	2.35
Blocked	10	0
	DMB Assay	Company Lite
Heparin-Sepharose (Pharmacia)	2.64±0.98	
Heparin-Agarose (Sigma)	1.11±0.06	0.3

We performed the equilibrium binding experiment on the new heparin-sepharose microbeads. The microbeads formulated in our laboratory bound less bFGF than those microbeads supplied by Pharmacia (Figure 7-8). There appears to be no correlation between heparin concentration within the microbeads and the amount of bFGF bound to the microbeads.

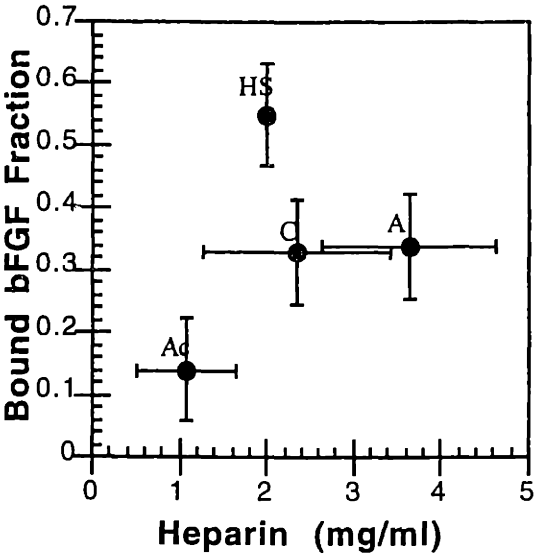

Figure 7-8. Heparin content modification. Data included are heparin-sepharose microbeads from Pharmacia (HS), high activation (A), low activation (C), and acetonitrile activation (Ac) heparin sepharose microbeads. Data points represent the mean of triplicate vials ± standard deviations.

The effect of increasing the heparin concentration in the entire solution volume was evaluated by increasing the total volume of heparin-sepharose microbeads. The volume of microbeads was kept constant by the inclusion of sepharose microbeads. bFGF concentration was kept constant at 62.5 nM. Each data point represents triplicate vials. The results were not similar to the predicted equilibrium expression (Figure 7-9). Conservative estimates are given for K_D and the number of bFGF binding sites on heparin (n). As the model predicts the fraction of bFGF should approach unity as the heparin concentration is increased (Equation 7-9). Experimental limit appears to be 80%.

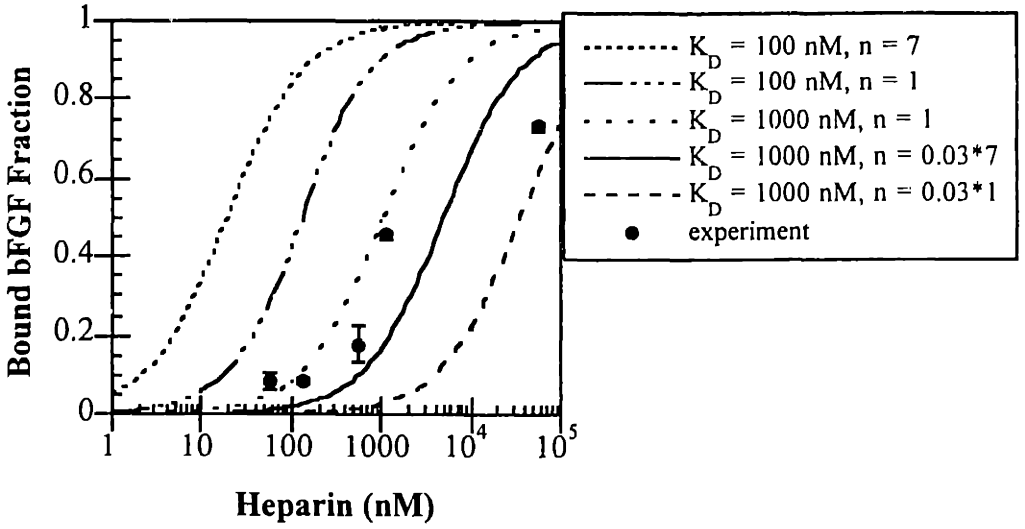

Figure 7-9. Saturation binding. Heparin concentration was increased by increasing the heparin sepharose microbead population in the incubation mixture. bFGF remained constant at 62.5 nM; total volume was 100 µl. The curves are the model predictions. Each data point represents the mean of triplicate vials ±standard deviations.

A possible explanation for this could be that we have two populations of bFGF in solution which exhibit different affinities for heparin. To evaluate this possibility we incubated 62.5 nM bFGF with 55600 nM heparin (equivalent in solution) for 2 hours. A sample of the supernatant was removed for counting. The remainder of the supernatant was incubated with fresh 55600 nM heparin for 2 hours. A sample of this supernatant showed that 15% of the bFGF remaining in solution after the first incubation bound to fresh heparin-sepharose.

7.6 Conclusions

The heparin-sepharose-alginate release system has been proposed for use in the clinical setting. Assumptions about the binding kinetics have been made based on results obtained in free solution and on cell surfaces. The results from this study show that this leads to false

interpretation of the data. In this study we investigated the kinetics of bFGF incorporation into the beads, the diffusion limits, and the saturation binding properties of heparin-sepharose gels.

We have shown that the heparin binding capacity for bFGF is significantly less than that predicted from previous experiments. We have shown that non-specific binding is not significant in describing bFGF immobilization to heparin-sepharose microbeads. Increasing the availability for bFGF binding to heparin by mechanical fragmentation does not increase the bound bFGF fraction. Changing the concentration of heparin within the beads itself did not significantly change the fraction of bFGF immobilized to the heparin-sepharose microbeads.

7.7 References

1. Thompson, J., K. Anderson, J. DiPietro, J. Zweibel, M. Zameta, W. Anderson, and T. Maciag, Site-directed neovessel formation in vivo. Science. **241**: 1349-1352 (1988).

2. Tabata, Y., S. Hijikata, and Y. Ikada, Enhanced vascularization and tissue granulation by basic fibroblast growth factor impregnated in gelatin hydrogels. Journal of Controlled Release. **31**: 189-199 (1994).

3. Nguyen, M., Y. Shing, and J. Folkman, Quantitation of angiogenesis and antiangiogenesis in the chick embryo chorioallantoic membrane. Microvascular Research. **47**: 31-40 (1994).

4. Edelman, E., M. Nugent, and M. Karnovsky, Perivascular and intravenous administration of basic fibroblast growth factor: Vascular and solid organ deposition. Proceedings of the National Academy of Sciences. **90**: 1513-1517 (1993).

5. Edelman, E., M. Nugent, L. Smith, and M. Karnvsky, Basic fibroblast growth factor enhances the coupling of intimal hyperplasia and proliferation of vasa vasorum in injured rat arteries. Journal of Clinical Investigation. **89**: 465-473 (1992).

6. Thompson, J., C. Haudenschild, K. Anderson, J. DiPietro, W. Anderson, and T. Maciag, Heparin-binding growth factor 1 induces the formation of organoid neovascular structures in vivo. Proceedings of the National Academy of Sciences. **86**: 7928-7932 (1989).

7. Knighton, D., G. Phillips, and V. Fiegel, Wound healing angiogenesis: Indirect stimulation by basic fibroblast growth factor. The Journal of Trauma. **30**(12 Supplement): S134-S144 (1990).

8. Norrby, K., Basic fibroblast growth factor and *de Novo* mammalian angiogenesis. Microvascular Research. **48**: 96-113 (1994).

9. Nabel, E., Z. Yang, G. Plautz, R. Forough, X. Zhan, C. Haudenschild, T. Maciag, and G. Nabel, Recombinant fibroblast growth factor-1 promotes intimal hyperplasia and angiogenesis in arteries in vivo. Nature. **362**: 844-846 (1993).

10. Sprugel, K., J.M. Pherson, A. Clowes, and R. Ross, Effects of growth factors in vivo I. Cell ingrowth into porous subcutaneous chambers. American Journal of Pathology. **129**(3): 601-613 (1987).

11. Bashkin, P., S. Doctrow, M. Klagsbrun, C. Svahn, J. Folkman, and I. Vlodavsky, Basic fibroblast growth factor binds to subendothelial extracellular matrix and is released by heparitinase and heparin-like molecules. Biochemistry. **28**: 1737-1743 (1989).

12. Passaniti, A., R. Taylor, R. Pili, Y. Guo, P. Long, J. Haney, R. Pauly, D. Grant, and G. Martin, A simple, quantitative method for assessing angiogenesis and antiangiogenic agents using reconstituted basement membrane, heparin, and fibroblast growth factor. Laboratory Investigation. **67**(4): 519-528 (1992).

13. Edelman, E., E. Mathiowitz, R. Langer, and M. Klagsbrun, Controlled and modulated release of basic fibroblast growth factor. Biomaterials. (1991).

14. Nugent, M., O. Chen, and E. Edelman. Controlled release of fibroblast growth factor: Activity in cell culture. in Materials Research Society. 1992. Boston: Materials Research Society.

15. Yamamura, K., T. Sakurai, K. Yano, T. Nabehsima, and T. Yotsuyanagi, Susatained release of basic fibroblast growth factor from the synthetic vascular prosthesis using hydroxypropylchitosan acetate. Journal of Biomedical Materials Research. **29**: 203-206 (1995).

16. Hickey, M. and W. Morrison, An improved matrx-type controlled release system for basic fibroblast growth factor. Biochemical and Biophysical Research Communications. **201**(3): 1066-1071 (1994).

17. Stagnor, J. and E. Samols, Induction of angiogenesis by growth factors: relevance to pancreatic islet transplantation, in Angiogenesis: Key Principles-Science-Technology-Medicine, R. Steiner, P. Weisz, andR. Langer, Editors. 1992, Birkhäuser-Verlag: Basel. p. 381-385.

18. Andrade, S., T. Fan, and G. Lewis, Qunatitative in-vivo studies oin angiogenesis in a rat sponge model. Journal of Experimental Pathology. **68**: 755-766 (1987).

19. Fajardo, L., J. Kowalski, H. Kwan, S. Prionas, and A. Allison, Methods in laboratory investigation: The disc angiogenesis system. Laboratory Investigation. **58**(6): 718-724 (1988).

20. Andrade, S., Y. Bakhle, I. Hart, and P. Piper, Effects of tumour cells on angiogenisi and vasoconstrictor responses in sponge implants in mice. (1992).

21. Maragoudakis, M., N. Tsopanoglou, M. Bastaki, and G. Haralabopoulos, Evaluation of promoters and inhibitors of angiogenesis using basement membrane biosynthesis as an index, in Angiogenesis in Health and Disease, M. Maragoudakis, P. Gullino, andP. Lelkes, Editors. 1992, Plenum Press: New York. p. 275-285.

22. Nicosia, R. and A. Ottinetti, Growth of microvessels in serum-free matrix culture of rat aorta. Laboratory Investigation. **63**(1): 115-122 (1990).

23. Norrby, K., On the quantitative rat mesenteric-window angiogenesis, in Angiogenesis: Key Principles-Science-Technology-Medicine, R. Steiner, P. Weisz, andR. Langer, Editors. 1992, Birkhäuser Verlag: Basel. p. 282-286.

24. Vu, M., C. Smith, P. Burger, and G. Klintworth, Methods in laboratory investigation: An evaluation of methods to quantitate the chick chorioallantoic membrane assay in angiogenesis. Labo ıtory Investigation. **53**(4): 499-508 (1985).

25. Dellian, M., B. Witwer, H. Salehi, F. Yuan, and R. Jain, Quantitation and physiological characterization of angiogenic vessels in mice. American Journal of Pathology. **149**: 59-71 (1996).

26 Bernstein, H., V. Yang, and R. Langer, Distribution of Heparinase Covalently Immobilized to Agarose: Experimental and Theoretical Studies. Biotechnology and Bioengineering. **30**: 196-207 (1987).

27. Anderson, J. and J. Quinn, Restricted transport in small pores. A model for steric exclusion and hindered particle motion. Biophysical Journal. **14**: 130 (1974).

28. Yuan, F., M. Dellian, D. Fukumura, M. Leunig, D. Berk, V. Torchillin, and R. Jain, Vascular permeability in a human tumor xenograft: Molecular size dependence and cutoff size. Cancer Research. **55**: 3752-3756 (1995).

29. Do, D., D. Clark, and J. Bailey, Modeling Enzyme Immobilizaton in Porous Solid Supports. Biotechnology and Bioengineering. **24**: 1527-1546 (1982).

30. Mach, H., D. Volkin, C. Burke, R. Linhardt, J. Fromm, D. Loganathan, and L. Mattsson, Nature of the interaction of heparin with acidic fibroblast growth factor. Biochemistry. **32**: 5480-5489 (1993).

31. Nugent, M. and E. Edelman, Kinetics of basic fibroblast growth factor binding to its receptor and heparan sulfate proteoglycan: A mechanism for cooperativity. Biochemistry. **31**(37): 8876-8883 (1992).

32. Gospodarowicz, D., J. Cheng, G.-M. Lui, A. Baird, and P. Böhlent, Isolation of brain fibroblast growth factor by heparin-sepharose affinity chromatography: Identity with pituitary fibroblast growth factor. Proceedings of the National Academy of Sciences. **81**: 6963-6967 (1984).

33. Shing, Y., J. Folkman, R. Sullivan, C. Butterfield, J. Murray, and M. Klagsbrun, Heparin affinity: Purification of a tumor-derived capillary endothelial growth factor. Science. **223**: 1296-1298 (1984).

34. Esch, F., N. Ueno, A. Baird, F. Hill, L. Denoroy, N. Ling, D. Gospodarowicz, and A. Guillemin, Primary Structure of bovine brain acidic fibroblast growth factor. Biochemical and Biophysical Research Communications. **133**(2): 554-562 (1985).

35. Abraham, J., J. Whang, A. Tumoro, A. Mergia, J. Friedman, D. Gospodarowicz, and J. Fiddes, Human bFGF: Nucleotid sequence and genomic organization. Embo Journal. **5**(10): 2523-2528 (1986).

36. Dionne, C., G. Crumley, F. Bellot, J. Kaplow, G. Searfoss, M. Ruta, W. Burgess, M. Jaye, and J. Schlessinger, Cloning and expression of two distinct high-affinity receptors cross-reacting with aFGF and bFGF. EMBO Journal. **9**(9): 2685-2692 (1990).

37. Rogelj, S., M. Klagsbrun, R. ATzmon, M. Kurokawa, A. Haimovitz, Z. Fuks, and I. Vlodavsky, Basic fibroblast growth factor is an extracellular matrix component required for

supporting the proliferation of vascular endothelial cells and the differentiation of PC 12 cells. Journal of Cell Biology. **109**: 823-831 (1989).

38. Rusnati, M., D. Coltrini, P. Caccia, P. Dell'Era, G. Zoppetti, P. Oreste, B. Valsasina, and M. Presta, Distinct role of 2-O-,N-, and 6-O-sulfate groups of heparin in the formation fo the ternary complex with basic fibroblast growth factor and soluble FGF receptor-1. Biochemical and Biophysical Research Communications. **203**(1): 450-458 (1994).

39. Baird, A., D. Schubert, N. Ling, and R. Guillemin, Receptor- and heparin-binding domains of basic fibroblast growth factor. PNAS. **85**: 2324-2328 (1988).

40. Montesano, R., M. Pepper, J. Vassalli, and L. Orci, Modulation of angiogenesis in vitro, in Angiogenesis: Key Principles-Science-Technology-Medicine, R. Steiner, P. Weisz, andR. Langer, Editors. 1992, Birkhäuser Verlag: Basel. p. 129-136.

41. Folkman, J. and M. Klagsbrun, Angiogenic factors. Science. **235**: 444-447 (1987).

42. Shing, Y., J. Folkman, C. Haudenschild, D. Lund, R. Crum, and M. Klagsbrun, Angiogenesis is stimulated by a tumor-derived endothelial growth factor. Journal of Cellular Biochemistry. **29**(4): 275-87 (1985).

43. Casu, B., Structure of Heparin and Heparin Fragments. Annals of New York Academy of Sciences. **556**: 1-17 (1989).

44. Danishefsky, I., L. Rosenfeld, L. Kuhn, B. Lahiri, and C. Whyzmuzis, Location of specific units in heparin and heparan sulfate. Annals New York Academy of Sciences. **556**: 29-35 (1989).

45. Saksela, O., D. Moscatelli, A. Sommer, and D. Rifkin, Endothelial cell-derived heparan sulfate binds basic fibroblast growth factor and protects it from proteolytic degradation. Journal of Cell Biology. **107**: 743-751 (1988).

46. Zhang, J., L. Cousens, P. Barr, and S. Sprang, Three-dimensional structure of human basic fibroblast grwoth factor, a structural homolog of interleukin 1B. PNAS. **88**: 3446-3450 (1991).

47. Eriksson, A., L. Cousens, L. Weaver, and B. Matthews, Three-dimensional structure of human basic fibroblast growth factor. PNAS. **88**: 3441-3445 (1991).

48. Chen, B., T. Arakawa, C. Morris, W. Kenney, C. Wells, and C. Pitt, Aggregation pathway of recombinant human keratinocyte growth factor and its stabilization. Pharmaceutical Research. **11**(11): 1581-1587 (1994).

49. Venkataraman, G., V. Sasisekharan, A. Herr, D. Ornitz, G. Waksman, C. Cooney, R. Langer, and R. Sasisekharan, Preferential self-association of basic fibroblast growth factor is stabilized by heparin during receptor dimerization and activation. Proceedings of the National Academy of Sciences. **93**: 845-850 (1996).

50. Volkin, D., P. Tsai, J. Dabora, J. Gress, C. Burke, R. Linhardt, and C. Middaugh, Physical stabilization of acidic fibroblast growth factor by polyanions. Archives of Biochemistry and Biophysics. **300**(1): 30-41 (1993).

51. Presta, M., M. Statuto, A. Isacchi, P. Caccia, A. Pozzi, A. Gualandris, M. Rusnati, L. Bergonzoni, and P. Sarmientos, Structure-function relationship of basic fibroblast growth factor:

Site-directed mutagenesis of a putative heparin-binding and receptor binding region. Biochemical and Biophysical Research Communications. **185**(3): 1098-1107 (1992).

52. Ishai-Michaeli, R., C. Svahn, M. Weber, T. Chajek-Shaul, H. Ekre, and I. Vlodavsky, Importance of size and sulfation of heparin in release of basic fibroblast growth factor from the vascular endothelium and extracellular matrix. Biochemistry. **31**: 2080-2088 (1992).

53. Habuchi, H., S. Suzuki, T. Saito, T. Tamura, T. Harada, K. Yoshida, and K. Kimata, Structure of a heparan sulphate oligosacchride that binds to basic fibroblast growth factor. Biochemical Journal. **285**: 805-813 (1992).

54. Maccarana, M., B. Casu, and U. Lindahl, Minimal sequence in heparin/heparan sulfate required for binding of basic fibroblast growth factor. Journal of Biological Chemistry. **268**(32): 23898-23905 (1993).

55. Turnbull, J., D. Fernig, Y. Ke, M. Wilkinsons, and J. Gallagher, Identification of the basic fibroblast growth factor binding sequence in fibroblast heparan sulfate. Journal of Biolgical Chemistry. **267**(15): 10337-10341 (1992).

56. Ishihara, M., D. Tyrell, G. Stauber, S. Brown, S. Cousens, and R. Stack, Preparation of affinity-fractionated, heparin-derived oligosacchrides and their effects on selected biological activities mediated by basic fibroblast growth factor. Journal of Biological Chemistry. **268**(7): 4675-4683 (1993).

57. Aviezer, D., E. Levy, M. Safran, C. Svahn, E. Buddecke, A. Schmidt, G. David, I. Vlodavsky, and A. Yayon, Differential structural requirements of heparin and heparan sulfate proteoglycans that promote binding of basic fibroblast growth factor to its receptor. Journal of Biological Chemistry. **269**(1): 114-121 (1994).

58. Arakawa, T., J. Wen, and J. Philo, Stoichiometry of heparin binding to basic fibroblast growth factor. Archives of Biochemistry and Biophysics. **308**(1): 267-273 (1994).

59. Thompson, L., M. Pantoliano, and B. Springer, Energetic characterization of the basic fibroblast growth factor-heparin interaction: Identification of the heparin binding domain. Biochemistry. **33**: 3831-3840 (1994).

60. Coltrini, D., M. Rusnati, G. Zoppetti, P. Oreste, A. Isacchi, P. Caccia, L. Bergonzoni, and M. Presta, Biochemical bases of the interaction of human basic fibroblast growth factor with glycosaminoglycans. European Journal of Biochemistry. **214**: 51-58 (1993).

61. Ishihara, M., P. Shaklee, Z. Yang, W. Liang, Z. Wei, R. Stack, and K. Holme, Structural features in heparin which modulate spedcific biological activities mediated by basic fibroblast growth factor. Glycobiology. **4**(4): 451-458 (1994).

62. Ornitz, D., A. Herr, M. Nilsson, J. Westman, C. Svahn, and G. Waksman, FGF binding and FGF receptor activation by synthetic heparan-derived di- and trisaccharides. Science. **268**: 432-436 (1995).

63. Guimond, S., M. Maccarana, B. Olwin, U. Lindahl, and A. Rapraeger, Activating and inhibitory heparin sequences for FGF-2 (Basic FGF) : Distinct reguirements for FGF-1, FGF-2, FGF-4. Journal of Biological Chemistry. **268**(32): 23906-23914 (1993).

64. Spivak-Kroizman, T., M. Lemmon, I. Dikic, J. Ladbury, D. Pinchasi, J. Huang, M. Jaye, G. Crumley, J. Schlessinger, and I. Lax, Heparin-induced oligermerization of FGF molecules is

responsible for FGF receptor dimerization, activation, and cell proliferation. Cell. **79**: 1015 - 1024 (1994).

65. Li, L.-Y. and A. Seddon, Fluorospectrometric analysis of heparin interaction with fibroblast growth factors. Growth Factors. **11**: 1-7 (1994).

66. Moscatelli, D., Basic fibroblast growth factor dissociates rapidly from heparan sulfates but slowly from receptors. Journal of Biological Chemistry. **267**(36): 25803-25809 (1992).

67. Bikfalvi, A., E. Dupuy, A. Inyang, N. Fayein, G. Leseche, Y. Courtois, and G. Tobelem, Binding, internalization, and degradation of basic fibroblast growth factor in human microvascular endothelial cells. Experimental Cell Research. **181**: 75-84 (1989).

68. Pantoliano, M., R. Horlick, B. Springer, D.V. Dyck, T. Tobery, D. Wetmore, J. Lear, A. Nahapetian, J. Bradley, and W. Sisk, Multivalent ligand-receptor binding interaction in the fibroblast growth factor system produce a cooperative growth factor and heparin mechanism for receptor dimerization. Biochemistry. **33**: 10229-10248 (1994).

69. Amsterdam, A., Z. Er-El, and S. Shaltiel, Ultrastructure of beaded agarose. ARchives of Biochemistry and Biophysics. **171**: 673-677 (1975).

70. Waki, S., J. Harvey, and A. Bellamy, Study of agarose gels by electron microscopy of freeze-fractured surfaces. Biopolymers. **21**: 1909-1926 (1982).

71. Porath, J., K. Aspberg, H. Drevin, and R. Axén, Preparation of Cyanogen Bromide-Activated Agarose Gels. Journal of Chromatography. **86**: 53-56 (1973).

72. Lindon, J., R. Rosenberg, E. Merrill, and E. Salzman, Interaction of human platelets with heparinized agarose gel. Journal of Laboratory and Clinical Medicine. **91**(1): 47-59 (1978).

73. Farndale, R., D. Buttle, and A. Barrett, Improved quantitation and discrimintation of sulphated glycosaminoglycans by us of dimetheylmethylene blue. Biochimica et Biophysica Acta. **883**: 173-176 (1986).

74. Danishefsky, I., F. Tzeng, M. Ahrens, and S. Klein, Synthesis of heparin-sepharoses and their binding with thrombin and antithrombin-heparin cofactor. Thrombosis Research. **8**: 131-140 (1976).

75. Ebert, C. and S. Kim, Immobilized heparin-spacer arm effects on biological interactions. Thrombosis Research. **26**: 43 (1982).

76. Funahashi, M., I. Matsumoto, and N. Seno, Preparation of three types of heparin-sepharose and their binding activities to thrombin and antithrombin III. Analytical Biochemistry. **126**: 414-421 (1982).

77. Taylor, K. and G. Jeffree, A new basic metachormatic dye, I:9-dimethyl methylene blue. Histochemical Journal. **1**(3): 199-204 (1969).

78. Sasaki, H., A. Hayashi, H. Kitagaki-Ogawa, I. Matsumoto, and N. Seno, Improved method for the immobilization of heparin. Journal of Chromatography. **400**: 123-132 (1987).

79. Iverius, P., Coupling of glycosaminoglycans to agarose beads (Sepharose 4B). Biochemical Journal. **124**: 677-683 (1971).

80. Tay, S., E. Merrill, E. Salzman, and J. Lindon, Activity toward thrombin-antithrombin of heparin immobilized on two hydrogels.

81. Pekna, M., R. Larsson, B. Formgren, U. Nilsson, and B. Nilsson, Complement activation by polymehtyl methacrylate minimized by end-point heaprin attachement. Biomaterials. **14**(3): 189-192 (1993).

82. Lindon, J., E. Salzman, E. Merrill, A. Dincer, D. Labarre, K. Bauer, and R. Rosenberg, Catalytic activity and platelet reactivity of heparin covalently bonded to surfaces. Journal Lab.Clin.MEd. **105**(2): 219-226 (1985).

83. Dincer, A., J. lindon, and E. Salzman, Covalent immobilization of heparin on polymethacrylate surfaces. Chemical Engineering Communication. **30**: 155 (1984).

84. Larm, O., R. Larsson, and P. Olsson, A new non-thrombogenic surface prepared by selective covalent binding of heparin via a modified reducing terminal residue. Biomaterials, Medical Devices, and Artificial Organs. **11**(2&3): 161-173 (1983).

85. Larsson, R., O. Larm, and P. Olsson, The search for thromboresistance using immobilized heparin. Annals of the New York Academy of Sciences. **516**: 102-115 (1987).

Chapter 8:
CHARACTERISTIC PORE CUTOFF SIZE IN GROWTH FACTOR-INDUCED VESSELS

8.1 Motivation and Background

Continued tumor growth is dependent on the induction of vasculature. The intensity of the development of the network has been correlated with prognosis [1]. The induction and maintenance of the tumor vascular network is thought to be dependent on tumor secreted factors (growth factors, cytokines, inhibitors, and proteases) [2-6]. For example, vascular endothelial growth factor (VEGF), a potent permeability factor and angiogenic factor, has been localized to the plasma membrane of the mouse ovarian tumor microvessel endothelium [7], human hepatocellular carcinoma [8], human breast cancer [9], and gastrointestinal adenocarcinoma [10].

As the number of identified factors which affect endothelial proliferation, migration and tubulogenesis increases (Table 8.1), the complexity of the interactions among chemicals and cells increases. Further understanding of these factors role in initiation and maintenance of vascular tortuosity [11], chaotic flow [12], and hyperpermeability [13] is needed. A critical prerequisite to further understanding of the actions of these factors in the in situ setting is a method to deliver them directly to the tissue and study the resulting dynamic changes in situ. As discussed in the previous chapter, we began to investigate a potential quantitative delivery system. However, as a first step in this investigation, we utilized a qualitative delivery system. Nguyen et al developed an in situ angiogenesis assay system which allows sustained release of a heparin-binding growth factors and observation of the angiogenic vessels [14]. This assay was translated to the mammalian setting by Dellian et al [15].

The basis of both assays was the use of sucralfate as a heparin analog to bind heparin-binding growth factors. Sucralfate (aluminum sucrose octasulfate) is a cyclodextrin which is a nonreducing, water soluble oligosaccharide [17] with high affinity for heparin binding growth factors [18]. The sucralfate provides a method of sustained heparin binding growth factor release,

and a low background vessel formation. The assay allows for continuous observation of the process of vascularization, non-invasive measurements of vascular parameters, and vertical stimulation of vessels as a result of delivery of a single heparin-binding growth factor.

Table 8-1. Initiators and Inhibitors of Angiogenesis and Endothelial Cell Growth

Angiogenic Factors/Mitogens		Inhibitors of Angiogenesis/Mitogenesis	
Angiotropin	Angiogenin	Angiostatin	Platelet Factor-4
B61	Angiotensin	Angioinhibin	IL-1
Copper (Cu)	FGF family	Gold Thiomalate	IL-6
TGFβ	EGF/TGF-α	TNF-α	TGF-β
Soluble E-selectin	PDEGF	bFGF soluble receptor	Interferons α and β
Heparinase	VEGF	Collagenase inhibitors	TIMP-1, TIMP-2, TIMP-3
Hyaluronic Acid	Substance P	Heparinase	D-Penicillamine
Integrins: $\alpha_v\beta_3$, $\alpha_v\beta_5$	G-CSF	Hyaluronic Acid	Thrombospondin-1
IL-8	GM-CSF	Platelet Factor 4	Prolactin fragment
Fibrin	IL-4	Protamine	Ganglioside GM3
Gangliosides GD3, GM1, GM2	Proliferin	Placental proliferin-related protein	Cartilage-derived inhibitor
Macrophage-derived factor	Prostaglandins E_1, E_2	Bacterial-derived angiogenesis inhibitors	Fungal-derived angiogenesis inhibitors
Pleotropin	Nicotinamide	Suramin	
Erythropoitin	Endothelin		

adapted from Jain et al and Bicknell [2, 16]

In the study desribed in this chapter we will focus on just two of the angiogenic factors listed in Table 8-1. bFGF and VEGF may directly or indirectly influence the tumor microvasculature morphology. bFGF is one of the most potent known angiogenic factor [4, 14, 19-26]. Picomolar quantities can induce angiogenesis in vivo [27]. bFGF belongs to the fibroblast growth factor family consisting of eight structurally related proteins. These include acidic FGF (FGF-1), basic FGF (FGF-2), keratinocyte growth factor, int-2, hst-Kaposi FGF, FGF-5, and FGF-6. bFGF is 45% homologous to *hst*, an oncogene similar to Kaposi's sarcoma oncogene. It is 30% homologous to *int-2*, another oncogene. bFGF is a 16-25 kDa basic protein. As with all fibroblast growth factors, it exhibits unusually high affinity for heparin. bFGF acts on

endothelial cells grown on a collagen matrix to promote migration and synthesis of plasminogen activator [28]. (A more detailed discussion of bFGF's chemical properties can be found in Chapter 7).

VEGF is secreted by a wide variety of cultured, transplanted, and primary human tumors [29-31]. VEGF is thought to aid the angiogenic process by inducing endothelial proliferation [6, 13, 32, 33]. The same molecule is also known as VPF (vascular permeability factor) [6, 13]. On a molar basis VEGF increases the vascular permeability 50,000 times that of histamine [6, 13, 34]. This hyperpermeability aids in extravasation of fibrinogen into the interstitium which may result in the formation of an extravascular fibrin gel, a substrate for endothelial and tumor cell growth [35, 36]. This transient hyperpermeability is not blocked by antihistamines or other inhibitors of inflammatory mediators [30].

VEGF is a 34,000-42,000 kDa protein [30, 31, 34]. It is a dimeric, disulfide-bonded protein, the two polypeptides contain identical N-termini but with chain heterogeneity [34]. VEGF is homologous to placenta growth factor and platelet-derived growth factor [37, 38]. It interacts with two specific tyrosine kinases, flt-1 and KDR, that are predominantly expressed on endothelial cell surfaces. VEGF is a heparin binding growth factor, although its affinity is much lower than that of the fibroblast growth factor family.

In situ hybridization has demonstrated upregulation of VEGF mRNA in numerous human tumors: lung, thyroid, breast, gastrointestinal, kidney, bladder, ovary, uterine cervix, and glioblastoma multiforme [36]. In addition to neoplasms, increased vascularization plays a role in other diseases such as diabetic retinopathy, psoriasis, endometriosis, and rheumatoid arthritis. Increased VEGF levels have been reported in all of these disease processes. bFGF has not been reproducibly found to be elevated in these diseases. Yuan et al showed that neutralization of endogenous VEGF results in decreased microvascular permeability, diameter, and tortuosity and eventually to vascular regression [39].

In addition to the effect growth factors, cytokines, inhibitors, proteases, and many other factors have within tumors; there are many clinical situations in which vigorous vascularization is

desired. These include disorders of impaired perfusion such as chronic wound healing in the diabetic patient and burn trauma. The therapeutic value of local induction and maintainence of vascularization would decrease the morbidity and mortality of these disorders. Some studies have illustrated the benefit of local injection of VEGF in improvement of perfusion of ischemic limbs in rabbits [36]. As was discussed in the previous chapter researchers have also been investigating methods of bFGF delivery to induce angiogenesis in ischemic myocardium [40].

The importance of VEGF and bFGF in initiating and maintaining increased vasculature in certain tumors and in other pathologies has been firmly established. The complex milieu of the tumor microenvironment does not enable us to make conclusions about the biological effect of an individual cytokine. Utilizing the chronic angiogenic assay described above allows us to investigate the effect on the pore cutoff size of factor-derived microvessels. We tested the hypothesis that the action of a single growth factor would exhibit less of an effect on the microvessel pore cutoff size than the action of the tumors on the microvessel pore cutoff size.

8.2 Materials and Methods

Dorsal Chamber Implantation. The method used is described in Chapter 3.

Collagen Gel Implantation. The procedure utilized was described previously [15]. Briefly, human recombinant bFGF (Gibco BRL, Gaithersberg MD) or human recombinant VEGF (Pepro Tech, Rocky Hill, NJ) was suspended in aluminum sucrose octasulfate (sucralfate; courtesy of Bukh Meditec, Copenhagen, Denmark), and collagen type I (Vitrogen 100, Celtrix, Santa Clara, CA) in the following ratios: 600 ng of bFGF or 600 ng of VEGF dissolved in 24 µl of 0.1% BSA (Sigma, St. Louis MO), 176 µl of collagen, plus 6.5 mg of sucralfate. Collagen was previously neutralized to pH 7.4 by the addition of 1 part sodium bicarbonate solution (11.76 g/l) and 1 part 10x Minimal Essential Medium (MEM, Gibco BRL), to 8 parts collagen. A 20 µl volume of the growth factor suspension was placed on a 3 mm x 3 mm square of nylon mesh (Tetko, Briarcliff Manor, NY). The suspension was allowed to gel for approximately 20 minutes at 35°C in a humid

environment. A second nylon mesh was placed on top of the gelled solution. This unit was then transferred to the tissue in the dorsal chamber. The chambers were closed again with a clean glass coverslip. Care was taken to assure avoidance of air bubbles in the preparation. All preparations and implantations were performed under sterile conditions.

Liposome Preparation. Liposomes were prepared as described in Chapter 3

Microscopy. The experimental setup is described in Chapter 3.

Particle extravasation. The procedure is the same as that described in Chapter 3.

8.3 Results and Discussion

Dellian et al determined that peak response to high dose growth factor (3000 ng/ml) was seen on the 25th day in the dorsal chamber [15]. In their study they obtained dose dependent blood vessels formation which was significant over controls. A higher dose (30,000 ng/ml) of bFGF did not result in an enhanced vascularization response. All experiments were performed at 3000 ng/ml of bFGF or VEGF. Each gel contained 60 ng of bFGF or VEGF. Previously it was shown that at concentrations a low as 10-100 ng/day bFGF induced massive capillary formation in the chorioallantoic membrane assay [27]. Qualitatively, we did not see such a vigorous response. This is likely due to the differences in the assay preparation. In addition, as discussed in Chapter 6, different sites exhibit different rates of angiogenesis as well as different pore cutoff sizes.

Angiogenic vessels were initially observed after 4 days, but maximal response was observed at 25 days. Images of the time course of vascularization in VEGF gels is shown in Appendix I (Figure I-1). Maximal vascular growth was observed within 14 days with the CAM assay [14]. This further illustrates the differences in the models. The tissue within the CAM assay is being stimulated by a number of unidentified factors as it is basically a developing embryo. In

the dorsal chamber there is no tissue stimulation except that induced by the gels. The time course of maximal response to growth factor stimulation is longer than that seen for tumor stimulation of an angiogenic response.

The time course of vascularization with the solitary growth factors (experiments conducted on day 26 or 27) was much longer than vascularization within tumors (experiments conducted on day 15). This is most likely due to the fact that numerous cytokines are being released by the tumors. In addition, it has been shown that bFGF and VEGF act synergistically [41].

The vessels considered to be induced by the growth factors were those that grew toward the coverslip and that traversed the collagen gel and the 2 layers of mesh. The presence of the growth factors induced angiogenesis over control gels containing collagen and sucralfate was previously demonstrated [14, 15]. Qualitative observation noted that there was increased numbers of vessels in gels containing growth factor over controls, but we did not quantitate this vascular response.

The number and morphology of vessels induced by the two growth factors were similar (Figure 1-2). This is an intriguing result since VEGF is reportedly a more potent angiogenic factor than bFGF. The vessel density and diameter in this experiment were uniformly less than that of the tumors studied in the dorsal chamber on the same day after implantation. Observations indicated a similar tortuosity to the tumors.

The pore cutoff size in bFGF-induced vessels was between 200 nm and 380 nm (Figure 8-1). This is on the lower end of the tumor-induced vessel pore cutoff size. The bFGF amount that is delivered locally may not be able overwhelm the host regulatory machinery as well as the release of various cytokines by tumors. In addition, the release of one cytokine may not stimulate the release of other cytokines in the local host tissue as the release of cytokines within the tumor tissue may stimulate more tumor secreted cytokines.

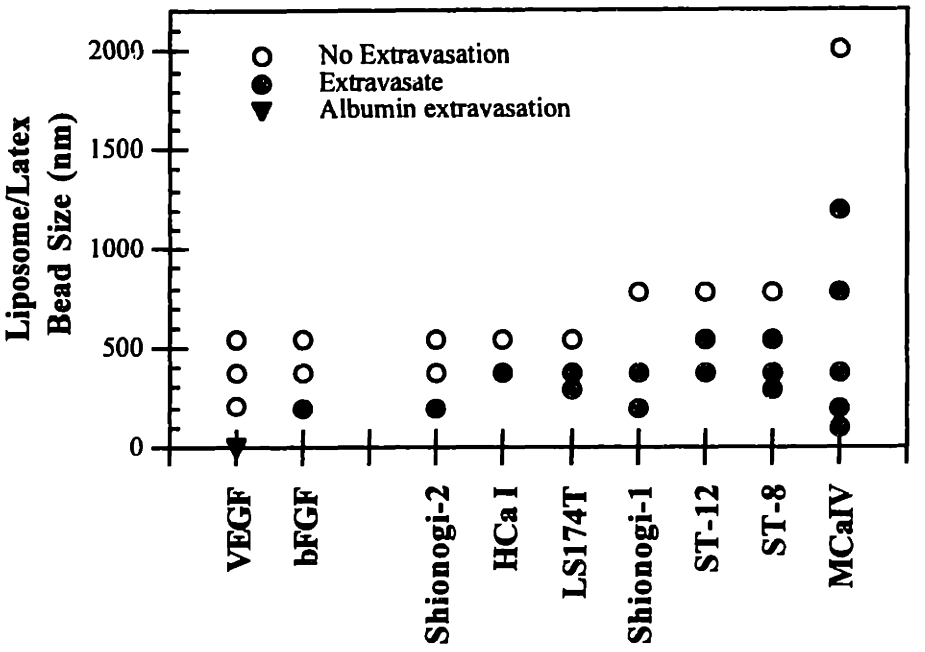

Figure 8-1. Growth factor-induced vessels in comparison with tumor-induced vessels

The pore cutoff size in VEGF-induced vessels was indistinguishable from normal microvasculature. Recently it was shown that topical administration of VEGF rapidly and directly induces formation of fenestrations and increased vesicle clustering and fusion in nonfenestrated endothelium of skeletal muscle and skin [42]. Elvax pellets containing VEGF induced microvessels containing fenestrations and open junctions [43]. Normal fenestral diaphragms contain a luminal anionic glycocalyx, however the fenestrae induced by tumors and VEGF-transfected cells was significantly less anionic than normal fenestral diaphragms in the intestine and pancreas [43]. The increased number of fenestrations and the biochemical difference in the fenestral diaphragm may account for the increased permeability of VEGF induced vessels. The size of the observed fenestrations was around 60 nm. This indicates that the mechanism of transvascular transport of nanoparticles is most likely not via the fenestrae. Our results indicate that the increases in permeability seen with VEGF stimulation are independent of pore cutoff size.

The vessels growing in from the side were also examined for extravasation. These may be the result of inflammation due to irritation by the nylon mesh. Increase capillary permeability can occur during wound healing and chronic inflammation. This is a rare occurrence unlike increased permeability exhibited by post-capillary venules [42]. There was no extravasation in these vessels or in the normal tissue surrounding the gel.

8.4 Conclusions

The results from this study and previous studies [15, 25, 26, 44] indicate that the delivery of growth factors does impart some local tissue response. The previous studies of tumors implanted in the dorsal chamber illustrated that the majority of the tumors that grew exhibited significantly increased pore cutoff sizes. Collagen gels containing bFGF or VEGF were used to study the influence of a specific angiogenic factor on the pore cutoff size. The pore cutoff size in bFGF-induced vessels seems to be similar to that found in the tumors. The VEGF-induced vessels exhibited no observable increase in pore cutoff size over normal vasculature. We postulated that the tumor regulates the local microenvironment by overwhelming the hosts regulatory machinery. In the studies illustrated here, while the growth factors do exert some effect on the local microenvironment it is not as vigorous as that caused by tumors, possibly implicating an incomplete stimulus for regulation of the microvascular pore cutoff size.

However, conclusions are difficult to make with the gel and the Elvax pellets because the following important parameters are not known: 1) the total amount of growth factor in the device, 2) the amount of growth factor in the gel that is bound to sucralfate, 3) the interaction of these growth factors with sucralfate, collagen, and Elvax, 4) the transport of the growth factors from the device and the release rates, 5) the amount of biologically active growth factor released, and 6) the partitioning into the tissue space. In addition, these parameters may significantly differ between VEGF and bFGF, thus comparisons between the two growth factors is not possible.

8.5 References

1. Folkman, J. and Y. Shing, Angiogenesis. Journal of Biological Chemistry. **267**: 10931-10934 (1992).

2. Bicknell, R. and A. Harris, Novel growth regulatory factors and tumor angiogenesis. European Journal of Cancer. **27**(6): 781-785 (1991).

3. Fenselau, A., Tumor and related angiogenesis factors, in Growth and Maturation Factors, G. Guroff, Editor. 1984, John Wiley & Sons: New York. p. 88-129.

4. Knighton, D., G. Phillips, and V. Fiegel, Wound healing angiogenesis: Indirect stimulation by basic fibroblast growth factor. The Journal of Trauma. **30**(12 Supplement): S134-S144 (1990).

5. Peverali, F., S. Mandriota, P. Ciana, R. Marelli, P. Quax, D. Rifkin, G.D. Valle, and P. Mignatti, Tumor cells secrete an angiogenic factor that stimulates basic fibroblast growth factor and urokinase expression in vascular endothelial cells. Journal of Cellular Physiology. **161**: 1-14 (1994).

6. Senger, D., L. Brown, K. Claffey, and H. Dvorak, Vascular permeability factor, tumor angiogenesis and stroma generation. Invasion Metastasis. **14**: 385-394 (1994-95).

7. Q-Hong, J. Nagy, D. Senger, H. Dvorak, and A. Dvorak, Ultrastructural localization of vascular permeability factor/vascular endothelial growth factor (VPF/VEGF) to the abluminal plasma membrane and vesiculovacuolar organelles of tumor microvascular endothelium. Journal of Histochemistry and Cytochemistry. **43**(4): 381-389 (1995).

8. Suzuki, K., N. Hayashi, Y. Miyamoto, M. Yamamoto, L. Ohkawa, Y. Ito, Y. Sasaki, Y. Yamaguchi, H. Nakase, K. Noda, N. Enomoto, K. Arai, Y. Yamada, H. Yoshihara, T. Tujimura, K. Kawano, K. Ysohikawa, and T. Kamada, Expression of vascular permeability factor/vascular endothelial growth factor in human hepatocellular carcinoma. Cancer Research. **56**: 3004-3009 (1996).

9. Brown, L., B. Berse, R. Jackman, K. Tognazzi, A. Guidi, H. Dvorak, D. Senger, J. Connolly, and S. Schnitt, Expression of vascular permeability factor (vascular endothelial growth factor) and its receptors in breast cancer. Human Pathology. **26**: 86-91 (1995).

10. Brown, L., B. Berse, R. Jackman, K. Tognazzi, E. Manseau, D. Senger, and H. Dvorak, Expression of vascular permeability factor (vascular endothelial growth factor) and its receptors in adenocarcinomas of the gastrointestinal tract. Cancer Research. **53**: 4727-4735 (1993).

11. Skinner, S., P. Tutton, and P. O'Brien, Microvascular architecture of experimental tumors in the rat. Cancer Research. **50**: 2411-2417 (1990).

12. Jain, R., Determinants of tumor blood flow: a review. Cancer Research. **48**: 2641-2658 (1988).

13. Dvorak, H., L. Brown, M. Detmar, and A. Dvorak, Vascular permeability factor/Vascular endothelial growth factor, microvascular hyperpermeability, and angiogenesis. American Journal of Pathology. **146**(5): 1029-1039 (1995).

14. Nguyen, M., Y. Shing, and J. Folkman, Quantitation of angiogenesis and antiangiogenesis in the chick embryo chorioallantoic membrane. Microvascular Research. **47**: 31-40 (1994).

15. Dellian, M., B. Witwer, H. Salehi, F. Yuan, and R. Jain, Quantitation and physiological characterization of angiogenic vessels in mice. American Journal of Pathology. **149**: 59-71 (1996).

16. Jain, R., Delivery of molecular medicine to solid tumors. Science. **271**: 1079-1080 (1996).

17. Folkman, J., P. Weisz, M. Joullie, W. Li, and W. Ewing, Control of angiogenesis with synthetic heparin substitutes. Science. **243**: 1490-1493 (1989).

18. Folkman, J., S. Szabo, and Y. Shing, Sucralfate affinity for fibroblast growth factor. Journal of Cell Biology. **111**: 223A (1990).

19. Tabata, Y., S. Hijikata, and Y. Ikada, Enhanced vascularization and tissue granulation by basic fibroblast growth factor impregnated in gelatin hydrogels. Journal of Controlled Release. **31**: 189-199 (1994).

20. Thompson, J., K. Anderson, J. DiPietro, J. Zweibel, M. Zameta, W. Anderson, and T. Maciag, Site-directed neovessel formation in vivo. Science. **241**: 1349-1352 (1988).

21. Thompson, J., C. Haudenschild, K. Anderson, J. DiPietro, W. Anderson, and T. Maciag, Heparin-binding growth factor 1 induces the formation of organoid neovascular structures in vivo. Proceedings of the National Academy of Sciences. **86**: 7928-7932 (1989).

22. Sprugel, K., J. McPherson, A. Clowes, and R. Ross, Effects of growth factors in vivo I. Cell ingrowth into porous subcutaneous chambers. American Journal of Pathology. **129**(3): 601-613 (1987).

23. Norrby, K., Basic fibroblast growth factor and *de novo* mammalian angiogenesis. Microvascular Research. **48**: 96-113 (1994).

24. Nabel, E., Z. Yang, G. Plautz, R. Forough, X. Zhan, C. Haudenschild, T. Maciag, and G. Nabel, Recombinant fibroblast growth factor-1 promotes intimal hyperplasia and angiogenesis in arteries in vivo. Nature. **362**: 844-846 (1993).

25. Edelman, E., M. Nugent, L. Smith, and M. Karnovsky, Basic fibroblast growth factor enhances the coupling of intimal hyperplasia and proliferation of vasa vasorum in injured rat arteries. Journal of Clinical Investigation. **89**: 465-473 (1992).

26. Edelman, E., M. Nugent, and M. Karnovsky, Perivascular and intravenous administration of basic fibroblast growth factor: Vascular and solid organ deposition. Proceedings of the National Academy of Sciences. **90**: 1513-1517 (1993).

27. Folkman, J. and M. Klagsbrun, Angiogenic factors. Science. **235**: 444-447 (1987).

28. Montesano, R., M. Pepper, J. Vassalli, and L. Orci, Modulation of angiogenesis in vitro, in Angiogenesis: Key Principles-Science-Technology-Medicine, R. Steiner, P. Weisz, andR. Langer, Editors. 1992, Birkhäuser Verlag: Basel. p. 129-136.

29. Berse, B., L. Brown, L.V.D. Water, H. Dvorak, and D. Senger, Vascular permeability factor (vascular endothelial growth factor) gene is expressed differentially in normal tissues, macrophages, and tumors. Molecular Biology Cell. **3**: 211-220 (1992).

30. Senger, D., S. Galli, A. Dvorak, C. Perruzza, V. Harvey, and H. Dvorak, Tumor cells secrete a vascular permeability factor that promotes accumulation of ascites fluid. Science. **219**: 983-985 (1983).

31. Senger, D., D. Connolly, C. Perruzza, D. Alsup, R. Nelson, R. Leimgruber, J. Feder, and H. Dvorak, Purification of a vascular permeability factor (VPF) from tumor cell conditioned medium. Federation Proceedings. **46**: 2102 (1987).

32. Leung, D., G. Cachianes, W. Kuang, D. Goeddel, and N. Ferrara, Vascular endothelial growth factor is a secreted angiogenic mitogen. Science. **246**: 1306 (1989).

33. Gospodarowicz, D., J. Abraham, and J. Schilling, Isolation and characterization of a vascular endothelial cell mitogen produced by pituitary-derived folliculostellate cells. Proceedings of the National Academy of Science. **86**: 7311-7315 (1989).

34. Senger, D., D. Connolly, L.V.D. Water, J. Feder, and H. Dvorak, Purification and NH_2-terminal amino acid sequence of guinea pig tumor-secreted vascular permeability factor. Cancer Research. **50**: 1774-1778 (1990).

35. Brown, L., B. Berse, R. Jackman, K. Tognazzi, E. Manseau, H. Dvorak, and D. Senger, Increased expression of vascular permeability factor (vascular endothelial growth factor) and its receptors in kidney and bladder carcinomas. American Journal of Pathology. **143**(5): 1255-1262 (1993).

36. Ferrara, N. and T. Davis-Smyth, The biology of vascular endothelial growth factor. Endocrine Reviews. **18**(1): 4-25 (1997).

37. Maglione, D., V. Guerriero, C. Viglietto, P. Delli-Bovi, and M. Persico, Isolation of a human placenta cDNA coding for a protein related to the vascular permeability factor. Proceedings of the National Academy of Science. **88**: 9267-9271 (1991).

38. Conn, G., M. Bayne, D. Soderman, P. Kwok, K. Sullivan, T. Palisi, D. Hope, and K. Thomas, Amino acid and cDNA sequences of a vascular endothelial cell mitogen that is homologous to platelet-derived growth factor. Proceedings of the National Academy of Science. **87**: 2628-2632 (1990).

39. Yuan, F., Y. Chen, M. Dellian, N. Safabakhsh, N. Ferrara, and R. Jain, Time-dependent vascular regression and permeability changes in established human tumor xenografts induced by an anti-vascular growth factor/vascular permeability factor antibody. Proceedings of the National Academy of Science-USA. **93**: 14765-14770 (1996).

40. Harada, K., W. Grossman, M. Friedman, E. Edelman, P. Prasa, C. Keighley, W. Mannint, F. Sellke, and M. Simons, Basic fibroblast growth factor improves myocardial function in chronically ischemic porcine hearts. Journal of Clinical Investigation. **94**: 623-630 (1994).

41. Pepper, M., N. Ferrara, L. Orci, and R. Montesano, Potent synergism between vascular endothelial growth factor and basic fibroblast growth factor in the induction of angiogenesis in vitro. Biochemical and Biophysical Research Communication. **189**(2): 824-831 (1992).

42. Roberts, W. and G. Palade, Increased microvascular permeability and endothelial fenestration induced by vascular endothelial growth factor Journal of Cell Science. **108**: 2369-2379 (1995).

43. Roberts, W. and G. Palade, Neovasculature induced by vascular endothelial growth factor is fenestrated. Cancer Research. **57**: 765-772 (1997).

44. Nugent, M., O. Chen, and E. Edelman. Controlled Release of Fibroblast Growth Factor: Activity in Ceil Culture. in Materials Research Society. 1992. Boston: Materials Research Society.

Chapter 9.
CONCLUSIONS AND FUTURE WORK

This thesis characterized the transvascular transport of macromolecules and nanoparticles in tumor microvessels. The initial studies identified the pore cutoff sizes and microvessel permeability in a variety of tumors. Following this analysis, we investigated the effect on the pore cutoff size of modulations within the tumor and host microenvironment. In a final analysis, we investigated the controlled delivery of a growth factor and the pore cutoff sizes of growth factor induced microvessels. The following conclusions were drawn from the work presented in this thesis:

1) Every tumor studied has a characteristic pore cutoff size. This size ranged between 200 nm to 1.2 μm.

2, The majority of tumors have a pore cutoff size between 400 and 800 nm. This indicates that the primary structure for macromolecular and particle diffusive transvascular transport in tumors is via opened gaps (widened interendothelial junctions or transendothelial gaps).

3) The transvascular transport of BSA is not influenced by the pore cutoff size. There are two possible explanations for this; transport can occur via 1) vesicles or receptor-mediated transport (albondin), or 2) through the pores; there is no hindrance to transport through the pores because $r_s/r_p << 1$.

4) Tumor growth and vascular modification do not modulate the pore cutoff size once the tumor vasculature is established. This indicates that the balance of microenvironment regulation between the tumor and the host occurs rapidly (within 7 days in these studies).

5) Tumor regression induced by hormone withdrawal in a hormone-responsive tumor had a significant effect on the pore cutoff size. Within 48 hours after hormone ablation, the tumor microvessels were impermeable to FITC-BSA.

6) A decrease in the pore cutoff size was seen in 3 of 4 tumors transplanted in the brain as compared with the striated skin muscle indicating that the host microenvironment plays a role in the modulation of the vascular structure in tumors.

7) Less than 3% of the heparin in heparin-sepharose beads is available or active to bind bFGF. This cannot be explained by diffusion limitations or differences in bFGF affinity for heparin.

8) The equilibrium binding characteristics are different than predicted from free solution equilibrium binding theory. This indicates that assumptions about the behavior of immobilized heparin (or other polysaccharides) cannot be extrapolated from that observed in solution.

9) Chronic application of bFGF induced vessels with pore cutoff sizes similar to tumor microvessels. VEGF induced vessels did not exhibit an increased pore cutoff size as compared with normal vessels.

The results of this work have lead to many questions, some of which are currently being addressed. Future areas of research in the transvascular transport of macromolecules and particles in tumors are listed below. Through these proposed studies, further knowledge of the structures of transport pathways and mechanisms of transvascular transport may aid in improving cancer treatment.

1) We initiated ultrastructural studies of MCa IV microvasculature. These electron microscopy studies support the functional observations discussed in this thesis. Open endothelial gaps were of a range of 100 - 1000 nm. Without serial sections we could not determine if these were interendothelial or transendothelial. In addition, to observed tumor cell migration through open gaps, 100 nm liposomes were also seen extravasating through open gaps [1]. Currently, ultrastructural studies are underway to investigate the role of vascular endothelial cadherins, zonula occludens and other cell adhesion molecules in maintained the open gaps seen in tumor microvessels.

2) Measurement of mRNA and protein levels of VEGF, bFGF, and their receptors in dorsal chamber and cranial window tumors to investigate any correlation with pore cutoff size and further investigation into the competitive microenvironment theory.

3) Investigate the hindrance to transvascular transport of larger particles. Current studies are underway to augment the permeability of tumor microvessels by delivery of exogenous growth factors.

4) Future growth and regression studies should include measurements of tumor size, vascular density, permeability, along with the pore cutoff size. Also, include in this study measurement of hormone levels and mRNA and protein levels of VEGF, bFGF, and their receptors. Current in vitro studies are aimed at detecting local VEGF and VEGF receptors in cells grown in conditioned media from different in situ sites or over different aged cell cultures.

5) Expand the study initiated with Shionogi tumor to include other hormone-responsive tumors, specifically a human estrogen dependent breast tumor cell line or androgen dependent prostatic tumor cell line. (We initiated this study, however, the cell lines tried did not grow in the dorsal chamber; refer to Chapter 3). An additional study should include studies on revascularization after hormone ablation and the pore cutoff sizes in these tumors. Include in this study measurement of hormone levels and mRNA and protein levels of VEGF, bFGF, and their receptors.

6) Investigate the effect on the pore cutoff size with various modes of cancer treatment, such as angiogenesis inhibitors, radiation therapy, liposomal delivery of drugs, and conventional chemotherapy.

7) Expand the bFGF-immobilized-heparin model to include transport through a support matrix such as alginate. Utilizing the knowledge gained from the bFGF-immobilized-heparin study, design a chronic, quantitative in vivo angiogenesis assay.

8) Compare the site differences of tumor microvessel pore cutoff size with expression of P-glycoprotein. It is thought that expresion of the multidrug resistance gene can render the cells resistant to cancer therapeutic drugs through upregulation of P-glycoprotein.

In summary, this study demonstrates that tumors have characteristic pore cutoff sizes which appears to be maintained by the tumor milieu and the local microenvironment. An understanding of the limits and regulation of transvascular transport may offer modalities to increase the distribution of size of the transvascular transport passageways for optimized delivery of therapeutic agents.

References

1. Hobbs, S., W. Monsky, F. Yuan, W. Roberts, L. Griffith, V. Torchilin, and R. Jain, Regulation of transport pathways in tumor vessels: Role of tumor type and microenvironment. Proceedings of the National Academy of Sciences. **95**: 4607-4612 (1998).

Appendix A. In Situ Chronic Animal Models: A Brief History

The native microvasculature, growth of new vasculature, and cellular growth is observable with transparent chambers. A chamber makes possible the combination of descriptive characterization and quantitative analysis in a chronic in situ setting.

Transparent chambers for microscopic observation have been used for over seven decades. The first transparent chambers were implanted in the rabbit ear by Sandison in 1924 [1]. This chamber was used to study the development of granulation tissue. A major disadvantage of the system was that allografts did not survive. In 1945 Algire adapted the rabbit ear chamber for use in the dorsal skinfold of the mouse [2]. His initial interest was to investigate developing microcirculation in transplanted tumors. Advantages of this system are repeated observation and good optical clarity.

In the late 1970s these chambers were used for the direct, quantitative , study of hemodynamics and morphologic parameters in the microcirculation in hamsters [3]. In 1992 the chambers were adapted for use in SCID (Severe Combined Immunodeficient) mice [4], and in 1993 in nude mice [5]. The chambers have been used extensively to study microvasculature of tumor implants [4, 6-14].

SCID mice lack both a functional immune system and mechanisms for DNA repair [15]. The absence of both T and B lymphocytes is due to a site-specific recombination pathway [16]. The use of immunocompromised mice increases the take rate of transplanted tumors and allows for xenotransplantation.

References

1. Sandison, J., A new method for the microscopic study of living growing tissues by the introduction of a transparent chamber in the rabbit's ear. Anatomical Record. **28**: 281-287 (1924).

2. Algire, G. and H. Charkley, Vascular reactions of normal and malignant tissues in vivo.I. Vascular reaction of mice to wounds and to normal and neoplastic transplants. Journal of the National Cancer Institute. **6**: 73-85 (1945).

3. Endrich, B., F. Hammersen, and K. Messmer, Capillary ultrastructure and microcirculatory function of malignant tumors, in Advances in Experimental Medicine and Biology, S. Chien, Editor. 1988, Plenum Press: New York. p. 205-214.

4. Leunig, M., F. Yuan, M. Menger, Y. Boucher, A. Goetz, K. Messmer, and R. Jain, Angiogenesis, microvascular architecture, microhemodynamics, and interstitial fluid pressure during early growth of human adenocarcinoma LS174T in SCID mice. Cancer Research. **52**: 6553-6560 (1992).

5. Lehr, H.-A., M. Leunig, M. Menger, and K. Meßmer, Dorsal skinfold chamber technique for intravital microscopy on striated muscle in nude mice. American Journal of Pathology. **143**(4): 1055-62 (1993).

6. Yuan, F., M. Leunig, D. Berk, and R. Jain, Microvascular permeability of albumin, vascular surface area, and vascular volume measured in human adenocarcinoma LS174T using dorsal chamber in SCID mice. Microvascular Research. **45**: 269-289 (1993).

7. Yuan, F., H. Salehi, Y. Boucher, U. Vasthare, R. Tuma, and R. Jain, Vascular permeability and microcirculation of gliomas and mammary carcinomas transplanted in rat and mouse cranial windows. Cancer Research. **54**: 4564-4568 (1994).

8. Yuan, F., M. Leunig, S. Huang, D. Berk, D. Papahadjoupolos, and R. Jain, Microvascular permeability and interstitial penetration of sterically stabilized (Stealth) liposomes in a human tumor xenograft. Cancer Research. **54**: 3352-3356 (1994).

9. Yuan, F., M. Dellian, D. Fukumura, M. Leunig, D. Berk, V. Torchillin, and R. Jain, Vascular permeability in a human tumor xenograft: Molecular size dependence and cutoff size. Cancer Research. **55**: 3752-3756 (1995).

10. Yuan, F., Y. Chen, M. Dellian, N. Safabakhsh, N. Ferrara, and R. Jain, Time-dependent vascular regression and permeability changes in established human tumor xenografts induced by an anti-vascular growth factor/vascular permeability factor antibody. Proceedings of the National Academy of Science-USA. **93**: 14765-14770 (1996).

11. Dellian, M., B. Witwer, H. Salehi, F. Yuan, and R. Jain, Quantitation and physiological characterization of angiogenic vessels in mice. American Journal of Pathology. **149**: 59-71 (1996).

12. Fukumura, D., H. Salehi, B. Witwer, R. Tuma, R. Melder, and R. Jain, Tumor necrosis factor a-induced leukocyte adhesion in normal and tumor vessels: Effect of tumor type, transplantation site, and host strain. Cancer Research. **55**: 4824-4829 (1995).

13. Fukumura, D., F. Yuan, M. Endo, and R. Jain, Role of nitric oxide in tumor microcirculation. American Journal of Pathology. **150**(2): 1-13 (1997).

14. Torres-Filho, I., M. Leunig, F. Yuan, M. Intaglietta, and R. Jain, Noninvasive measurement of microvascular and interstitial oxygen profiles in a human tumor in SCID mice. Proceedings of the National Academy of Science-USA. **91**(6): 2081-5 (1994).

15. Bosma, G., R. Custer, and M. Bosma, A severe combined immunodeficiency mutation in the mouse. Nature. **301**(10): 527-530 (1983).

16. Hendrickson, E., X. Qin, E. Bump, D. Schatz, M. Oettinger, and D. Weaver, A link between double-strand break-related repair and V(D)J recombination: the scid mutation. Proceedings of the National Academy of Sciences. **88**: 4061-4065 (1991).

Appendix B. Stealth® Liposomes

Liposomes are multi-lamellar bilayers of lipids enclosing an aqueous phase (Figure B-1). The hydrophilic head groups are always in contact with the aqueous phase. The lipid composition varies but usually the predominant type is a phospholipid. The presence of cholesterol increases the liposome stability. Negative charge prevents aggregation and increases encapsulation efficiency [1]. An aqueous suspension of solutes is shaken over a dried lipid film to form liposomes.

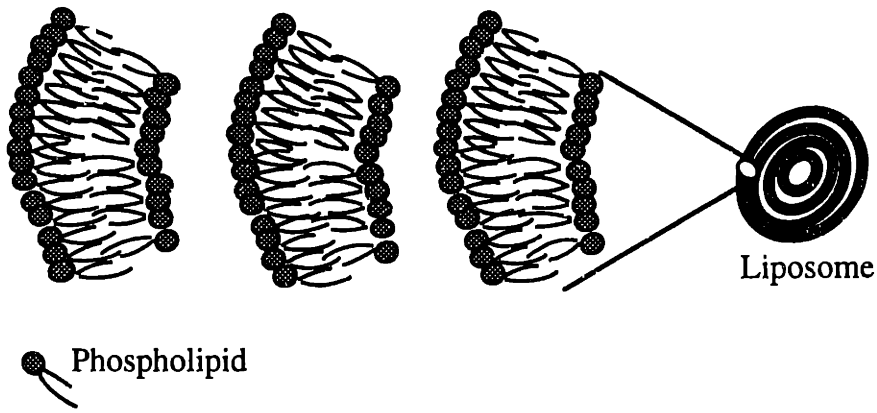

Figure B-1. Schematic of liposome structure

It was hypothesized over thirty years ago that liposomes could be used as drug carriers. The potential advantages are:

- Prolonged effect of the encapsulated drug
- Increased concentration at the site of action leading to amplification of effect
- Decreased tissue and systemic toxicity
- Increased protection from host response
- Increased uptake by phagocytic cells
- Local, directed, and selective drug release
- Delivery of drugs which are only activated in the cellular environment
- Transport across hydrophobic barriers
- No chemical modifications of drug necessary

Appendix B. Stealth® Liposomes

- Mimic certain cell functions

However, conventional liposomes when injected into the bloodstream are recognized as foreign bodies by the host's immune system and rapidly cleared by the phagocytic cells within the liver and spleen [1]. These conventional liposomes accumulate in the liver and spleen (90% of injection) within a couple of hours. The rate of elimination depends on many parameters such as size, charge, and fluidity of the liposome. The circulation time increases with decreasing size, negative charge density, and bilayer fluidity [2].

If the cells of the reticuloendothelial system (RES) are the targets then conventional formulations are optimal. This clearance is significantly reduced by incorporating polyethylene glycol-linked lipids (2000 - 5000 MW) [3]. These liposomes are termed Stealth® for their ability to sustain their anonymity in the bloodstream. They exhibit first-order clearance rates independent of dose. The circulation time is increased up to 48 hours and the tissue distribution is much improved over conventional liposomes (Table B-1). In addition to the increased percentage of the dose remaining in the circulation, there is also increased uptake in solid tumors, enhanced antitumor activity of encapsulated drugs, and dose independent clearance kinetics [3, 4].

Table B-1. Tissue Distribution of Stealth® Liposomes

Tissue	Localization (%)
Blood	29
Liver	18
Spleen	3
Heart	0.1
Skin	16
Elsewhere	21

[3]

References

1. Lasic, D. and Martin, F., eds. Stealth Liposomes. Pharmacology and Toxicology: Basic and Clinical Aspects, ed. M. Hollinger. 1995, CRC Press: Boca Raton.

2. Gregoriadis, G. Engineering liposomes for targeted drug delivery: Progress and problems. Trends in Biotechnology. **13:** 527-537 (1995).

3. Papahadjopoulos, D., Allen, T., Gabizon, A., Mayhew, E., Matthay, K., Huang, S., Lee, K., Woodle, M., Lasic, D., Redemann, C., and Martin, F. Sterically stabilized liposomes: Improvements in pharmacokinetics and antitumor therapeutic efficacy. Proceedings of the National Academy of Sciences-USA. **88:** 11460-11464 (1991).

4. Huang, S., Lee, K., Hong, K., Friend, D., and Papahadjopoulos, D. Microscopic localization of sterically stabilized liposomes in colon carcinoma-bearing mice. Cancer Research. **52:** 5135-5143 (1992).

Appendix C. Intravital Fluorescent Microscopy Photographs for Chapter 3

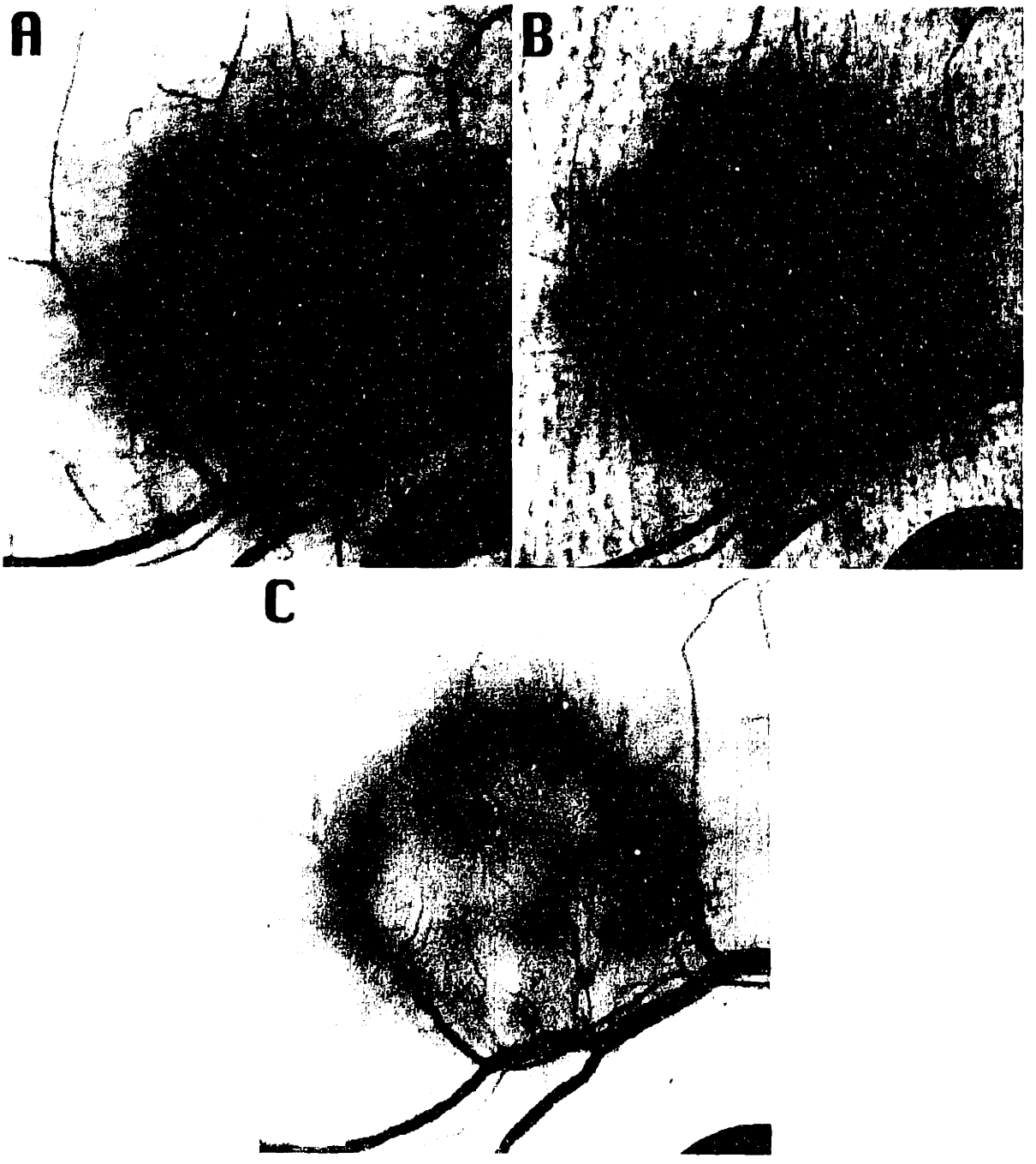

Figure C-1. HCa I growth in the dorsal chamber. Image of the same tumor at A) 6 days, B) 12 days, and C) 15 days after tumor implantation

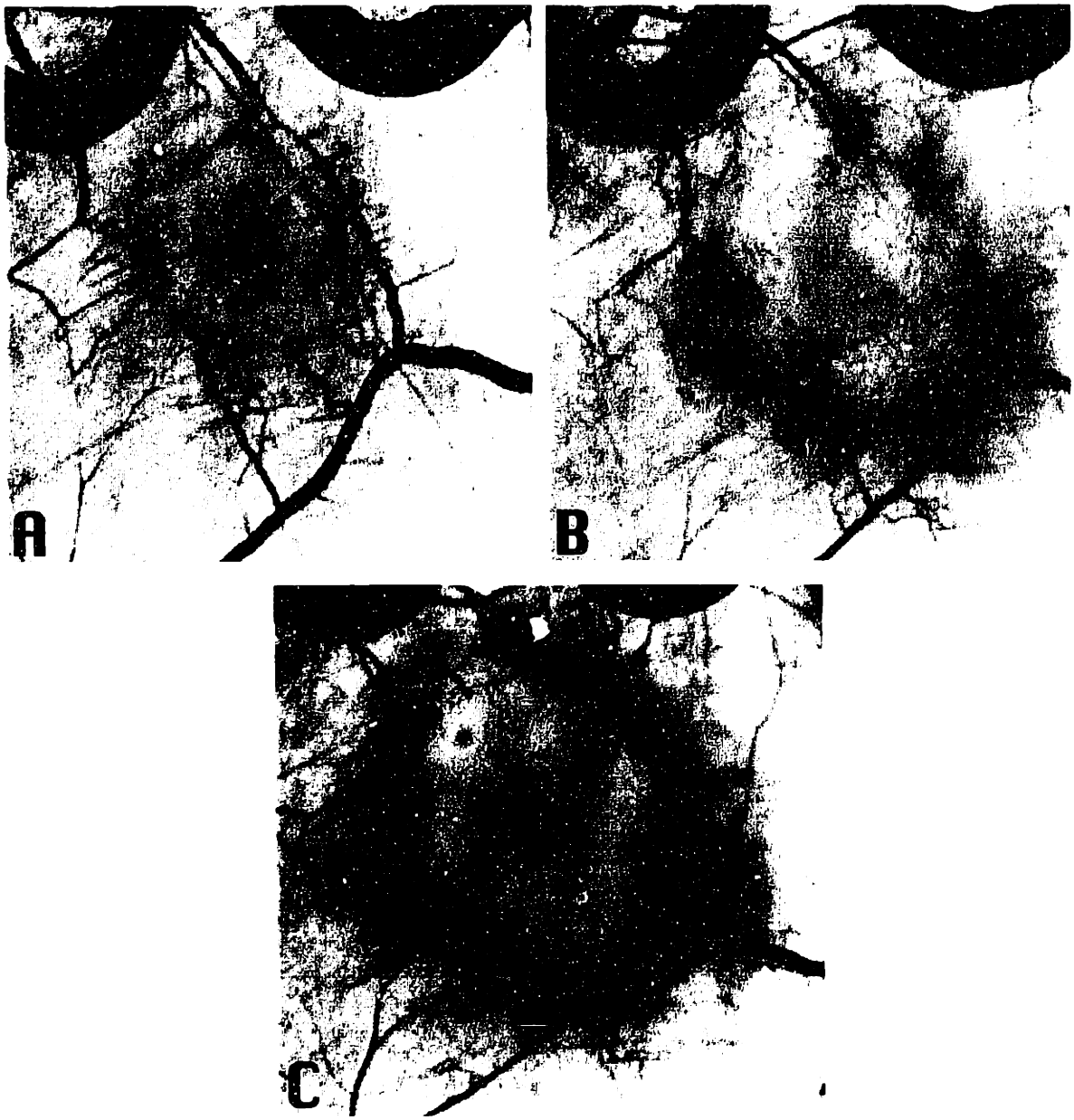

Figure C-2. ST-8 growth in the dorsal chamber. Image of the same tumor at A) 5 days, B) 10 days, and C) 12 days after tumor implantation.

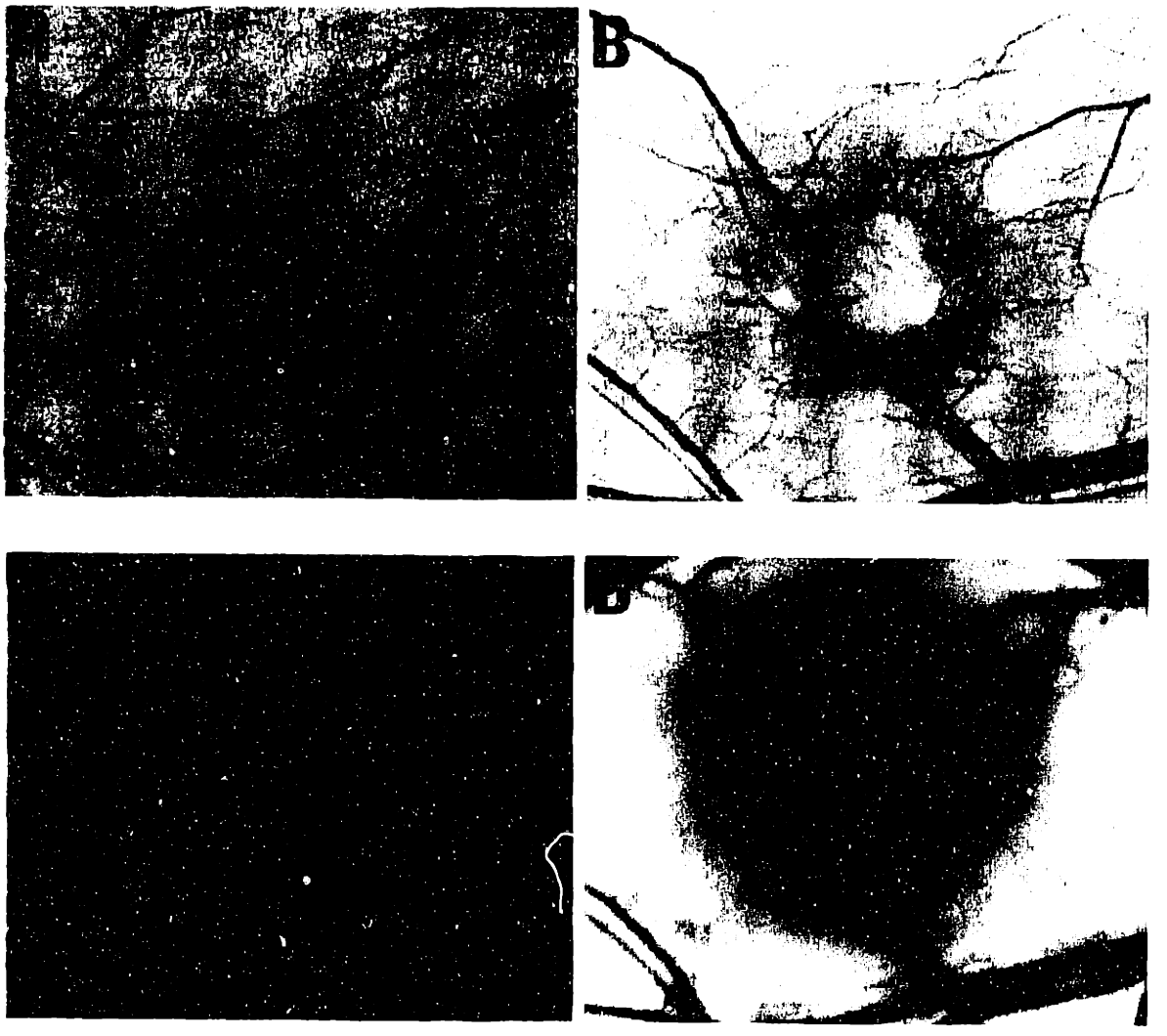

Figure C-3. MCa IV growth in the dorsal chamber. Image of the same tumor at A) 6 days, B) 9 days, C) 15 days, and D) 20 days after tumor implantation.

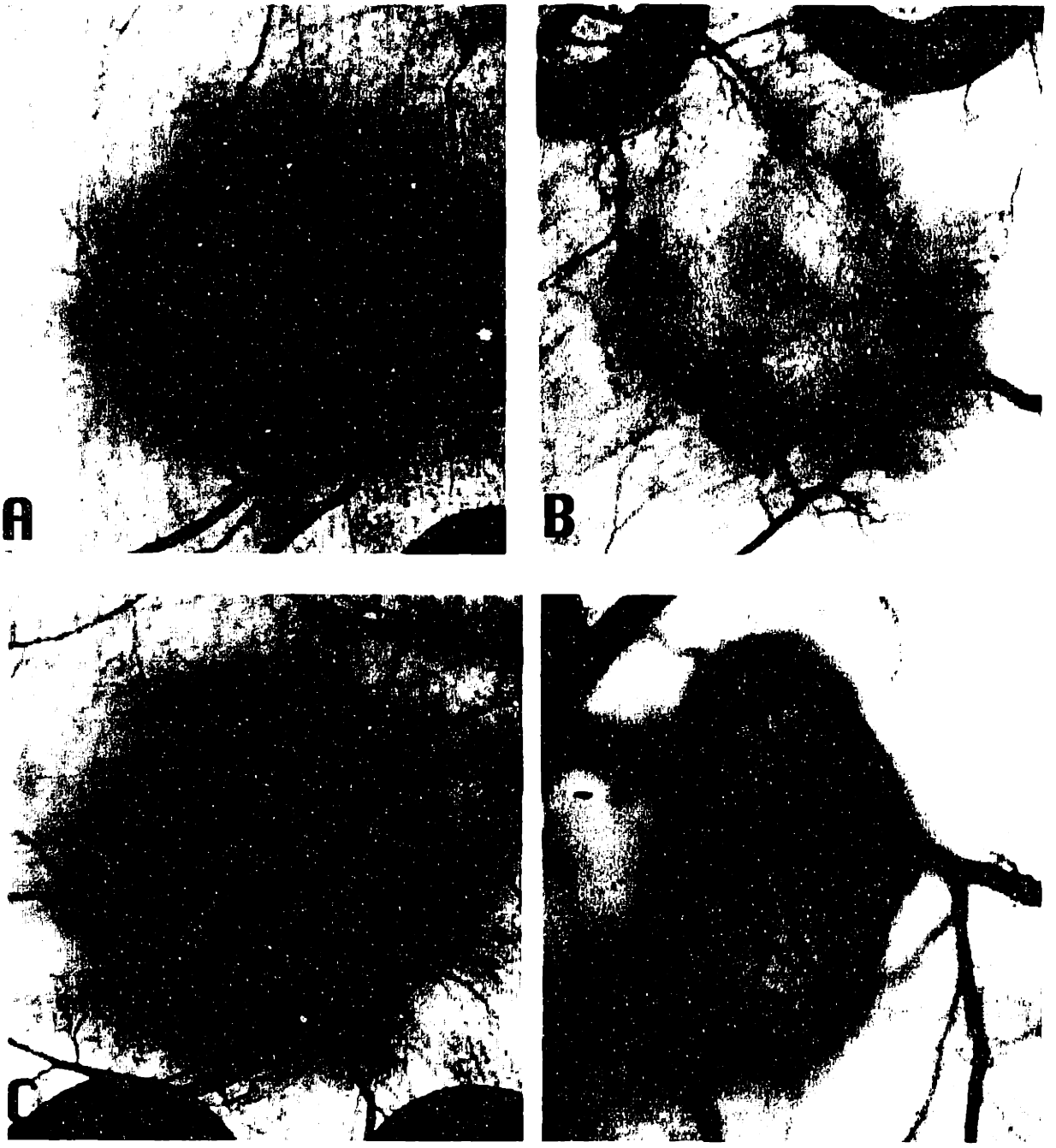

Figure C-4. Characteristic vascular patterns of tumors implanted in the dorsal chamber.
A) HCa I, 12 days after implantation
B) ST-8, 10 days after implantation
C) Shionogi, 11 days after implantation
D) MCa IV, 23 days after implantation

2 μm latex beads

1.2 - 2 μm latex beads

780 nm latex beads

380 nm liposomes

233 nm liposomes

94 nm liposomes

Figure C-5. Pore cutoff size for Mca IV in the dorsal chamber (25x)

Appendix D. Microvascular Permeability Derivation

The effective vascular permeability was derived in Yuan et al [1]. The volume of the monitoring window (V) was equal to the area of the window multiplied by the thickness of the tissue. The area of the monitoring window was 0.51 x 0.44 mm^2 (0.224 mm^2). The depth of the tissue varied from 0.5 to 2.0 mm. The effective permeability of a single microvessel is related to the diffusive permeability, the solute reflection coefficient, and the convective flux as discussed in Chapter 4. The definition of average effective permeability is

$$J_s = PSC_p \tag{D-1}$$

where J_S is the total solute flux across the total surface area within the volume, V. C_p, the plasma concentration of solute is assumed to be much greater than the interstitial concentration of solute (C_{int}) and also to be the same in all vessels. P represents the average effective permeability of vessels in the monitoring volume.

The increase in macromolecules within the monitoring window is assumed to be due to extravasation since the length of the window is much greater than the diameters of the vessels. Therefore, the mass balance is given by

$$\frac{dN_t}{dt} = J_s + \frac{dN_{tv}}{dt} \tag{D-2}$$

where N_t is the total number of macromolecules in the volume. N_{tv} is the number of macromolecules in the intravascular space. N_{tv} is related to the plasma concentration of solute by

$$N_{tv} = V_{ves}C_p(1 - H_{Tm}) \tag{D-3}$$

where V_{ves} is the vessel volume within the monitoring volume, V. H_{Tm} is the average hematocrit in the monitoring volume. Initially, there is no extravasation from the vessels, therefore N_t is equivalent to N_{tv}.

The average fluorescence intensity in the monitoring window is defined as

$$I_m = \frac{1}{A}\int_A I_t dA = \frac{\Psi(h)k}{V} N_t \qquad \text{(D-4)}$$

where I_t is the total fluorescence intensity which is related to the total concentration of fluorescently labeled molecules in the volume, the depth of light collection, the tissue attenuation of the light, and the intensity of background tissue within the dorsal chamber. A is the area of the large monitoring window, P is the optical correction function which is a function of the light attenuation from excitation and emission, and the depth of the tissue.

The integrated intensity across a single vessel per unit length (F_p) is obtained by placing a smaller window over a portion of the vessel. The amount of fluorescent molecules within the vessels immediately after injection is much greater than the amount extravasated, therefore

$$F_p = \frac{1}{4}\pi d^2 k C_p (1 - H_T) \qquad \text{(D-5)}$$

where d is the vessel diameter, H_T is the local hematocrit. The average fluorescence intensity before extravasation can be used to measure vascular volume (V_{ves}). As was stated above all the fluorescent molecules are located intravascularly. Combining equations D-3 to D-5 leads to the following expression for the vascular volume

$$\frac{V_{ves}}{V} = \frac{\pi}{4} d^2 \frac{I_{m0}}{F_p \Psi(h)} \left[\frac{1 - H_T}{1 - H_{Tm}} \right] \qquad \text{(D-6)}$$

Appendix D. Microvascular Permeability Derivation

The permeability -surface area product per unit volume is calculated by combining equations D-1 through D-6 (Substitute D-1 into D-2, substitute D-3 and D-4 into the result and rearrange, substitute D-6 into the result and rearrange, finally substitute D-5 into the result)

$$\frac{PS}{V} = \frac{\pi d^2 (1 - H_T)}{4 F_p \Psi(h)} \left(\frac{1}{I_{m0}} \frac{dI_m}{dt} + \frac{I_{m0}}{K} \right) \qquad \text{(D-7)}$$

where $K = -C_p/(dC_p/dt)$. From this we can calculate the average permeability of tumor vessels

$$P = (1 - H_{Tm}) \frac{V_{ves}}{S} \left(\frac{1}{I_{m0}} \frac{dI_m}{dt} + \frac{I_{m0}}{K} \right) \qquad \text{(D-8)}$$

References

1. Yuan, F., M. Leunig, D. Berk, and R. Jain, Microvascular permeability of albumin, vascular surface area, and vascular volume measured in human adenocarcinoma LS174T using dorsal chamber in SCID mice. Microvascular Research. **45**: 269-289 (1993).

Appendix E. Microvascular Permeability Data

Table E-1. Microvascular Permeability Measurements

Animal	$I_{backround}$	I_o	dI/dt ($x10^{-4}$)	$(dI/dt)/I_o$ ($x10^{-4}$)	S/V_{ves} (1/cm)	1/K (1/s)	P(cm/s) ($x10^{-7}$)
hca-11	0.224	2.02	6.864	3.8218	2499	0.00011	1.5953
hca-12	0.281	1.91	23.44	14.3892	3144	0.00011	3.9905
hca-13	0.3	2.38	12.27	5.899	34515	0.00011	0.16425
hca-21	0.223	0.57	3.217	9.4064	2984	0.00011	2.8519
hca-22	0.365	0.67	2.204	7.1558	3835	0.00011	1.7437
st8-21	0.1672	0.77	2.76	4.556	2743	0.00011	1.6702
st8-11	0.141	0.46	2.346	7.3542	1823	0.00011	3.7564
st8-12	0.121	0.23	0.2134	1.9225	3775	0.00011	0.64854
st8-13	0.18	0.19	0.4946	41.2167	3695	0.00011	9.2765
st8-22	0.149	0.52	2.41	6.4267	1856	0.00011	3.2848
mca-11	0.2	0.83	4.874	7.7984	3441	0.00011	2.0947

Appendix F. Intravital Fluorescent Microscopy Photographs for Chapter 5

Appendix F. Intravital Fluorescent Microscopy Photographs for Chapter 5

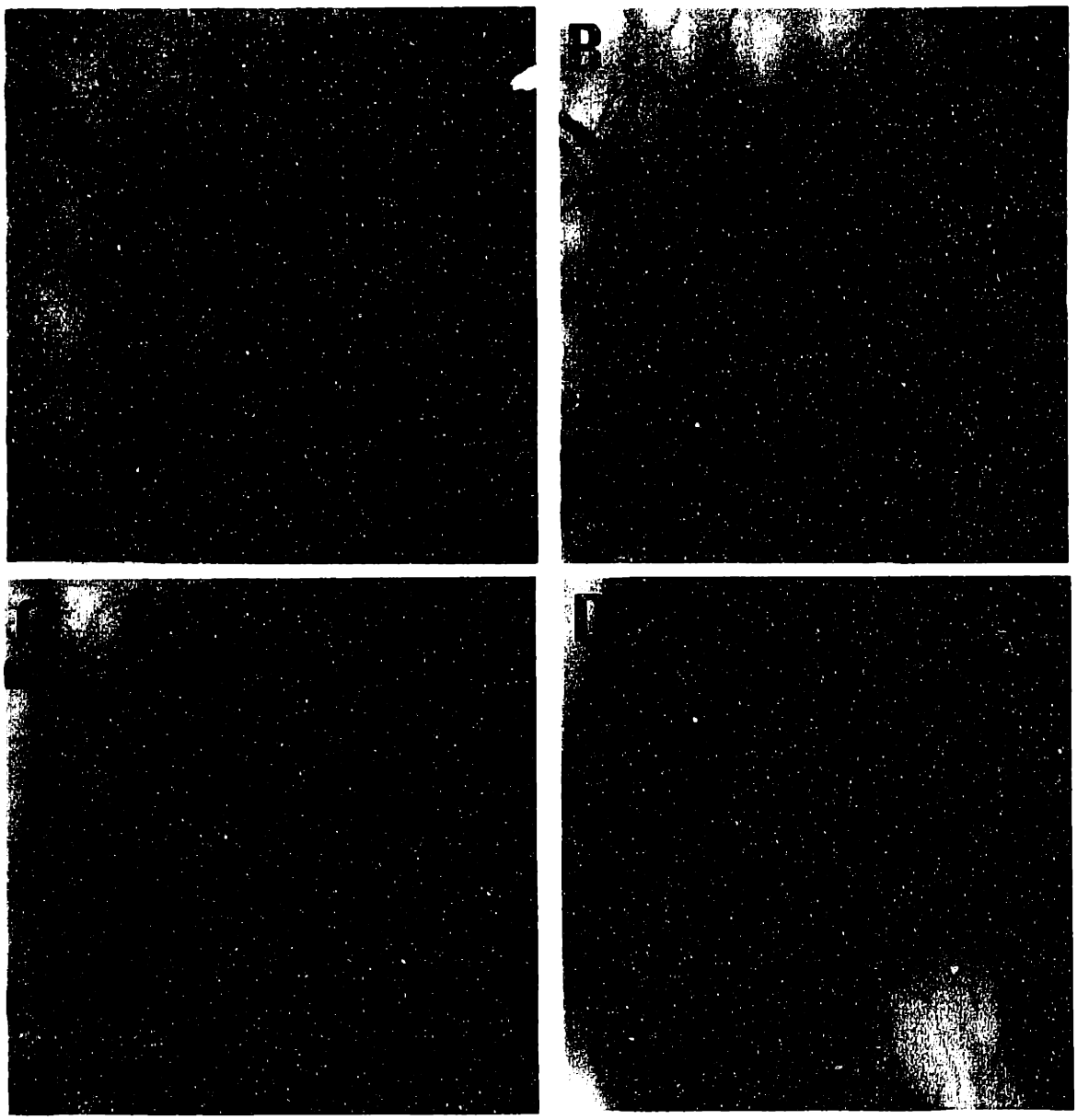

Figure F-1. Images of the same Shionogi tumor in the dorsal chamber.
A) 5 days before sham operation (5 days after implantation)
B) day of sham operation (10 days after implantation)
C) 5 days after sham operation (15 days after implantation)
D) 12 days after sham operation (22 days after implantation)

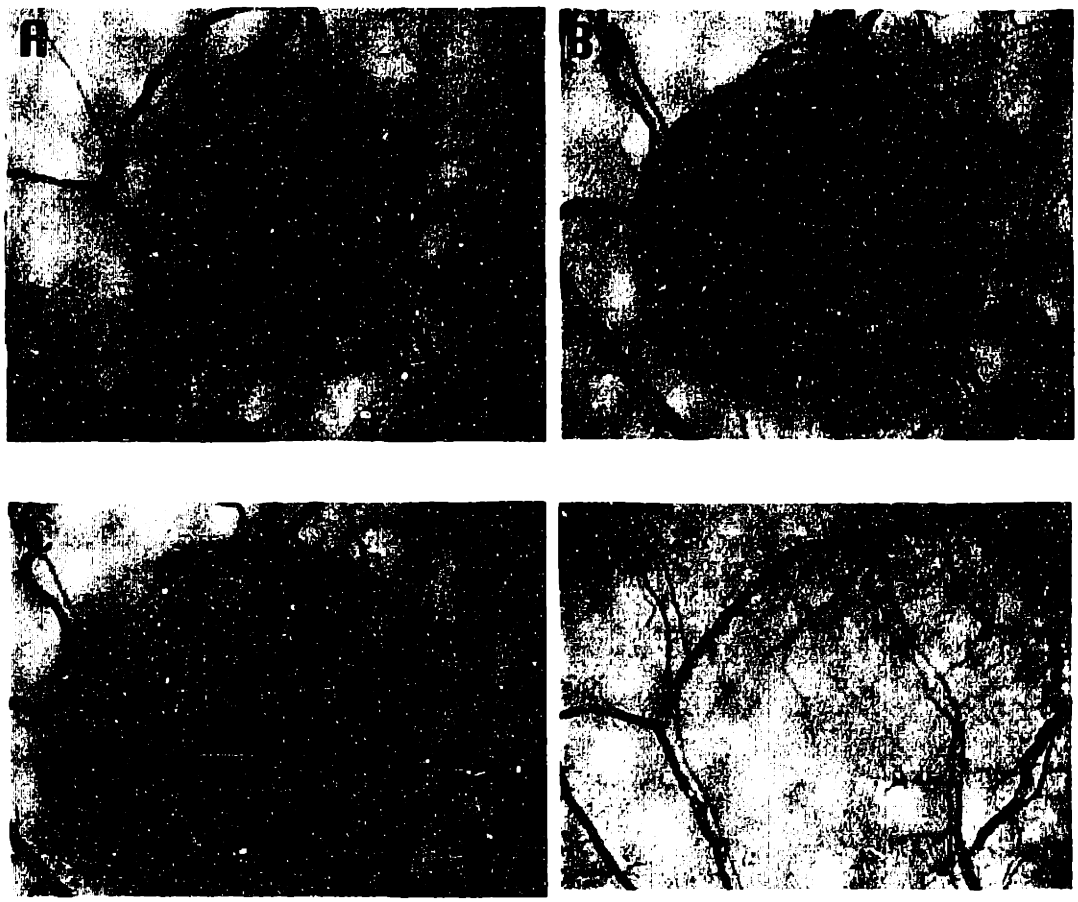

Figure F-2. Images of the same Shionogi tumor in the dorsal chamber.
A) 5 days before orchiectomy (5 days after implantation)
B) day of orchiectomy (10 days after implantation)
C) 5 days after orchiectomy (15 days after implantation)
D) 12 days after orchiectomy (22 days after implantation)

Appendix G. Intravital Fluorescent Microscopy Photographs for Chapter 6

Appendix G. Intravital Fluorescent Microscopy Photographs for Chapter 6

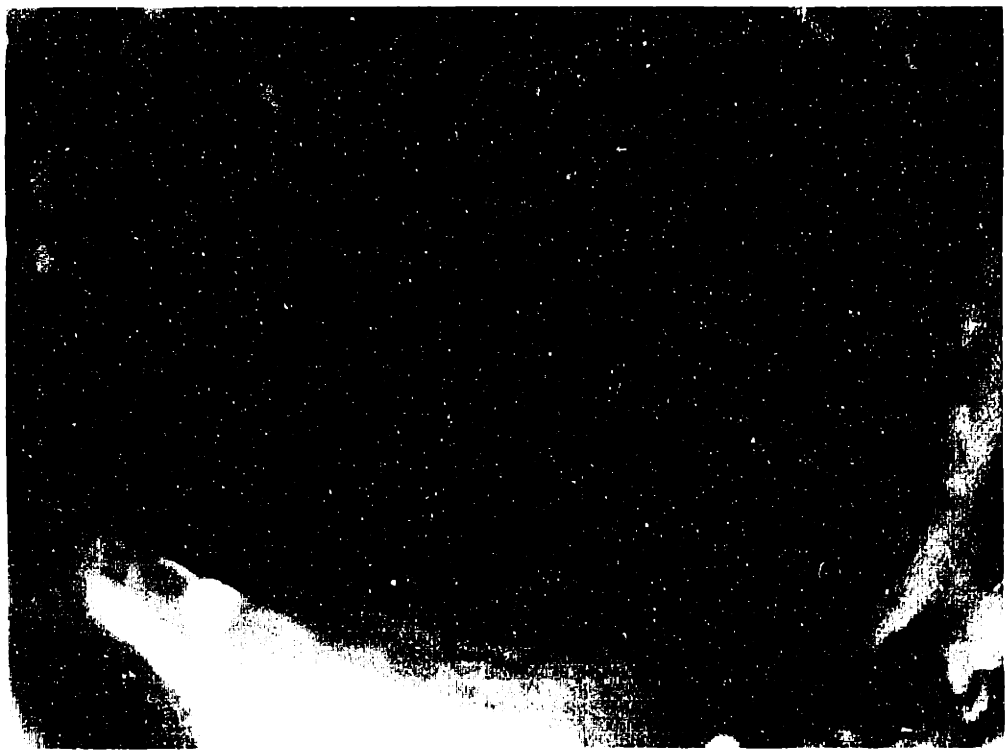

Figure G-1. Overview of the cranial window. A 15 day old U87 is located on the pial surface of the upper hemisphere.

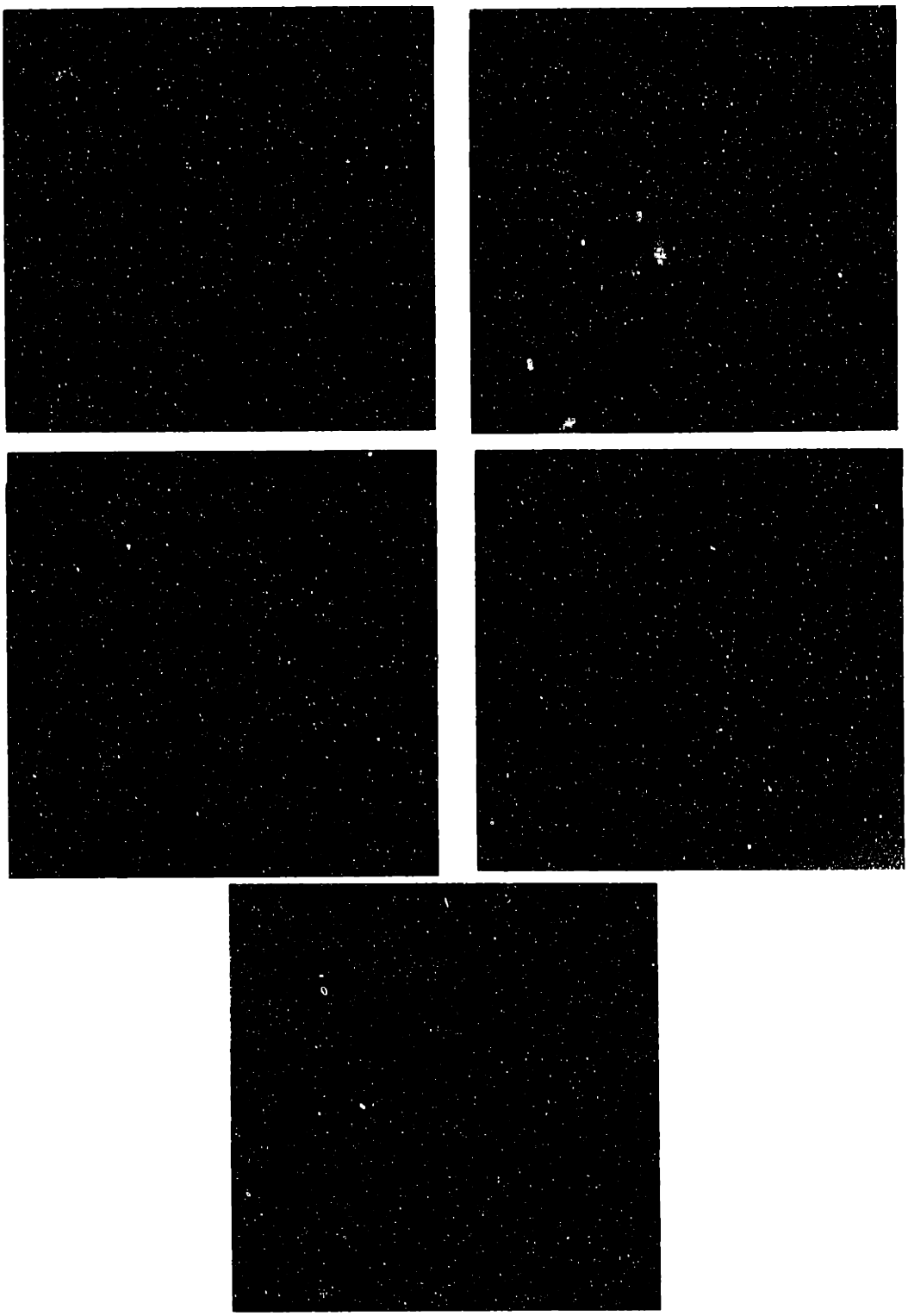

Figure G-2. Pore cutoff size representation in the cranial window.
A) HCa I: no extravasation of 400 nm liposomes (2.5x magnification)
B) HCa I: extravasation of 210 nm liposomes (2.5x magnification)
C) MCa IV: vessel perfusion shown with FITC dextran,
there was no extravasation of 780 nm latex beads (1.6x magnification)
D) MCa IV: no extravasation of 550 nm liposomes (2.5x magnification)
E) MCa IV: extravasation of 400 nm liposomes (25x magnification)

Appendix H. bFGF-Heparin Binding Data

TCA Precipitation Data

N1

Preincubation fraction protein associated

Volume (µl)	CPM ppt	CPM super
10	1093.8	485.8

To each vial

CPM total	3716.5
Volume (µl)	25
FGF* (µg)	0.008
FGF (µg)	0.1

Calculations

%protein associated CPM	0.69
%free label CPM	0.31
FGFtotal/FGF*	13.5
FGF*/CPM	3.11E-06

N2

Preincubation fraction protein associated

Volume (µl)	CPM ppt	CPM super
5	370.8	207.8
	373.8	267.6

To each vial

CPM total	2917.8
Volume (µl)	25
FGF* (µg)	0.008
FGF (µg)	0.1

Calculations

%protein associated CPM	0.61
%free label CPM	0.39
FGFtotal/FGF*	13.5
FGF*/CPM	4.49E-06

N3

Preincubation fraction protein associated

Volume (µl)	CPM ppt	CPM super
5	5539.5	2047.9
	4080.3	1705.9

To each vial

CPM total	7441.8
Volume (µl)	10
FGF* (µg)	0.008
FGF (µg)	0.1

Calculations

%protein associated CPM	0.72
%free label CPM	0.28
FGFtotal/FGF*	13.5
FGF*/CPM	1.49E-06

N4

Preincubation fraction protein associated

Volume (µl)	CPM ppt	CPM super
5	3107.8	1450.8
	2843.9	1426.8

To each vial

CPM total	13843.8
Volume (µl)	15
FGF* (µg)	0.008
FGF (µg)	0.1

Calculations

%protein associated CPM	0.67
%free label CPM	0.33
FGFtotal/FGF*	13.5
FGF*/CPM	8.57E-07

N5

Preincubation fraction protein associated

Volume (µl)	CPM ppt	CPM super
5	1495.8	566.8
	1383.7	494.8

To each vial

CPM total	3520.8
Volume (µl)	10
FGF* (µg)	0.008
FGF (µg)	0

Calculations

%protein associated CPM	0.73
%free label CPM	0.27
FGFtotal/FGF*	1
FGF*/CPM	3.11E-06

N6

Preincubation fraction protein associated

Volume (µl)	CPM ppt	CPM super
5	1647.3	702.7
	1657.7	544.8

To each vial

CPM total	11288.8
Volume (µl)	25
FGF* (µg)	0.008
FGF (µg)	0.1

Calculations

%protein associated CPM	0.73
%free label CPM	0.27
FGFtotal/FGF*	13.5
FGF*/CPM	9.76E-07

Appendix H. bFGF-Heparin Binding Data

TCA Precipitation Data continued

N7		
Preincubation fraction protein associated		
Volume (µl)	CPM ppt	CPM super
5	828.2	392.8
	831.4	390
To each vial		
CPM total		5862.8
Volume (µl)		20
FGF* (µg)		0.008
FGF (µg)		0.1
Calculations		
%protein associated CPM		0.68
%free label CPM		0.32
FGFtotal/FGF*		13.5
FGF*/CPM		2.01E-06

Heparin Content Determination in Activated and Coupled Sepharose Beads

A. Heparin Standards

Heparin (µg)	Absorbance	A-Backgd
50/100	0.995	0.6444
30/100	1.0014	0.6508
15/100	0.8564	0.5058
9.99/100	0.7758	0.4252
7.5/100	0.7261	0.3755
3/100	0.5037	0.1531
0/100	0.3506	0

B. Heparin Content over the Microbeads

Activation	Absorbance	A-Backgrd	dilution factor	Hsample	Hsolution(µg)
A	0.463	0.1124	2.67E+03	1.87718482	5005.82618
	0.5275	0.1769	1602	3.75300276	6012.31043
	0.9628	0.6122	320.4	16.4125927	5258.5947
	0.7861	0.4355	640.8	11.273724	7224.20234
Ac	0.4897	0.1391	2827.232	2.6536862	7502.58654
	0.5591	0.2085	1696	4.67200814	7923.72581
	0.9946	0.644	339.2	17.3374146	5880.85102
	0.8201	0.4695	678.4	12.2625273	8318.8985
C	0.4325	0.0819	2270.454	0.99017013	2248.13574
	0.4673	0.1167	1362	2.00223935	2727.04999
	0.8276	0.477	272.4	12.4806456	3399.72787
	0.6138	0.2632	544.8	6.26281809	3411.9833

Appendix H. bFGF-Heparin Binding Data

Heparin Content Determination in Activated and Coupled Sepharose Beads continued

C. Heparin Content within the microbeads

Activation	Hsolution Ave (mg)	Std. dev	Hinit(mg)	Hbead (mg)	Vbead (ml)	C (mg/ml)
A	5.875233	0.9958	8.2	2.32476659	0.64	3.632448
Ac	7.406515	1.0703	8.2	0.79348453	0.74	1.072276
C	2.946724	0.5651	3.85	0.90327578	0.385	2.346171

Appendix I. Intravital Fluorescent Microscopy Photographs for Chapter 8

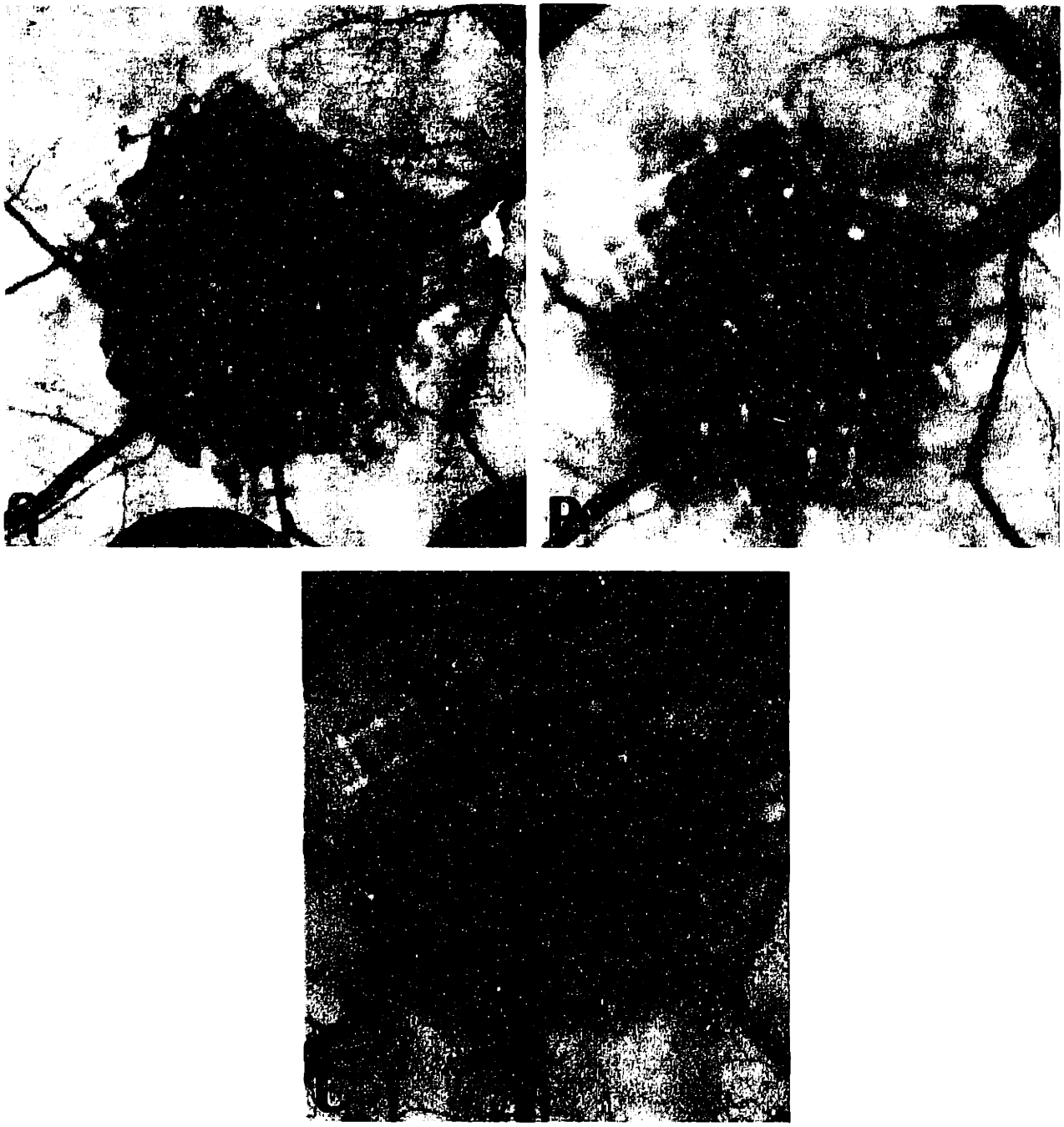

Figure I-1.Vascular growth into a collagen gel containing VEGF in the dorsal chamber.
A) 6 days, B) 11 days, and C) 20 days after gel implantation.

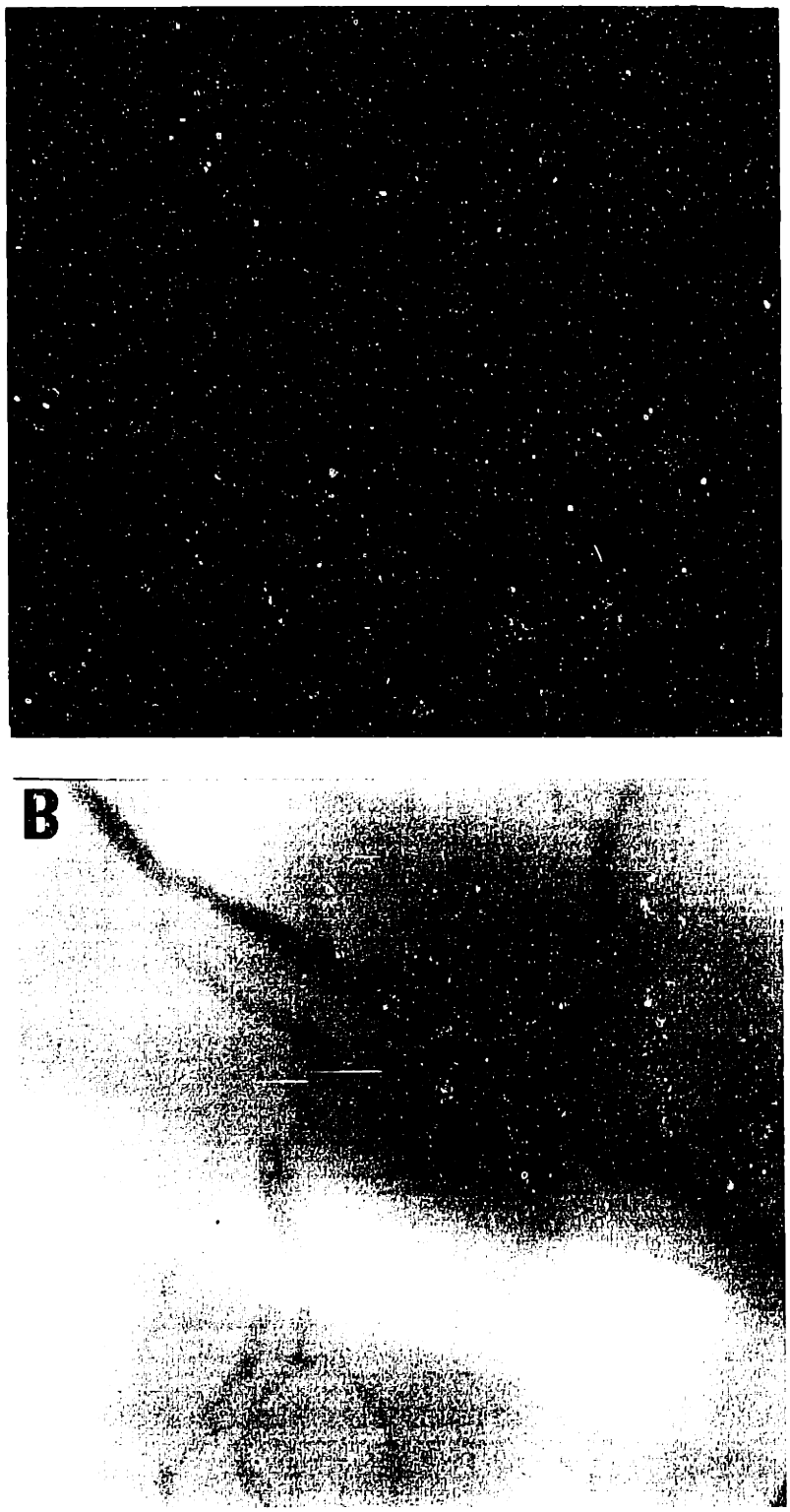

Figure I-2.Comparison of bFGF and VEGF induced vascular patterns.
A) Fluorescent image of bFGF gel (2.5x magnification)
B) Non-fluorescent image of VEGF gel (2.5x magnification)

Appendix J. Pore Cutoff Studies Data

Pore Cutoff Size Determination in Dorsal Chambers			Pore Cutoff Size Determination in Cranial Window	
Tumor line	Extravasation size (nm)	No extravasation size (nm)	Extravasation size (nm)	No extravasation size (nm)
MCa IV	100	2000	380	550
	200			780
	380			
	580			
	780			
	1200			
ST-8	290	780	400	780
	380			
	550			
LS174T	290	550		
	384			
	480			
HCa 1	384	550	210	400
ST-12	380	780		
	550			
ST-melanoma		380		
		550		
Shionogi 1	200	780	100	400
	380			550
Shionogi 2	200	380		
		550		
VEGF	7	380		
		550		
bFGF	200	380		
		550		
U87			7	100
				370

	Tumor Growth		Tumor Regression	
Day	Extravasation size (nm)	No extravasation size (nm)	Extravasation size (nm)	No extravasation size (nm)
-2	200	550	200	550
0	200	400	200	400
2	200	400		7
				100
				200
				400
				550
4	200	400		200
				400
6				200
				400
				550

Appendix K. Nomenclature

BBB	blood-brain barrier
bFGF	basic fibroblast growth factor
BSA	bovine serum albumin
BTB	blood-tumor barrier
C	pore fluid bFGF concentration
C_{bulk}	bulk fluid bFGF concentration
C_{int}	interstitial solute concentration (moles/cm^3)
C_p	plasma solute concentration (moles/cm^3)
d_n	vessel diameter
D	molecular diffusivity in water at 20°C
D_{eff}	effective diffusivity
D_{gel}	diffusivity in the gel
ECM	extracellular matrix
FITC	fluorescein isothiocyanate
F_p	integrated intensity across single vessel per unit length
HCa I	murine hepatocarcinoma
H_T	local hematocrit
H_{Tm}	average hematocrit of microvessels
I	average fluorescence intensity
I_b	background tissue fluorescence intensity
I_m	average fluorescence intensity in monitoring window
I_o	initial average fluorescence intensity
I_t	total fluorescent intensity
J_s	solute flux (moles/s)
J_v	fluid volume flux (cm^3/s)
k	proportionality constant
K	plasma clearance
K_d	hindered diffusion factor
K_D	equilibrium dissociation constant
K_f	fluorescence proportionality constant
L_n	vessel length
LS174T	human colon adenocarcinoma
M	total number of vessels on the tumor surface
MCA IV	murine mammary carcinoma
MW	molecular weight
N_t	total number of macromolecules per volume
N_{tv}	total number of macromolecules in intravascular space
P_p	plasma hydrostatic pressure
P_{int}	interstitial hydrostatic pressure
Pe	Peclet number
q	partition coefficient
Rho	rhodamine
PDGF	platelet derived growth factor
r_p	pore radius
r_s	solute radius
r_{sphere}	radius of sepharose microbead
R_T	number of binding sites for bFGF on heparin molecule
S	bound complex concentration
SCID	severe combined immunodeficiency
Shionogi	murine androgen dependent mammary carcinoma
ST-8	anaplastic, murine origin

Appendix K. Nomenclature

Shionogi	murine androgen dependent mammary carcinoma
ST-8	anaplastic, murine origin
ST-12	anaplastic, murine origin
TGF-β	transforming growth factor
U87	human glioblastoma
V_{bulk}	volume of solution
VEGF	vascular endothelial growth factor
V_{ves}	total vessel volume
VVO	vesiculo-vacuolar organelles
ε	void fraction of sepharose gel
γ	tortuosity of sepharose gels
λ	ratio of solute radius to pore radius
π_p	plasma oncotic pressure
π_{int}	interstitial oncotic pressure
Φ	partition coefficient
$\Psi(h)$	optical correction function
σ	solute reflection coefficient